UNIVERSITY OF TRENTO - Italy
Department CIBIO

International PhD Program in Biomolecular Sciences

Department of Cellular, Computational and Integrative Biology – CIBIO

XXXII Cycle

"Pleiotropic effect of MATR3 in pluripotent stem cells"

Tutor:

Prof. Alessandro Provenzani

University of Trento, CIBIO

Advisor:

Ph.D. Rosa Loffredo

Ph.D. Thesis of

Daniele Pollini

University of Trento, CIBIO

Academic Year 2018/2019

Original authorship

Declaration:

I, Daniele Pollini, confirm that this is my own work and the use of all material from other sources have been properly and fully acknowledged.

Contents

ABSTRACT

Matrin3 (MATR3) is an RNA binding protein involved in many roles in the nucleus, such as chromatin architecture and gene expression regulation, modulating transcriptional and post-transcriptional processes as RNA splicing and mRNA stabilization. Nevertheless, some functions of MATR3 within the cells are not entirely clear. MATR3 has been associated with Amyotrophic Lateral Sclerosis (ALS), a neurodegenerative disease that damages motor neuron (MN) cells and leads to progressive muscle paralysis and respiratory failure. A better understanding of MATR3 activity within cell physiology could represent an essential breakthrough for studying MATR3-associated pathologies. Using MATR3-silenced human pluripotent stem cell (hiPSC) line model, we collected data on the MATR3 role in the pluripotency and in the neural induction and differentiation. We found that the downregulation of MATR3 alters the expression level of crucial self-renewal factors such as OCT4, NANOG, KLF4, and LIN28A. We observed MATR3 acts at multiple levels of the gene expression, i.e. regulating YTHDF1 expression, and in RNA metabolism, having a role in mRNA stabilization and translation. The reduction of stemness potential caused by MATR3 downregulation creates a defect during the neurodifferentiation process, which does not arrest motor neurons formation but induces selective alterations that may affect motor neurons functionality. Indeed, several morphological and molecular abnormalities were observed during the neuronal differentiation, such as the alterations of the formation of neuroepithelial rosettes that arise in a reduction of neurite lengths and arborization in neuronal cells. On this basis, we investigated neuronal differentiation in the brain organoids grown from iPSCs derived from ALS patients fibroblasts. We show, for the first time, that MATR3 is a critical factor in orchestrating the stemness network through transcriptional, post-transcriptional, and translational regulation, therefore affecting the differentiation of mature neurons.

ABBREVIATIONS

AD	Alzheimer Disease
ALS	Amyothrofical Lateral Sclerosis
ChIP	Chromatin Immunoprecipitation
CNS	Central Nervus System
CTIP2	COUP-TF-interacting protein2
DPRs	Di-Peptide Repeats
DSB	Double-Strand Breaks
EBs	Embryoid Bodies
ESC	Embryonic Stem Cell
FTD	Frontotemporal Dementia
HDACs	Histone Deacetylase
HR	Homologous Recombination
ICM	Inner Cell Mass
iPSC	induced Pluripotent Stem Cell
Ips	Intermediate Progenitors
lncRNAs	long non-coding RNAs
MATR3	Matrin 3
MNs	Motor Neurons
miRNA	micro RNA
mRNA	messenger RNA
NCIs	Neuronal Cytoplasmic Inclusions
NES	Nuclear Export Signal
NHEJ	Non-Homologous end Joining
NLS	Nuclear Localization Signal
oRGs	outer Radial Glial cells
PSC	Pluripotent Stem Cell
PTB	Polypyrimidine Tract Binding
PTMs	Post-Translational Modifications
RBMs	RNA Binding Proteins
RNPs	Ribonucleoproteins
ROS	Oxygen species
RRM	RNA Recognition Motif
SSB	Single-Strand Breaks
SVZ	Sub-Ventricular Zone
TBR1	T-box brain protein 1
TE	Trophectoderm
vRGs	ventricular Radial Glial cells
VZ	Ventricular Zone

1. INTRODUCTION

1.1 Pluripotent Stem Cells (PSCs)

1.1.1 Overview

Pluripotent stem cells (PSCs) have the ability to differentiate into any cell that is ultimately derived from the three embryonic germ layers (mesoderm, ectoderm and endoderm) (Trounson, 2007; Wu *et al.*, 2016; Carvalho, 2017). This characteristic is showed by the cells residing in the inner cell mass (ICM) of the blastocyst, named Embryonic Stem Cell (ESC), during the first steps of the embryogenesis (Johnson *et al.*, 2008). The primary characteristic of PSC is the undifferentiated state that allows their abilities to self-renew and differentiate into mature cells (Gardner, 2013). During the process of maturation, the loss of pluripotency and commitment to specific cell lineages lead to essential changes within the cell, such as the profound changes in chromatin structures. The chromatin changes induce a change in gene expression that include the down-regulation of the pluripotency factors and consequently the up-regulation of differentiation regulators (Figure 1) (Johnson *et al.*, 2008; Berdasco and Esteller, 2011; Chagastelles and Nardi, 2011; Bhartiya and Nagvenkar, 2013; Tsz Kin Ng, Daniel Pelaez and Cheung, 2013). In adult mammals, PSCs are not present, but adult stem cells are quiescent within adult tissues. They can infrequently divide to generate two different cells, a stem cell clone and a transiently-amplifying cell, that allow regenerating contemporize a new stem cell but also a new somatic cell (Tsz Kin Ng, Daniel Pelaez and Cheung, 2013).

The ESC, derived from the inner cell mass of a blastocyst before gastrulation, is considered the prototype of pluripotent stem cells (Radzisheuskaya *et al.*, 2013; Tsz Kin Ng, Daniel Pelaez and Cheung, 2013). However, the exploitation of human ESC has limitations, i.e. ESCs are not easy to obtain, and besides, their use is prohibited or limited in some countries in the world for ethical reasons (Bhartiya and Nagvenkar, 2013).

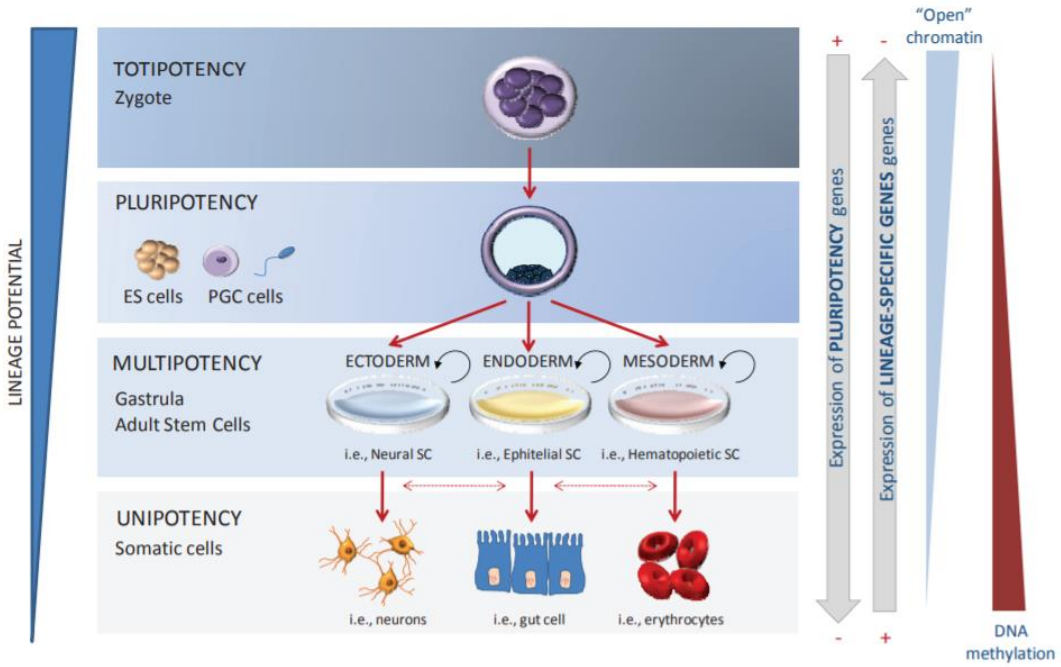

Figure 1. Stemness lineage, from the totipotent stem cell, formed during the reproduction with the fusion of the spermatozoa and oocyte to form the zygotes cell; through by the pluripotency state and multipotency state to the unipotent stem cell the last step of the differentiation in specific-tissue cell lineage, somatic cells. In this representation was reported graphically the main changes happened during the differentiation of stem cells, such as the genetic changes with the remodelling chromatin and expression of the factors gene involved in stemness (Berdasco and Esteller, 2011).

In 2006 Takahashi and Yamanaka found a cocktail of 4 genes (OCT4, SOX2, KLF4 and cMYC) able to reprogram somatic cells and induce the formation of pluripotent stem cells, called induced pluripotent stem cells (iPSCs) (Takahashi and Yamanaka, 2006). One of the mainstream and valuable applications of iPSCs is their use to recreate the so-called “disease in a dish”. Indeed, the possibility to obtain iPSCs directly from the patient’s cells allows recreating *in vitro* disease models with the same genetic background of the patient (Rowe and Daley, 2019). iPSC-based models offer the possibility to develop a more in-depth understanding of the pathological mechanisms involved in human diseases, especially neurological diseases. For example, the use of animal models such as the transgenic mice for Alzheimer disease study has the limitation of being a different species, and this could not rightly or entirely recapitulate the main features of the disease (Puzzo *et al.*, 2015; Onos *et al.*, 2016).

Moreover, besides disease modelling, iPSCs are redefining drug screening and regenerative medicine. iPSC technology allows the screening of therapeutic molecules by providing drug development models that are disease- and patient-specific (Rowe and Daley, 2019).

However, several issues exist in the application of hiPSCs in cell therapy. For example, one of the most efficient methods to obtain the iPSCs is to use retro- or lentivirus system. Retroviruses possess some properties that make iPSCs that are produced unfit for human cell therapy, i.e. viral DNA integration into the host cell (Medvedev, Shevchenko and Zakian, 2010). Moreover, the overexpression of *Oct4*, *Sox2*, *Klf4*, and *c–Myc* could lead to neoplastic development (Qi and Pei, 2007; Cai *et al.*, 2015; Hadjimichael *et al.*, 2015).

1.2 Pluripotency

1.2.1 Mechanisms to maintain self-renewal

To date, our knowledge about how the pluripotency circuit is maintained is incomplete. However, the major pathways responsible for pluripotency maintenance are known and well characterized. It is widely reported that self-renewal state is due to the expression of the main transcription factors as OCT4, NANOG, and SOX2 cell surface glycolipid as SSEA-3 and SSEA-4 and glycoprotein TRA-1-60 and TRA-1-81 and to the functional enzymatic activity as telomerase and alkaline phosphatase (Ilic *et al.*, 2012). We can, in part, describe how human ESCs maintain self-renewal. Indeed, several networks have been identified to work synergically to maintain pluripotency. For the correct self-renewal, the TGFβ/ACTIVIN and FGF signalling is required (in mouse, dictated by LIF and BMP4 (Figure 2) (Ilic *et al.*, 2012)). TGFβ/ACTIVIN activates the SMAD transcription functions (Shi and Massague, 2003) while FGF way activates the phosphorylation events in the MAP kinase cascade (Chang and Karin, 2001). The TGFβ/ACTIVIN mediated SMAD signalling (and respective LIF pathway in mouse), is directly involved in transcription of *NANOG*, *KLF4* and *SOX2* (Figure 2) (Hall *et al.*, 2009; Niwa *et al.*, 2009; R. Xu *et al.*, 2009). Another highly conserved pathway that is necessary to maintain the self-reward is the Wnt pathway (Hao *et al.*, 2006). Wnt network is crucial to forming a complex between receptors Frizzled and LRP5/6, the interaction that allows the releasing of β-catenin that moves in the nucleus where can play a role as a coactivator for T-Cell-factor, a transcription factor to activate Wnt-responsive genes (Singh and Brivanlou, 2013). TCF, the transcription mediator of Wnt signalling, is direct involves in OCT4, NANOG, and SOX2 expression (Cole *et al.*, 2008). TCF has also engaged directly with other transcription factors work as NANOG, OCT4, and SOX2, thus indicating an essential role of Wnt pathways where its mediated

interacts in the core of transcription pluripotency (Singh and Brivanlou, 2013). The crucial pluripotency factors OCT4, NANOG, SOX2, LIN28A, and KLF4 roles also in self-renewal are described in the next chapters.

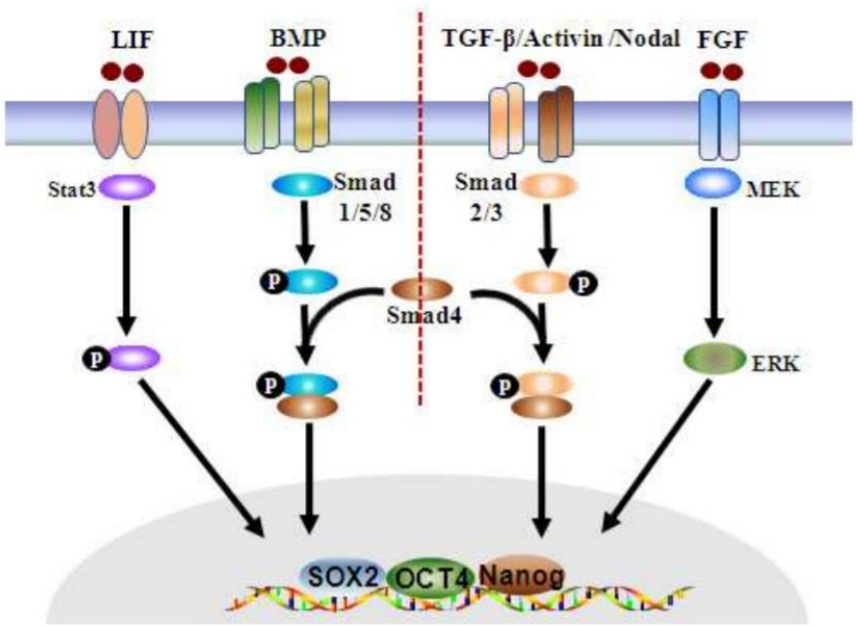

Figure 2. Representation of the main exogenous growth factors signal pathways that regulate the transcription factors in ES cell pluripotency. The left panel was represented principal mouse pathways and in the right the principal human pathways (Han, Wang and Hao, 2013).

1.2.2 OCT4 in pluripotency maintenance

OCT4 (also known as OCT3, OCT 3/4) is a member of the POU (Pit-Oct-Unc) transcription factor family (HR *et al.*, 1990), and is encoded by the Pou5f1 gene. POU proteins are known as DNA binding-proteins, controlling the expression of their target genes through binding octameric sequence motif of an AGTCAAAT *consensus* sequence (Pan *et al.*, 2002; Shi and Jin, 2010; Young, 2012). The expression of OCT4 is characteristic of the stemness stage, indeed its expression was reported during embryonic development, initially in blastomeres, subsequently in the ICM and the primitive endoderm factors downregulate it in trophectoderm (TE) (Pesce and Scholer, 2001; Pan *et al.*, 2002). During the development, OCT4 is still expressed in the embryonic ectoderm, while it is downregulated at the gastrulation stage (Pesce and Scholer, 2001; Pan *et al.*, 2002). The primordial germ cells are the only cells that express OCT4 even after the commitment (Pesce and Scholer, 2001; Pan *et al.*, 2002).

OCT4 is transcriptionally regulated by cis-acting elements located upstream of the *OCT4* gene and methylation of chromatin structures (Ben-shushan *et al.*, 1993; Pan *et al.*, 2002). DNA methylation sites are localized in three different regulatory elements, i.e. distal enhancer, proximal enhancer and proximal promoter (Niwa, 2007). The DNA methylation of these three elements reflects the transcriptional status of the *OCT4* gene, where high levels of methylation inhibit the transcription of *OCT4*. Indeed these three elements are methylated by Dnmt3a and Dnmt3b during the differentiation of ES cells (Hattori *et al.*, 2004; Kellner and Kikyo, 2012). Moreover, post-translational mechanisms affect the stability and the activity of the protein OCT4, e.i. the transcription activity of POU factors is known to be regulated by phosphorylation modification (Brehm *et al.*, 1997; Shi and Jin, 2010). Furthermore, few studies have reported some post-translational modifications (PTMs) that occur on OCT4, such as the modification on the monosaccharide O-linked β-N-acetylglucosamine (O-GlcNAc) (Webster *et al.*, 2009; Berg *et al.*, 2010). The ubiquitination that promotes the OCT4 degradation through the 26S proteasome (Xu *et al.*, 2004; H. Xu *et al.*, 2009) and the sumoylation that appears to jointly control OCT4 protein amount at an appropriate level in ESCs (Wei, Scho and Atchison, 2007).

The OCT4 function in pluripotency is determined by the balance between the cellular amount of OCT4 and its PTMs (Pan *et al.*, 2002). High level of OCT4 expression drives stem cells towards endoderm and mesoderm lineages, while low level of OCT4 brings the ES cells to differentiate in TE (Figure 3) (Niwa, Miyazaki and Smith, 2000; Pan *et al.*, 2002; Niwa, 2007). OCT4 cooperates

with other factors to activate or repress gene targets. OCT4 is able to modulate the expression of the targets through the cooperative binding with SOX2; for example, OCT4/SOX2 activates the transcription of FGF4, a stem cell-specific growth factor (Curatola and Basilico, 1990). The octamer motif recognized by OCT4/SOX2 is the regulatory sequence present within the FGF4 enhancer. It has also been found in other stem cell factors enhancers, i.e. *OCT4* itself, *NANOG* and *SOX2.* This highlights the importance of OCT4 in stemness and, at the same time, could be considered the primary factor in determining ES fate.

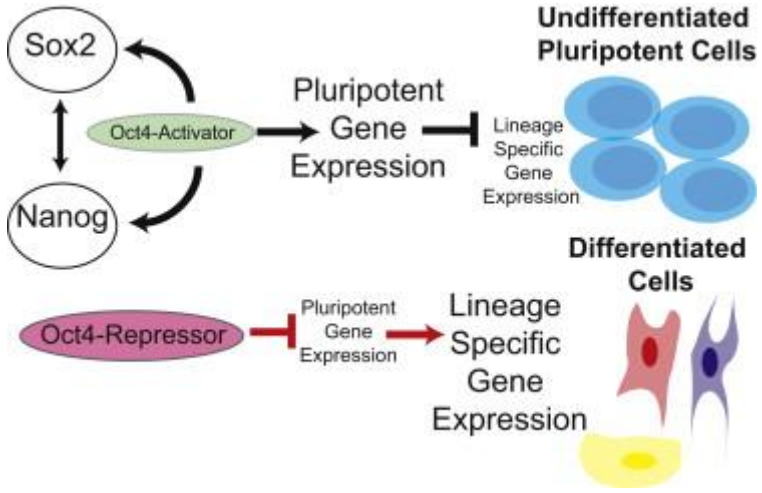

Figure 3. Schematic representation of the double role of OCT4; as an activator, to maintain the pluripotency and as a repressor to promote the differentiation (Hammachi *et al.*, 2012).

1.2.3 NANOG in pluripotency maintenance

One of the essential pluripotency factors involved in ES cell self-renewal is NANOG. The name of NANOG derives from the Celtic mythology name of the Otherworld "Tír Na nÓg", Land of the Young (Allouba *et al.*, 2015). Nanog was found to play a role in regulating cell fate of pluripotent ICM during embryonic mouse development. *In vivo*, it maintains the pluripotent epiblast and prevents the differentiation towards the primitive endoderm, and disappears in the trophectoderm in the blastocyst stage (Chambers *et al.*, 2003; Pan and Thomson, 2007).

NANOG protein consists of 305 amino acids that assemble three domains: the N-terminal, the homeodomain (highly conserved in Hox genes), and the C-terminal. NANOG can bind the DNA consensus sequence 5'-TAAT[GT][GT]-3' or 5'-[CG][GA][CG]C[GC]ATTAN[GC]-3' of the genes

targets, as *OCT4* (Hayashi *et al.*, 2015). It acts as a transcription activator or repressor, cooperating with other master pluripotency factors as OCT4 and SOX2 (Gawlik-rzemieniewska and Bednarek, 2016). NANOG plays a critical role in SMAD signalling; inasmuch interacts directly with SMAD1 with a positive role to activate the SMAD1 complex and inhibits the BMP signalling (Suzuki *et al.*, 2006). The repression of BMP is important for the maintenance of pluripotency because BMP is an initial promotion of mesoderm differentiation with the regulation of Brachyury (one of the most important factors in mesoderm development) (Pan and Thomson, 2007). NANOG regulates the transcription of several pluripotency genes, e.i. it binds the enhancer region of REX1 to regulate its expression positively and to maintain the pluripotency state (Ben-Shushan *et al.*, 1998; Mitsui *et al.*, 2003).

NANOG has been reported to interact with chromatin-associated proteins such as the nucleosome-remodelling SWI/SNF complex, histone deacetylation complex NuRD and demethylase LSD1, that suggests a role in epigenetics control as well as the remodelling of the chromatin (Liang *et al.*, 2008). Even if the role of NANOG in the maintenance of the pluripotency is beyond doubt, it is not present in the pluripotency "Cocktail" for the reprogramming, as the role of NANOG could not be crucial in pluripotency. Moreover, the Nanog overexpression in mESCs could independently maintain the pluripotency by the Lif signal (Chambers *et al.*, 2003; Mitsui *et al.*, 2003). Instead, the overexpression of Oct4 and Sox2 leads to differentiation, respectively, towards the mesendodermal and neural ectoderm (Thomson *et al.*, 2017). The main reason why NANOG is not in the reprogramming "Cocktail" is that itself autorepression is mediated by the association of NANOG and Zfp281 protein with NuRD complex, that inhibits the activation of endogenous NANOG and block the translation in iPSCs (Fidalgo *et al.*, 2012).

1.2.4 SOX2 in pluripotency maintenance

SOX2 is a SOX family member, characterised by a conserved region named high-mobility-group (HMG) DNA binding domain (Zhang and Cui, 2014). SOX family was identified during the studies of mammalian testis-determination factor, SEX determining factor Y (Sry) (Zhang and Cui, 2014; Schaefer and Lengerke, 2019). SOX family is divided into eight categories (SOX A-H), where the SOXB group is divided into SOXB1 and SOXB2 groups, and SOX1, SOX2 and SOX3 are a member of SOXB1 group (Kamachi and Kondoh, 2013). However, in contrast to SOX1 and SOX3, SOX2 can play distinct functions in a different context, such as during embryonic development (Zhang and

Cui, 2014). During the development, SOX2 expression is maintained along with the commitment towards multipotent progenitors as neuronal or epithelial lineages. During neuronal commitment, at early embryogenesis, SOX2 is a crucial factor from the cerebral tubing to the neuronal cortex and finally to the subventricular zone of the lateral ventricle and the granular region in the hippocampus (SOX2 expression is also detected in the adult brain) (Zhao *et al.*, 2004; Feng and Wen, 2015).

Nevertheless, SOX2 plays a critical role in pluripotency; it is involved in several molecular mechanisms such as a transcription factor, an epigenetic regulator, and a signalling molecule (Vencken *et al.*, 2014). SOX2 levels are finely regulated to maintain the balance between the self-renewal, and the differentiation of ESCs (Boer *et al.*, 2007; Kopp *et al.*, 2008; Feng and Wen, 2011) SOX2 is usually found in pluripotency to work cooperatively with other, in dose-dependent, transcription factors as OCT4 and NANOG, and this highlights the importance of the balance of these factors in pluripotency (Boyer *et al.*, 2005). The regulation of SOX2 could occur at the post-translation level; indeed, several PTMs as methylation, acetylation, sumoylation, and phosphorylation can impact SOX2 activity (Zhang and Cui, 2014).

1.2.5 KLF4 in pluripotency maintenance

The Krüppel-factor 4 (KLF4) is a member of the Krüppel-like factor (KLF) family that is characterized by three conserved zinc finger transcription domains at the C-terminus (Schuh *et al.*, 1986). Through the zinc finger domains, KLF4 can bind GC-box or CACCC-boxes DNA sequences with different affinities (Shi and Ai, 2013). Moreover, KLF4 is endowed with one transactivation domain (TAD) and one repression domain, which modulate KLF4 transcriptional activity (that is affected by the affinity of its interaction with other proteins and/or by the binding affinity with the DNA target sequence) (Zhang *et al.*, 2010). KLF4 is expressed in various tissues where plays different roles depending on the targets, activating or repressing the transcription of genes to maintain the self-renewal, and affecting cell proliferation (can block cell proliferation by regulating the expression of cell cycle genes), differentiation and apoptosis (activator or repressor) (Rowland, Bernards and Peeper, 2005; Shields, Christy and Yang, 2008; Xinming Chen *et al.*, 2008; Li *et al.*, 2010; Shi and Ai, 2013; Ghaleb *et al.*, 2018).

In the early human embryogenesis, KLF4 is expressed from the early stage, at the state of eight cells, even before the morula formation (Bialkowska, Yang and Mallipattu, 2017). Indeed, it was co-localized with OCT4 on different target genes to regulate their transcription, such as NANOG, OCT4, SOX2, and C-Myc to maintain the pluripotency (Zhang *et al.*, 2010; Park *et al.*, 2019).

1.2.6 The self-renewal network, OCT4-SOX2-NANOG axis

Pluripotency is maintained by specific signals and interconnected networks where few actors play multiple critical roles in pluripotency as OCT4, NANOG, KLF4, and SOX2 (Shi *et al.*, no date; Nichols *et al.*, 1998; Takahashi *et al.*, 2007; Ng and Surani, 2011; Li, Carlos and Belmonte, 2018). These factors regulate their targets co-operatively, autoregulate themselves and gene circuits (Figure 4) (Akberdin *et al.*, 2018; Li, Carlos and Belmonte, 2018). Indeed, pluripotency factors provide to maintain their expression by autoregulatory and cross-regulatory interactions and activation of additional targets (Orkin *et al.*, 2008). At the same time, pluripotency factors prevent the expression of differentiation-promoting genes (Orkin *et al.*, 2008), for example, GATA-6 is an essential gene for primitive endoderm gene expression is regulated directly by NANOG (Wang *et al.*, 2006).

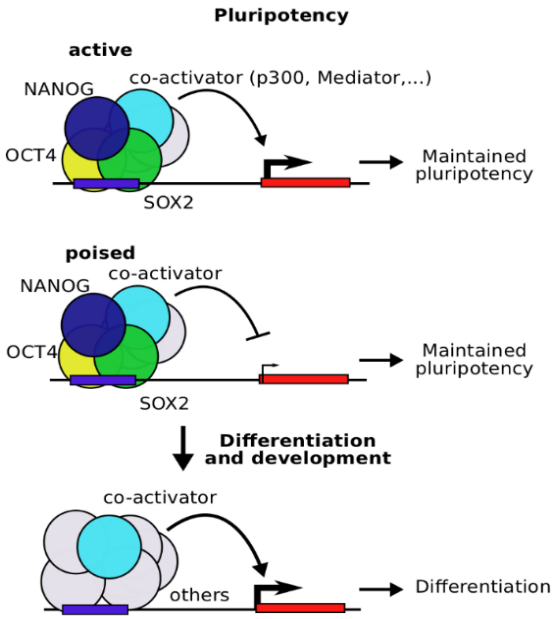

Figure 4. Most important pluripotency factors, OCT4, SOX2 and NANOG, work cooperatively in ESCs to maintain the pluripotency by activating gene expression, or poisoning expression leading to the differentiation development (Göke *et al.*, 2011).

These factors could interact with other complexes. For example, NANOG is associated with histone deacetylase (HDACs) and NuRD remodelling complex, while OCT4 is associate with PRC1 polycomb complex and Swi/Snf ATPase-dependent remodelling complex (Berg *et al.*, 2010; Fidalgo *et al.*, 2012). OCT4, in some cases, acts as a repressor of target genes through binding to the octamer motif, for example, at the proximal promoters of human chorionic gonadotropin genes (Liu and Roberts, 1996; Pan *et al.*, 2002). The above examples of interactions provide the ability of pluripotency factors to positively or negatively modulate the transcription of targets suppressing the expression differentiation factors (Orkin *et al.*, 2008; Hackett and Surani, 2014). OCT4, NANOG, and SOX2 factors act as the crux of the pluripotency gene regulatory network (Young, 2012). Chromatin immunoprecipitation (ChIP) coupled with DNA microarray experiments, identified the DNA sequence bound by OCT4, SOX2 and NANOG. Interestingly, a high frequency of co-occupancy was found within the same regions for these factors (Boyer *et al.*, 2005). Indeed, more than half of the OCT4 DNA recognition motifs are bound by SOX2 as well, and 90% of the OCT4 and SOX2 recognition regions were also recognized by NANOG (Boyer *et al.*, 2005; Pan and Thomson, 2007). 352 target genes were identified to be bound by OCT4, NANOG and SOX2, respectively the 3%, 9% and 7% promoters of 18.000 genes in human ES (Pan and Thomson, 2007; Kellner and Kikyo, 2012). The regulation loop created by OCT4, NANOG, SOX2, and FoxD3 maintains the expression of OCT4 at the average level to keep the correct pluripotency state. Sub-steady levels of OCT4 induce NANOG expression, while average levels repress it. NANOG and FoxD3 are the activators of OCT4 expression, but when the OCT4 level crosses the threshold level, NANOG became its repressor (Figure 5) (Pan and Thomson, 2007). The role of NANOG and OCT4/SOX2 in transcription has been previously reported, but the regulatory links between NANOG and OCT4/SOX2 complex have not fully elucidated. A study showed that the effect of NANOG depletion is the OCT4 and SOX2 downregulation, but, on the other hand, the overexpression of NANOG affects only OCT4 expression. Indeed, the NANOG overexpression leads to an increase of 150% of OCT4 mRNA, while SOX2 mRNA expression does not change (Loh *et al.*, 2006). Instead, in OCT4 overexpressing ESCs, NANOG expression was lower respect to wild type but higher in OCT4 silenced cells (Pan *et al.*, 2001; Karwacki-Neisius *et al.*, 2013).

The balance of these few factors is the key for the down-stream cascade through the activation of Smad1, Stat3 and Tcf3 which are the effectors of signalling pathways controlled by BMP, LIF and Wnt in mouse models (Loh *et al.*, 2006; Cole *et al.*, 2008; Xi Chen *et al.*, 2008). Moreover,

OCT4, SOX2 and NANOG co-operate and regulate other associated transcription factors, such as KLF4, Nac1, Zfp281, Dax1, Nr5a2, Tcfcp2l1 and Esrrb (Ng and Surani, 2011). The critical balance is kept controlling the transcription of their targets as autoregulating their expression, to maintaining the pluripotency state (Mitsui *et al.*, 2003; Chew *et al.*, 2005; Ng and Surani, 2011).

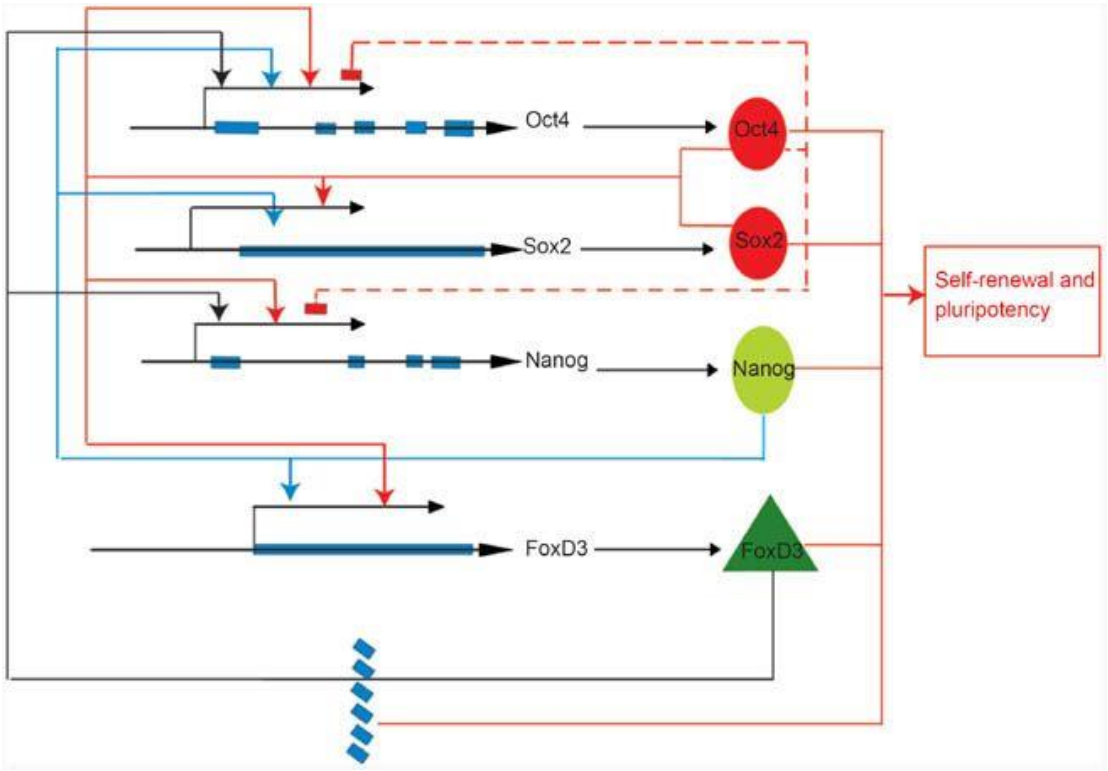

Figure 5. Transcriptional networks regulation by Oct4, Nanog, Sox2 and FoxD3 (Pan and Thomson, 2007).

1.3 Post-transcriptional regulation of the pluripotent state

While previous sections have focused on signalling pathways, transcriptional regulation, and epigenetic modifications, this section reports that post-transcriptional events also play an essential role in pluripotency maintenance (Shigunov and Dallagiovanna, 2015).

The RNA-binding proteins (RBPs) are a class of proteins that are essential mediators in post-transcriptional regulation and are involved in every aspect of mRNAs life (Shigunov and Dallagiovanna, 2015). RBPs allow the dynamic and rapid control of protein synthesis to adapt to cellular requirements, the control the RNA metabolism from the synthesis to the decay, from the pre-RNA splicing to mRNA localization, turnover, modifications, nuclear export, translation control and editing (Hualin *et al.*, 2014). Moreover, RBPs interact with specific cis-regulatory mRNA elements to form the ribonucleoproteins (RNPs), complexes able to regulate the RNAs expression and function (Janga and Mittal, 2011).

More than 800 RBPs encoded by the human genome have been identified, able to recognise 40 different types of domain motifs (Hualin *et al.*, 2014). RBPs have one or multiple RBP domains. The best-characterised RBP domains are: RNA Recognition Motif (RRM), K-homology domain (KH), RGG box (Arg-Gly-Gly), zing finger, double-stranded RNA-binding domain (dsRBD), PUF domain and Piwi/Argonaute/Zwille (PAZ) domain (Finn *et al.*, 2010; Oliveira *et al.*, 2017). RRM domain is the most familiar domain shared among RBPs. It is typically shaped to 90 amino acid and consists of four antiparallel β-strands, which form one β-sheet that is packed against two α-helices (Oliveira *et al.*, 2017). RBPs can be provided of one or more RRMs, that are able to bind short and longer RNAs with increased affinity and specificity (Oliveira *et al.*, 2017).

Although RBPs are ubiquitous, some of them have been reported to be active in a specific cell or tissue types, to contribute to maintaining the cell specificity (Musunuru, 2003). Nevertheless, the mechanisms with which RBPs drive the cell specificity remain poorly understood, even because of that, 39% of the RBPs have no been characterized yet (Li, Carlos and Belmonte, 2018). It is widely reported the association between the malfunction or altered expression of specific RBPs such as TDP43, FUS, MATR3, HuR/HuB/HuC/HuD etc. with several neurodegenerative diseases (Hanson, Kim and Tibbetts, 2012; Hualin *et al.*, 2014; Hashemikhabir, Neelamraju and Janga, 2015; Conlon and Manley, 2017). Indeed, neuro system cells produce a tissue-specific set of RBPs playing specific regulation, modulating differentiation and synaptic stimuli (Darnell, 2014). Consequently, mutations in this class of proteins could lead to pathogenic mechanisms of

degenerative diseases (Lemmens *et al.*, 2010; Darnell, 2014). In pluripotent stem cell, the alternative splicing plays an important role: it was found the number of isoforms belonging to some proteins is higher in stem cells than in differentiated cells, a phenomenon called "isoform specialization" (Figure 6) (Qian *et al.*, 2010; Chepelev and Chen, 2013). This highlights how PSCs require a high diversity of isoforms to maintain their identities, as the isoforms have no-redundant functions (Chepelev and Chen, 2013). Stem cell factors, such as NANOG and OCT4 genes, produce multiple isoforms. Nevertheless, these mRNAs have been undergoing various controls and regulations, as the polyadenylation (Elkon, Ugalde and Agami, 2013). The alternative polyadenylation could impact the protein output through affecting the stability, translation or localization of mRNAs (Wang, 2014).

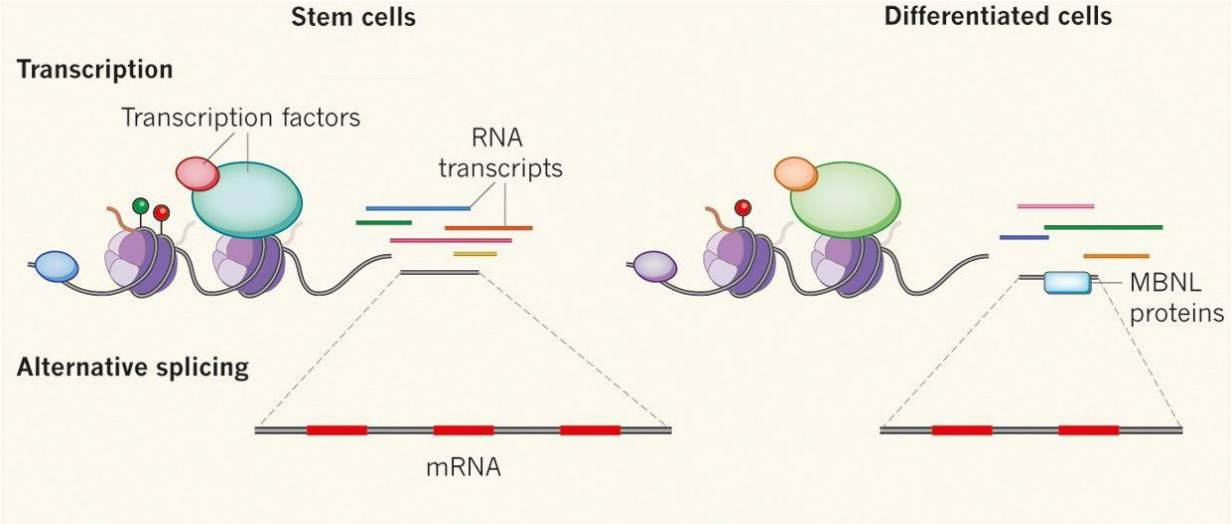

Figure 6. Schematic representation of different transcription and alternative-splicing between stem cells and differentiated cells (Aaronson and Meshorer, 2013).

The mRNA turnover is also a critical factor impacting on protein abundance (Neff *et al.*, 2012). Into the cells, the mRNA-turnover depends in part on the mRNA stability, which is determined negatively or positively by RBPs. Indeed, the latter inhibits or speed up the decay of target mRNAs or mRNAs translation. (Blackshear and Lai, 2003). The translational rate changes among all the cell types. Several studies reported that iPSCs are characterized by a low translation rate to maintain the undifferentiated state (Sampath *et al.*, 2008; Signer *et al.*, 2014; Blanco *et al.*, 2016). Furthermore, comparing PSCs and EBs, it emerges that the polysome density is higher in differentiating cells and that leads to an increase of RNA (± 50%), ribosomal RNA (± 20%) and

proteins (± 30%) (Tahmasebi, Amiri and Sonenberg, 2019). It is also reported that a low translation rate in PSCs has no impact on the proliferation and replication rate (Jackson, Hellen and Pestova, 2015; Blanco *et al.*, 2016; Tahmasebi, Amiri and Sonenberg, 2019).

An essential aspect to considerate about the regulation of the translation in PSCs and in adult cells is the N6-methyl-adenosine (m6A) methylation, which is the most prevalent on the mRNAs modification. The m^6A RNA modification is a post-transcriptionally cause by the methyltransferase complex, a class of proteins knows as writers (METTL3, METTL14 and WTAP). The methylation by METTL3 is required for maintaining the ground state of humans and regulate self-renewal and differentiation of PSCs (Batista *et al.*, 2014; Geula *et al.*, 2015; Wu *et al.*, 2019). METTL3 overexpression improves reprogramming efficiency. That means that m^6A modification may play pivotal physiological functions in regulating RNA metabolism in the pluripotency stage, leading to changes in the expression of pluripotency key factors as OCT4 (Chen, Y. Hao, *et al.*, 2015). Dysregulations of this modification have already been linked to cancer and other human diseases (Sibbritt *et al.*, 2013; Batista *et al.*, 2015). For a class of writers, there is a class of readers, proteins able to recognize the modifications, such as the m^6A methylation.

YTHDF1 is a member of YTH domain proteins, a family protein defined as readers of m^6A, and plays a crucial role in mediating the translation of m^6A-RNAs (Liao, Sun and Xu, 2018; Bai *et al.*, 2019; Wu *et al.*, 2019; Zhuang *et al.*, 2019). YTHDF1 and YTHDF3 binding to m^6A modifications enhance mRNA translation, while YTHDF2 recognizes m^6A mRNA within the GACU/A consensus to mediate degradation of m^6A transcripts (Chen, Y. Hao, *et al.*, 2015; Paris *et al.*, 2019). Moreover, YTHDF1 has a role in translation, interacting with eIF3 and facilitating translation initiation (Wang et al., 2015).

1.3.1 LIN28 plays key roles in pluripotency regulation.

LIN28 is an RBP that plays a crucial role in post-transcriptional control in PSCs. Indeed, its expression in ESCs is fundamental for the cell to maintain the pluripotency blocking the biogenesis of let-7 family of miRNA (Viswanathan, Daley and Gregory, 2013; Zhang, Ratanasirintrawoot, Chandrasekaran, Wu, *et al.*, 2016). The human LIN28 (LIN28A) and its paralog LIN28B are expressed in human cells and encode for 23 and 28kDa proteins respectively;

both expressed in ESC and tumors like neuroblastoma and silent in most of the adult tissues (Molenaar *et al.*, 2012; Mayr and Heinemann, 2013; Tsialikas and Romer-seibert, 2015). Nevertheless, LIN28 proteins are identified by their unique pairing of cold shock domain (CSD) and cysteine cysteine histidine cysteine (CCHC) zinc knuckle domain, which confers the ability to bind the RNA (Tsialikas and Romer-seibert, 2015). Lin28A and Lin28B have an extended sequence identity but differ for the nuclear localization signal and the tail region at the C-terminus which is present only in LIN28B (Piskounova *et al.*, 2008; Hyun *et al.*, 2014). Furthermore, LIN28A and LIN28B localize differently within the cells, i.e. LIN28A is predominantly in the cytoplasm, possibly shuttling to the nucleus. On the contrary, LIN28B is found predominantly in the nucleus (Balzer and Moss, 2007; Piskounova *et al.*, 2011).

The most crucial difference between LIN28A and LIN28B is the mechanism by which they inhibit let-7 miRNA. LIN28A recruits TUTase (Zcchc11/TUTase4) to block Dicer and indirectly let-7 biogenesis in the cytoplasm, while LIN28B represses let-7 by sequestering let-7 transcripts in the nucleus (Piskounova *et al.*, 2011). Furthermore, while the LIN28B role in the pluripotency is not well elucidated, the LIN28A function is better characterised. The influence of LIN28A to maintain the pluripotency emerges out of its role to facilitate the reprogramming of somatic cells to iPSCs (Yu *et al.*, 2012).

Studying conducted on mouse model reported that during the oocyte growth, there is an accumulation of RNA that plays a vital role in the embryo transition, where the maternal RNAs and proteins lead the oocyte into totipotent blastomeres (Flemr *et al.*, 2014). Moreover, Lin28 is expressed at the embryo stage and during the whole period of the organogenesis and will also be in some specific tissues in the adult stage (Yang and Moss, 2003). In PSCs, LIN28 is involved in the metabolism as a modulator of glucose metabolism mediated by let-7 dependent mTOR signalling (Zhu *et al.*, 2011). Furthermore, it was revealed Lin28 role in the regulation of the oxidative metabolism and modulation of the expression of metabolism genes is essential for the maintenance of pluripotency state (Zhang, Ratanasirintrawoot, Chandrasekaran, Li, *et al.*, 2016). Moreover, it was also reported the role of LIN28 in the modulation of translation in positive feedback for its targets (PENG *et al.*, 2011). The activation of LIN28A is turned on by mitogen-activated protein kinase (MAPK) / extracellular signal-regulated kinase (ERK) signalling. MAPK/ERK phosphorylates LIN28 protein activating to control mRNA translation (Tsanov *et al.*, 2017). It was also reported that LIN28 protein binds OCT4 mRNA (Qiu *et al.*, 2010).

1.3.2 RNA binding protein MATR3

Matrin3 (MATR3) is a highly conserved protein of 125 KDa, identified as an abundant component of the inner nuclear matrix, having the structural function to connect the nuclear membrane and the laminin proteins to intranuclear structures (Belgrader, Dey and Berezneyg, 1991; Nakayasu and Berezneyt, 1991). MATR3 is endowed of one nuclear localization signal (NLS) and one nuclear export signal (NES), two C2H2-type ZnF binding domains and two tandem RNA recognition motifs (RRM) (Figure 7) (Belgrader, Dey and Berezneyg, 1991; Hisada-Ishii *et al.*, 2007; Uemura *et al.*, 2017). The presence of multi-domains suggests the multiple functions of the protein as able to bind both DNA and RNA.

MATR3 has been recognized to be a key element of a subnuclear architecture promoting the activation of enhancers. The binding of the POU-homeodomain transcription factor Pit1 to its enhancers is mainly dependent on the presence of a MATR3 rich network. The MATR3-dependent physical organization of the chromatin allows the assembly of Pit1-β-catenin-SatB1 complex and the consequential activation of developmental gene transcriptional programs (Skowronska-Krawczyk *et al.*, 2014). Similarly, the long non-coding RNAs (lncRNA) *PINCR* recruits MATR3 and facilitates the association of p53 with the enhancers of its targets, favouring chromatin looping between the enhancers and promoters of these genes, thus supporting the DNA damage response (DDR) (Chaudhary *et al.*, 2017). Moreover, MATR3 is involved in RNA metabolism; PAR-CLIP analysis identified the consensus RNA sequences preferentially bound by MATR3, an intronic pyrimidine-rich sequence (Uemura *et al.*, 2017). MATR3 can regulate the levels of target mRNAs and lncRNAs (Salton *et al.*, 2011; Banerjee *et al.*, 2017; Iradi *et al.*, 2018) and nuclear mRNAs export (Zhang and Carmichael, 2001; Boehringer *et al.*, 2017). Furthermore, it was reported that MATR3 regulates the expression of target mRNAs directly by affecting their stability (Salton *et al.*, 2011). Moreover, MATR3 has well been characterised as a splicing factor (Coelho *et al.*, 2015; Uemura *et al.*, 2017). Indeed, MATR3 acts synergistically with Polypyrimidine tract binding (PTB) protein (a well-known splicing regulator RBP) (Kafasla *et al.*, 2012; Coelho *et al.*, 2015). It was reported that hundreds of genes with a subset of these splicing events co-regulated by interaction with PTB (Coelho *et al.*, 2015; Uemura *et al.*, 2017). Generally, MATR3 binds to an extended region within repressed exons and flanking introns and acts mainly as a splicing repressor (Coelho *et al.*, 2015).

As above reported, MATR3 is a nuclear protein, and its cytoplasmatic localization has been observed in rare cases, usually associated with neuron disease such as Amyotrophic Lateral Sclerosis (ALS). Indeed, MATR3 has also been found in neuronal cytoplasmic inclusions (NCIs) alone or associated with TDP-43 (Tada *et al.*, 2018), C9orf72 hexanucleotide repeat expansion Di-Peptide Repeats (DPRs) (Johnson *et al.*, 2014) or ectopic ALS-linked FUS mutant (Yamaguchi and Takanashi, 2016) in ALS-patient's cells.

Furthermore, MATR3 was showed to be a key element for Neural Stem Cells (NSCs) differentiation, and its role is regulated by ATM-mediated phosphorylation (Niimori-kita *et al.*, 2018). However, whether MATR3 has a role in pluripotency maintenance and cell fate commitment has not been unravelled yet.

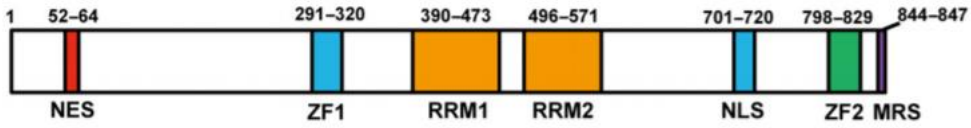

Figure 7. Schematic diagram of MATR3 structures protein (Uemura *et al.*, 2017).

1.4 Amyotrophic Lateral Sclerosis

Amyothrofical Lateral Sclerosis (ALS) is a neurodegenerative disorder that was characterized for the first time in 1869 by a neurologist named Jean-Martin Charcot (Rowland and Shneider, 2001; Zarei *et al.*, 2015). It is being characterized by the progressive paralysis that can lead to respiratory failure and death, within three to five years from the diagnosis, due to the degeneration of both upper and lower Motor Neurons (MNs) (Rowland and Shneider, 2001; Mateen, Carone and Sorenson, 2010; Chio *et al.*, 2012; Ajroud-driss and Siddique, 2015; Zarei *et al.*, 2015; Hardiman *et al.*, 2017; Oskarsson, Gendron and Staff, 2018). MNs have a crucial role in vertebrates because they are neuronal cells located in the central nervous system, which bridge the brain to the muscle (Stifani, 2014; Barkan and Zornik, 2019). Indeed, early ALS symptoms are the spinal-onset disease (the beginning of muscle weakness of the limbs), or the bulbar-onset disease (characterized by a difficulty to speech) and dysphagia (characterized by a difficulty to

swallowing) (Rowland and Shneider, 2001; Zarei *et al.*, 2015; Hardiman *et al.*, 2017; Oskarsson, Gendron and Staff, 2018).

The only 5-10% of the cases are genetic dominant inheritance factors that are named familial ALS (fALS), a group where is possible to understand the genetic history of the disease (Greenway *et al.*, 2006; Abhinav *et al.*, 2007), while the remaining 90-95% of the cases are defined sporadic ALS (sALS), where the mutation(s) may occur *ex novo* (Ferrara *et al.*, 2018). The division into the two groups was made for the first time in 1955 (Kurland and Mulder, 1955). In 1993 the first mutation associated with the ALS was found in the superoxide dismutase 1 (SOD1) gene. 20% of fALS cases harbour this mutation (Siddique *et al.*, 1991; Rosen *et al.*, 1993). To date, we know that more than thirty genes are associated with ALS. Those "hit" genes encode for proteins involved in the RNA metabolism, such as MATR3, FUS, C9ORF72, HNRNPA1, TARDBP, AGN (Greenway *et al.*, 2006; Sreedharan *et al.*, 2008; Kwiatkowski *et al.*, 2009; DeJesus-Hernandez *et al.*, 2011; Renton *et al.*, 2011; Kim *et al.*, 2013; Johnson *et al.*, 2014); or proteins involved in proteostasis and protein quality control such as SOD1, VPC, OPTN, UBQLN2, SQSTM1 and TBK1 (Rosen *et al.*, 1993; Johnson *et al.*, 2010; Maruyama *et al.*, 2010; Deng *et al.*, 2011; Fecto *et al.*, 2011; Freischmidt *et al.*, 2015).

Interestingly, many of the above mutations (mutations in genes such us TARDBP, VCP, TBL1 and C9orf72 repeat expansions (Nguyen, Van Broeckhoven and van der Zee, 2018)) could lead to frontotemporal dementia (FTD) as well. FTD is a heterogeneous neurodegenerative disorder with distinct clinical signs as changes in behaviour, language, executive control and motor symptoms (Olney, Spina and Miller, 2017; Ferrara *et al.*, 2018; Nguyen, Van Broeckhoven and van der Zee, 2018).

1.4.1 MATR3 in ALS

In 2009 a study associated with the first time a MATR3 mutation with the ALS disease (Senderek *et al.*, 2009). They found a heterozygous 254C-G transversion in exon 2 of the MATR3 gene, resulting in a ser85-to-cys (S85C) substitution (Senderek *et al.*, 2009). S85C mutation was also associated with vocal cord and pharyngeal weakness with distal myopathy (VCPDM), a progressive autosomal dominant distal myopathy that also results in dysphagia, dysphonia and vocal cord and pharyngeal weakness (Johnson *et al.*, 2014; Boehringer *et al.*, 2017).

In 2014 it was found that the S85C-MATR3 interacted with TARDBP protein more than the wild-type protein as its steady-state expression was lower respect the wild type, suggesting a structural effect of the mutation (Johnson *et al.*, 2014).

Over the last few years, several MATR3 mutations were associated with ALS. Interestingly, most of those are enclosed in two predominant amino acids clusters, i.e. amino acids 66-154 and amino acids 610-787 (Figure 8) (Boehringer *et al.*, 2017). However, the mechanisms that induce the disease are still unknown (Johnson *et al.*, 2014; K.-P. Lin *et al.*, 2015; Boehringer *et al.*, 2017; Marangi, Lattante, Niccolò, *et al.*, 2017).

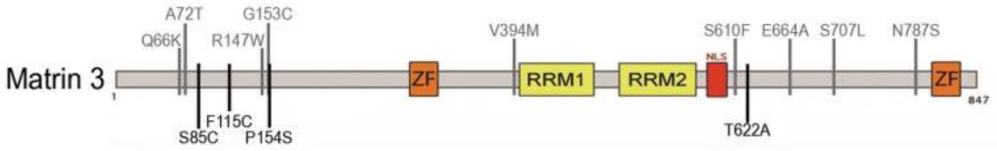

Figure 8. Mutations in the MATR3 sequence identified so far (Boehringer *et al.*, 2017).

Thus, MATR3 may exert an essential role in motor neuron function and survival, with a critical role in RNA metabolism (Johnson *et al.*, 2014; K. Lin *et al.*, 2015; Origone *et al.*, 2015; Leblond *et al.*, 2016; Marangi, Lattante, Doronzio, *et al.*, 2017). Indeed, more than 30 genes (such as TDP43, FUS, hnRNPA1, hnRNPA2B1 and MATR3) which are associated with ALS (Guerreiro, Brás and Hardy, 2015) have in common their involvement in RNA processing metabolism (Boehringer *et al.*, 2017).

As described previously, MATR3 is an RBP with multiple roles in RNA metabolism, such as splicing, stability and as we reported in this work in translation (Salton *et al.*, 2011; Coelho *et al.*, 2015). Interestingly, although the most of studies showed MATR3 is mainly a nuclear protein (Hisada-

Ishii *et al.*, 2007; Salton *et al.*, 2011; Skowronska-Krawczyk *et al.*, 2014), in some cases, MATR3 has also been found in neuronal cytoplasmic inclusions (NCIs) alone or associated with TDP-43, C9orf72 hexanucleotide repeat expansion Di-Peptide Repeats (DPRs) (Johnson *et al.*, 2014) or ectopic ALS-linked FUS mutant (Yamaguchi and Takanashi, 2016a).

The oxidative stress is considered one of the most contributory factors to ALS pathology (Pollari *et al.*, 2014; Xiao *et al.*, 2018). Indeed, it was reported how in ALS mouse models, the nerve terminals are sensitive to the oxygen species (ROS), with a massive impact on mitochondria functions. ROS's high production leads to an increased DNA damage response (Singh *et al.*, 2019). As MATR3 is also known to be involved in DNA damage response, this opens an exciting scenario to investigate the pathological mechanisms better and develop strategies to treat the MNs, and consequently propose possible therapeutic approaches (Pollari *et al.*, 2014).

1.4.2 MATR3 roles in DNA damage

The homeostasis, stability, and integrity of the cell and genome are essential in the cell life, and, as knows, cells have developed mechanisms to keep to guarantee the physiological balance and to respond to the stress stimuli. In PSCs, the balance between self-renewal and differentiation states could be critical for tissue homeostasis, and ROS partially regulates it (Figure 9) (Mohyeldin, N-Muvdi and Quin˜ones-Hinojosa, 2010; Bigarella, Liang and Ghaffari, 2014a; Cie *et al.*, 2017). The redox state is essential for maintaining the function of stem cells and for their fate (Lee *et al.*, 2018).

Neurons are particularly exposed to the DNA damage, in opposite to the PSCs, they are in a post-mitotic state, but with a critical metabolic rate and are susceptible to oxidative stress (Pan, Penney and Tsai, 2014). In neural development, DNA repair is fundamental because an unrepaired lesion at this stage could lead to dramatic consequences on the functional nervous system (McKinnon, 2009, 2013). Furthermore, the DNA damage increases with the cell senescence and numerous DNA lesions have been reported in neurons of fALS patients (Madabhushi, Pan and Tsai, 2014).

The two most common DNA damage reported are single-strand breaks (SSB) or double-strand break (DSB) (Pilié *et al.*, 2019). The repair pathways activated are dependent on the specific type of damage detected and repair machinery available. SSB is repaired from SSB repair or BEAR

repair mechanisms, while, the DSB is repaired by the Homologous Recombination (HR) or the Non-Homologous Endjoining (NHEJ) mechanisms (Chapman, Taylor and Boulton, 2012).

HR need an undamaged DNA template, extensive sequence homology between the broken DNA and donor DNA molecules, to repair the DSB (Mao *et al.*, 2008; Scully *et al.*, 2019). By contrast, the NHEJ is a high-capacity pathway that joins two DNA ends with minimal reference to DNA sequence and no regard for homology, generating deletions or insertions, with the possibility to accommodate limited base-pairing between the two processed DNA ends (Scully *et al.*, 2019). The Ku70/ku80 heterodimer bounds both end breaks at the beginning of the repair mechanism, which then recruits the DNA dependent protein kinase (PKcs). If necessary, the ends can be cut by nucleases or can be filled by DNA polymerases to create new compatible ends, and finally, the ligation complex (DNA ligase IV, XRCC4 and XLF) ligates the ends (Brandsma and van Gent, 2012). Moreover, it was reported that a heterodimer form by NONO-SFPQ is requested to stimulate DNA ligase IV-XRCC4, although this stimulation mechanism is not clear (Jaafar *et al.*, 2017).

In this scenario, it was not difficult to connect the roles of DNA repair to neurodegenerative diseases such as the ALS.

MATR3 was found to be a phosphorylation target of ATM during DDR and was reported to interact with SFPQ/NONO heterodimer, which interacts with the NHEJ machinery (Salton *et al.*, 2010; Nishida *et al.*, 2017). This opens the interesting scenario of studying MATR3 in DNA damage response in MNs and how its mutations/malfunctioning could lead to neurodegenerative disease.

ALS-related proteins like FUS and TDP43 have also been linked to DNA damage repair (Hill *et al.*, 2016; Gong *et al.*, 2017; Naumann *et al.*, 2018); and it is widely demonstrated that these proteins interact with MATR3 (Johnson *et al.*, 2014; Yamaguchi and Takanashi, 2016b). This thesis is also supported by the latest studies which give more cruciality to DNA repair mechanisms in neurodegeneration and underline the presence of markers of DNA damage in neurodegenerative neuronal samples and peripheral tissues of patients (McKinnon, 2009; Coppedè and Migliore, 2015; Penndorf, Witte and Kretz, 2018).

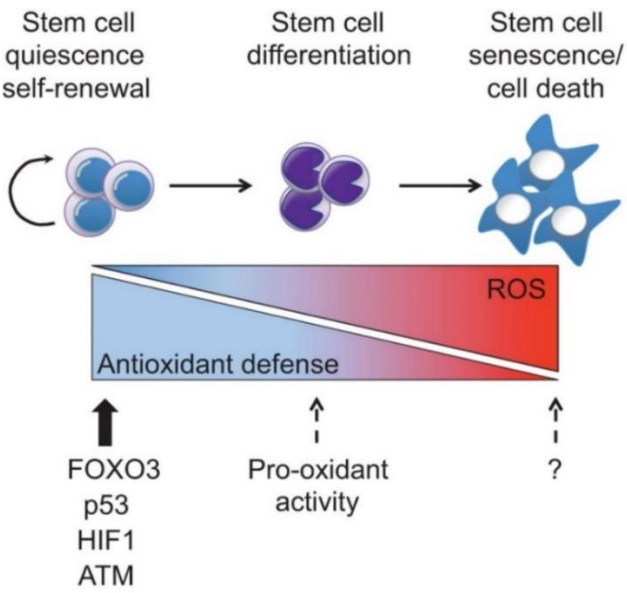

Figure 9. ROS effects on the stem cells. (Bigarella, Liang and Ghaffari, 2014b).

1.4.3 ALS in a dish

One of the most crucial challenges to study the ALS is to understand the mechanisms that lead to the MNs degeneration deeply, and this needs an accessible and powerful model able to explain the pathogenic causes of this disorder. To date, it is possible to rely on different models of study, such as cell cultures, animal models or, when possible, human post-mortem brains, especially useful for the investigation on the lethal pathological mechanisms (Damme, Robberecht and Bosch, 2017; Mohamed *et al.*, 2019). Over time, the combination of animal and cell models contributed tremendously to partially elucidate the causes and molecular mechanisms altered in neurodegenerative disorders (Mohamed *et al.*, 2019).

The main advantage of using mouse models is the possibility of getting genetically modified mice, which recapitulate the pathological conditions. Mainly, they give the possibility to investigate the neuroinflammatory response, which has been demonstrated to be an essential and critical aspect in neurodegeneration pathologies, including ALS. Furthermore, mouse models have helped to study the environment surrounding the MNs, e.i. it was possible to study the vascular system as it was reported the reduced expression of the vascular endothelial growth factor (VEGF) in ALS (Gurney *et al.*, 1994; Oosthuyse *et al.*, 2001; Chattopadhyay and Valentine, 2009; Philips and Robberecht, 2011; Damme, Robberecht and Bosch, 2017).

However, mouse models showed different limitations, i.e., many transgenic mouse models did not capture the entire spectrum of the human disease pathology (Shi *et al.*, 2017). Moreover, the animal model leads to a high clinical failure rate in drug development, inasmuch as it is inadequate compared to the human neurological system (Logan *et al.*, 2019). On this basis, it is clear that available experimental models have limited predictive ability for identifying novel therapies.

The introduction of the hiPSCs in medical research has opened a new perspective to study the diseases in "a dish". Due to their ability to differentiate into many lineages and preserve the patients' genetic information, this technology allows increasing our knowledge because of the possibility to recapitulate the pathological features seen in patients, including neurodegenerative diseases (Kim, 2015). hiPCSs made are also particularly advantageous for drug development and biomarker discovery. Indeed, it was reported that iPSC-derived neurons could better represent the biomarker changes happening in real patients (Liu *et al.*, 2014; Guyett, Hendrickson and Laha, 2018; Li, Chao and Shi, 2018). During these last years, an increasing number of iPSC lines have been generated, including iPSC derived from ALS patients, with a growing interest for both cell development and setting new therapeutic strategies and for studying the effects of genomic defects on cellular functions (Matus, Medinas and Hetz, 2014; Damme, Robberecht and Bosch, 2017; Fujimori *et al.*, 2018; Pollini *et al.*, 2018; Logan *et al.*, 2019). Indeed, iPSCs allow elucidating different aspects in ALS disease, such as the aggregation and/or cytoplasmic mislocalization of TDP-43, SOD1, FUS, MATR3 and in the case of C9orf72 repeat expansions. The formation of RNA foci and dipeptide repeat proteins, neurofilaments disorganization, defects in nucleocytoplasmic transport and much more (Chen, Qian, Du, Cao, Petersen, Liu, Blackbourn IV, *et al.*, 2014; Matus, Medinas and Hetz, 2014; Zhang *et al.*, 2015; Damme, Robberecht and Bosch, 2017).

Due to their potential to differentiate into any cell or tissue and the quick technologies advancements of the past decade, the development of organoid systems has been possible. This 3D *in vitro* culture systems contain a sub-population of self-renewing stem cells which is able to differentiate into multiple and organ-specific cell types. Those cellular sets exhibit spatial organization similar to the corresponding organ and are capable of recapitulating some functions of that organ providing an exceptional model (Lancaster *et al.*, 2013; Qian, Song and Ming, 2019). In particular cerebral organoids are able to exhibit a variety of cell lineage identities that form different parts of the brain such as the forebrain, midbrain and hindbrain have been set up (Lancaster *et al.*, 2013; Lancaster and Knoblich, 2014). Organoids can recapitulate the human

brain not only for the cellular morphology and cytoarchitecture but also for functions, which are inaccessible to direct experimentation (Di Lullo and Kriegstein, 2017; Qian, Song and Ming, 2019). One of the most significant advantages of using organoids lies in the possibility to overcome mouse models, that showed essential differences with humans. Not only the final structure of the brain is radically different, smooth neocortex in mouse and the highly convoluted in the human neocortex, and also the formation and the maturation of the neurons. Indeed, the division patterns of human and mouse neural stem cells exhibit significant differences. For example, most of the radial glia cells and primary neural stem cells are located in the ventricular zone in the developing mouse neocortex, while an abundant population of outer radial glia cells is in the subventricular zone and contribute to the evolutionary expansion of the human neocortex (Lui, Hansen and Kriegstein, 2011; Koo *et al.*, 2019).

The greatest strength of the brain organoids is their ability to form a structural “mini” brain, able to mimic endogenous pattering and drive effective dorsal and ventral forebrain differentiation. Where is possible to diversify the ventricular-like zone (VZ), that contains neural stem cells, over time, that is able to produce a cortical-like structure, which contains cells expressing markers of deep- and superficial-layer neurons such as the Reelin-positive Cajal-Retzius cells (Figure 10).

Nevertheless, it is hard to establish the exact neurodevelopmental age correspondence between organoid and *in vivo* human brain, while the organoid age of two months seems comparable with the fetus formation in the first trimester (Lancaster *et al.*, 2013).

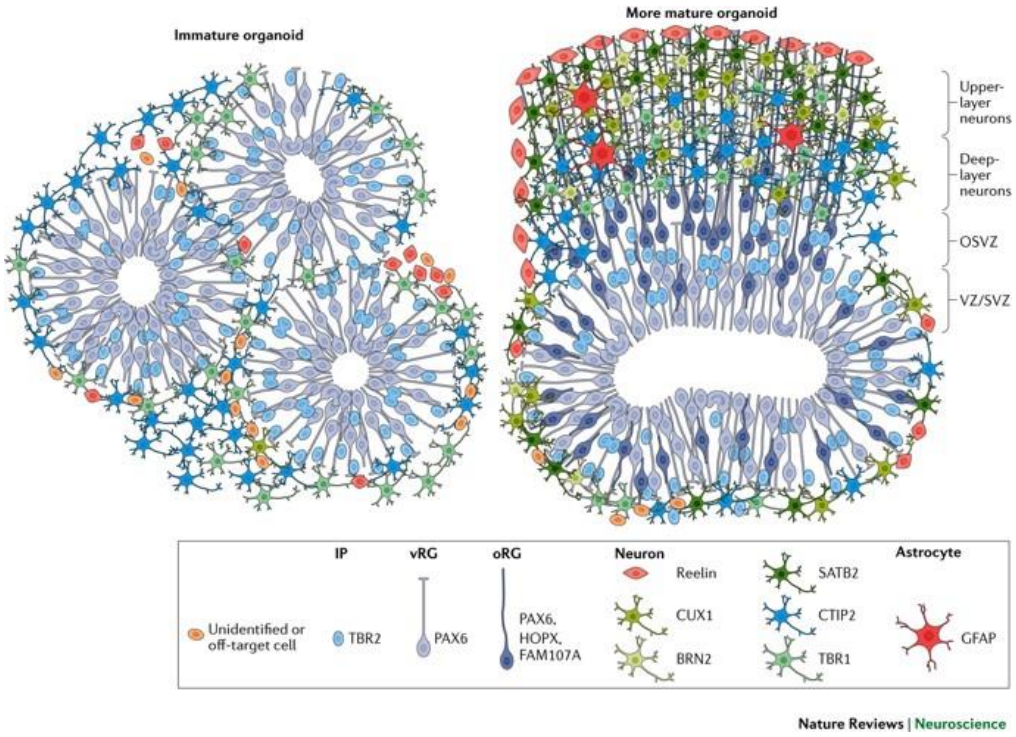

Figure 10. Representation of brain organoids at two different time points. On the left, an immature organoid whose structure is composed by neuroepithelial stem cells and ventricular radial glial cells (vRGs), that form the ventricular zone (VZ), and intermediate progenitors (IPs). There are cells expressing markers of early cortical plate neurons such as COUP-TF-interacting protein2 (CTIP2) and T-box brain protein 1 (TBR1). On the right, the mature organoid exhibits multilaminar organization with a well-delimitate structure, characterized by multiple progenitor areas, a VZ and a subventricular-like zone (SVZ), outer radial glial cells (oRGs) and glia and cortical layer markers positive cells (Di Lullo and Kriegstein, 2017).

Midbrain organoids have been extraordinarily useful for studying AD and PK diseases, because of their ability even to recapitulate extracellular amyloid aggregation and accumulation of hyperphosphorylated tau proteins (Choi *et al.*, 2014; Winanto *et al.*, 2019; Grenier, Kao and Diamandis, 2020). However, an organoid model to study ALS disease is still lacking. Indeed, as a part of the CNS, the spinal cord is a highly complex system to reproduce along with all its functions as for the different subclasses of MNs present. As a matter of fact, the same issue comes across, even using the 2D models. The iPSCs-derived MNs (obtained from retinoic acid-induced casualization and consecutive Sonic Hedgehog-induced ventralization) mostly include the hindbrain or cervical subtypes and do not represent all populations of MNs present in the spinal cord (Winanto *et al.*, 2019).

Nevertheless, few works reported the possibility of obtaining a suitable 3D system to study the ALS disease. One group generated a nerve organoid composed of a robust fascicle of axons that spontaneously assemble into a fascicle extended from a spheroid (Kawada *et al.*, 2017). Another group reported the achieving of a spinal cord organoid setting up using a modified version of the well-known Lancaster' protocol (Lancaster *et al.*, 2013; Hor *et al.*, 2018). Finally, the experimental procedures to create the ventral spinal cord organoids, featuring the presences of different spinal cell types, were also published (Hor *et al.*, 2018). Altogether, these studies demonstrate how spinal cord organoids could be generated, though the setting of this kind of organoids need to be improved, as the aim of their usage is to study the interaction between the nervous system and other non-neuronal systems that impact neuronal function (Chukwurah *et al.*, 2019).

It behoves to report a different strategy adopted to bypass the vascular system's absence in the brain organoids. It consists of organoid transplantation in the mouse brain, where the mouse endothelial cells form an active vascular system in the human brain organoid transplanted (Daviaud, Friedel and Zou, 2018; Mansour *et al.*, 2018; Pham *et al.*, 2019). Furthermore, one of the essential benefits, to use the brain organoids resides in the possibility to work with a model that can support preclinical drug studies and improve the high clinical failure rate in drug development, as well as suitable to model neurodevelopmental disorders with actual pathogeny (Koo *et al.*, 2019; Logan *et al.*, 2019). This highlights once again the power of this model and the high expectative that we have on it.

Nevertheless, the brain organoids present different limitations, such as the absence of a structured spatial organization, the immune system, and reasonable tissue size present in animal models (Grebenyuk and Ranga, 2019). Moreover, the absence of a vascular system hampers to support its correct growth, with consequent deficiency of oxygen and nutrients perceived mostly in the core of the organoids with a high level of apoptosis and consequently, the lost of large-scale and more reproducible tissue organization (Grebenyuk and Ranga, 2019; Koo *et al.*, 2019). To date, different pioneering works have been generated *in vitro* vasculature in the organoid system, intending to improve the model, so in the next future, human brain organoids could be easily combined with a vascular system able to support a long-term culture and can open a way to study neurovascular interactions (Cakir *et al.*, 2019; Grebenyuk and Ranga, 2019; Homan *et al.*, 2019; Koo *et al.*, 2019; Pham *et al.*, 2019).

2 PROJECT AIMS

ALS is a neurodegenerative disease that affects the motor neurons. Recently, it was reported that MATR3 mutations are associated with the onset of familial ALS. Nevertheless, so far, it has not been possible to explain the mechanistic connection between MATR3 mutations and this neurodegenerative disease.

Based on this, we decided to investigate the MATR3 roles intensely during cellular differentiation.

We used hiPSCs as the cellular model in order to understand whether MATR3 is important for undifferentiated cells to correctly commit and differentiate towards mature cells such as MNs by downregulating the endogenous gene via short hairpin RNA. We aimed at deciphering the role of MATR3 in pluripotency maintenance by dissecting its functions in gene expression regulation at different levels.

Finally, we aimed to understand how MATR3's mutations could lead to the onset of ALS disease. We reprogrammed ALS patient's fibroblasts to understand the impact of Q66K MATR3 mutation, in pluripotency maintenance, and in neuron commitment (2D and 3D models). We aimed to compare the effect of the mutation with the downregulation of the gene to clarify the extent to which the two defects share similar effects.

3 RESULTS

CONTRIBUTIONS

In this thesis, some results discussed by the Ph.D. candidate were performed in collaborations with other researchers.

Conceptualization: Alessandro Provenzani, Luciano Conti, Daniele Pollini;

Methodology: Daniele Pollini, Rosa Loffredo, Marina Cardano;

Investigation: Daniele Pollini (principal authors of the experiments), Rosa Loffredo (contribution for the differentiation in MNs), Annalisa Rossi (collaboration for the polysome assay), Mariachiara Micaelli (contribution for the RIP assay), Daniele Peroni (Mass Spectrometry);

Bioinformatics analysis and data curations: Erik Dassi, Daniele Pollini;

Supervision and Project Administration: Alessandro Provenzani.

Moreover, *to highlights experiments that were performed in collaborations with other researchers, under the figures have reported their contributions*.

3.1 MATR3 is essential for single cell growth of hiPSCs

We generated human iPSCs stably silenced for MATR3 to assess its role in stemness maintenance and differentiation. Human episomal iPSCs line A18945 was infected with lentiviral particles loaded with shRNA sequence targeting human *MATR3* (shMATR3), and stably silenced cells were selected. In the expanded polyclonal shMATR3-iPSC population, MATR3 protein levels were reduced to 60%, if compared to control transduced cells (shCtrl) (Figures 11.1 A and B). Both shCtrl and shMATR3 cells showed the same morphological features (Figure 11.1 C): dense cells, scant cytoplasm, large nucleoli, high nucleus/cytoplasm ratio and round and compact colonies (Wakui, 2017). Moreover, neither proliferation and viability differences (Figures 11.1 D and E) were observed between shCtrl and shMATR3 cells. Furthermore, Immunofluorescence (IF) analysis showed a not deleterious expression change of few self-renewal markers in both cell lines (Figure 11.1 F).

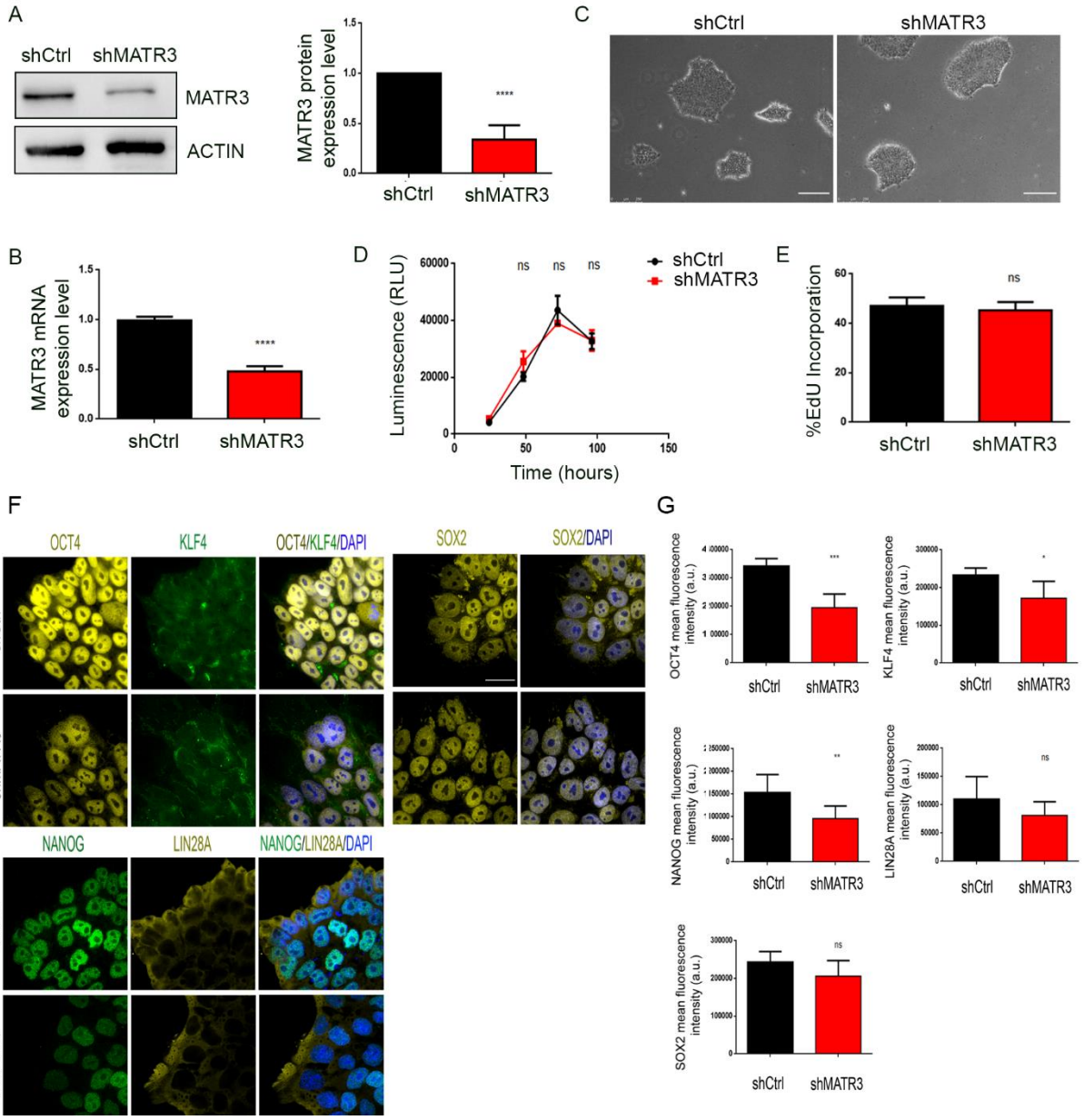

Figure 11.1 MATR3 is essential for single cell growth of hiPSCs

(A) MATR3 protein expression levels were analysed by Western Blot (WB) in hiPSCs stably infected with shMATR3 and shCtrl lentiparticles. β-ACTIN was used as housekeeping. MATR3 levels were quantified by densitometry analysis. The bar plots show the mean values of three independent experiments (right panel). The bar represents ± S.E.M. **(B)** *MATR3* RNA expression levels were measured by RT-qPCR in hiPSC line stably infected with shMATR3 and shCtrl lentiparticles. Statistical analysis performed using GraphPad Prism, *t*-test analysis (**** *P*<0.0001). (**C**) Images of shCtrl and shMATR3 hiPSCs (Scale bar 250 µm). **(D)** Growth curve of shCtrl and shMATR3 hiPSCs by OZBlue method. Data are presented as the mean ± S.E.M. of three biological replicates. Two-way ANOVA (*ns*, not significant). **(E)** EdU proliferation assay for shMATR3 and shCtrl hiPSCs. The percentage of EdU incorporating cells was measured by flow cytometry. Data present as means ± S.E.M (n=2); *t-test* (*ns*, not significant). **(F)** Immunofluorescence staining for pluripotency markers OCT4, KLF4, NANOG, LIN28A and SOX2. Cell nuclei were stained with DAPI in blue (Scale bar: 25µm). **(G)** The quantification of immunofluorescence intensity was performed using the

ImageJ mean fluorescence intensity measurement. Data are reported as mean ± S.E.M. for nine replicates from 2 different biological replicates, *P-value* was calculated using *t-test* (*ns*, not significant; * *P*<0.05; ** *P*<0.01; *** *P*<0.001).

We then investigated the effect of sub-optimal culturing conditions on shMATR3 cells, after single cells plating (Chen, Qian, Du, Cao, Petersen, Liu, Iv, *et al.*, 2014). We evaluated cell growth and morphology of shMATR3 cells after having seeded them as single cells or small colonies. Alkaline Phosphatase (AP) test revealed that shMATR3 cells have a significant deficit to grow measured in terms of number and area of the single cells and colonies in comparison to shCtrl cells (Figures 11G and 11H). This suggests that the downregulation of MATR3 does not impact on cell growth in standard culturing conditions but determines a deleterious effect after single-cell plating.

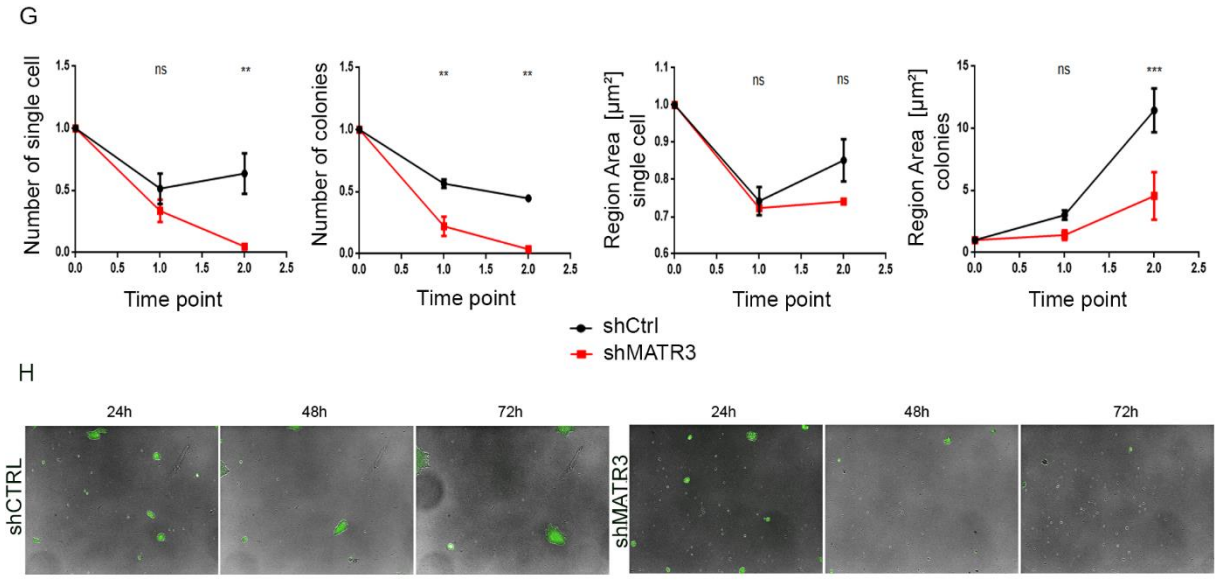

Figure 11.2 MATR3 is essential for single cell growth of hiPSCs

(G) Analyses of shMATR3 and shCtrl hiPSCs following single-cell seeding. Cells were incubated with AP Live Stain at each time point (time point, 24h, 48h and 72h respectively 0, 1 and 2 in the graph). Images were acquired with the Operetta High Content Screening System using 2X objective 0.08NA. The region Areas [µm^2] for the single cells and for the colonies are reported for each time point. One-way ANOVA (** *P*<0.01; *** *P*<0.001). **(H)** Alkaline Phosphatase (AP) assay performed on shCtrl and shMATR3 cell line single cell. The images were acquired with the Operetta High Content Screening System using 2X objective 0.08NA. Representative images are reported for each time point.

3.2 MATR3 allows the ability of proper iPSCs differentiation

Considering that MATR3 silencing negatively impacts on iPSCs growth in sub-optimal culturing conditions, we further explored its effect during trilineage commitment using the embryoid bodies (EBs) assay (Lin *et al.*, 2014) (Figures 12.1 A). Monitoring the principal phenotypical EBs features during the first week, we observed some differences between shMATR3 and shCtrl cultures (Figure 12.1 A). MATR3 silencing was associated with a significant reduction in the number of the spheres (± 50%) (Figure 12.1 B), and an alteration in shape, evaluated as Elongation Distortion Index (EDI), which is a derivative of Circularity (EDI = 1/Circularity - 1) (Figure 12.1 C) (Warkus *et al.*, 2016). After EBs plating in monolayer cultures for an additional week, shMATR3 (and shCtrl) EBs spontaneously differentiated in culture, towards cell types representatives of all the three germ layers, as confirmed by immunofluorescence analyses (Figure 12.1 D). MATR3 silencing determined, after 14 days of cultivation, an up-regulation of both mRNA and protein expression of neuroectodermal (TUBB3 and NESTIN), in agreement with previous data (Niimori-kita *et al.*, 2018) and endodermal (GATA4) markers (Vallier *et al.*, 2009), but not of mesodermal marker (αSMA) (Figure 12.1 E).

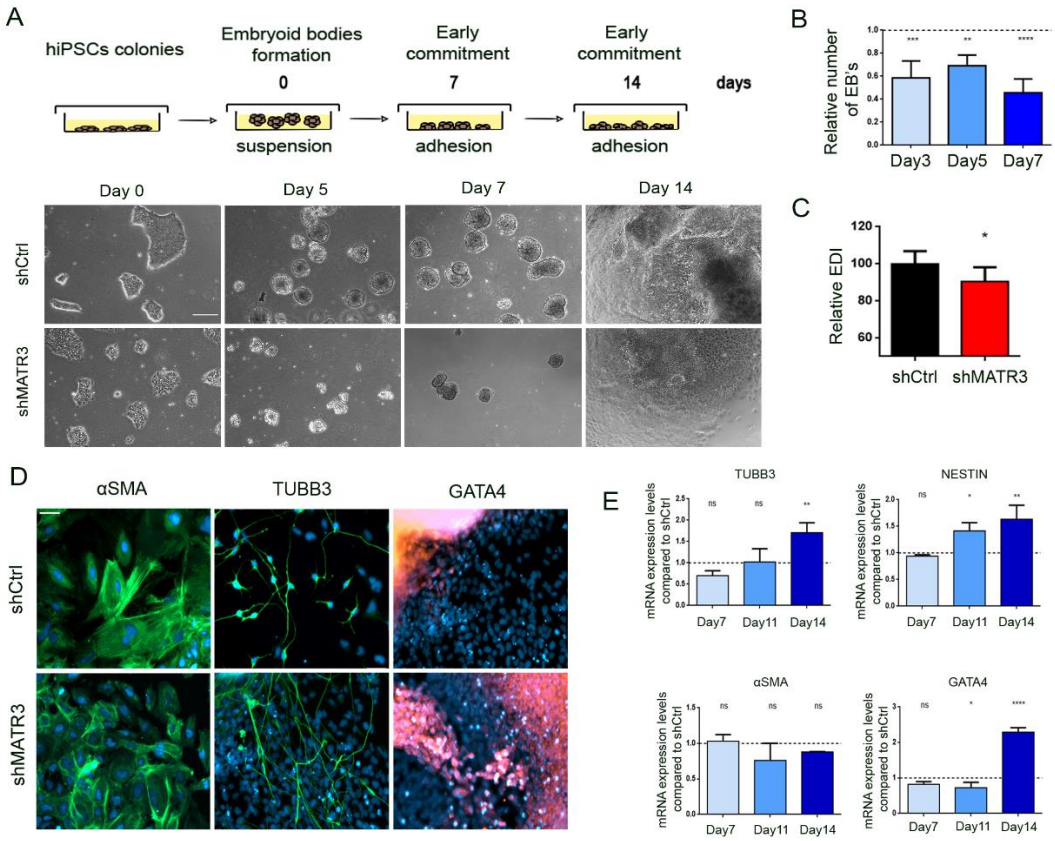

Figure 12.1 MATR3 allows the ability of proper iPSCs differentiation

(A) Schematic diagram of the protocol used to obtain and cultivate EBs. hiPSCs were dissociated and transferred to suspension cultures for seven days and then pated on Geltrex-coated culture plate for other 7 days in order to obtain spontaneous differentiation (upper panel). Time course of shCtrl and shMATR3 EBs cultures. Images detected by optical microscope (scale bar 250 µm)(bottom panel) **(B)** EBs count analysis performed with Harmony 4.1 software (Perkin Elmer) on images acquired with the Operetta High Content Screening System using 2X 0,08NA objective. Data are presented as the mean ± S.E.M. P-value was calculated using One-way ANOVA (** P<0.01; *** P<0.001; **** P<0.0001). **(C)** Analysis of the EDI, a derivative of Circularity (EDI = 1/Circularity - 1). Data are presented as the mean ± S.E.M. P-value was calculated using t-test (* P<0.05). **(D)** Immunofluorescence staining of specific markers for the three germ layers on 14 days-EBs. EBs were stained for Alpha-smooth muscle actin (α-SMA) (mesoderm), TUBB3 (ectoderm) and GATA-4 (endoderm) markers. Cell nuclei were stained with DAPI in blue. Scale bar indicated 50µm. **(E)** NESTIN and TUBB3 (Ectoderm), α-SMA (Mesoderm) and GATA-4 (Endoderm) mRNA levels were analysed by RT-qPCR in 14 days differentiating-EBs. β-ACTIN used as housekeeping and values normalized on the shCtrl reported at value 1 in the graph. Data are presented as the mean ± S.E.M. P-value was calculated by One-way ANOVA (* P<0.05; ** P<0.01; **** P<0.0001).

In order to better elucidate the MATR3 role during *in vitro* neuralization, we generated Neural Precursor Cells (NPCs) from shMATR3 (and shCtrl) iPSCs. After 12 days of neural induction (Jha, Rao and Malik, 2015) NPCs quality was assessed by FABP7 expression verification (Yun *et al.*, 2012; Leong *et al.*, 2013) (Figure 12.2 F). NPCs created radially organized structures called "neural rosette", in which Nestin-positive NPCs are distributed around a central lumen, expressing the tight junction protein ZO-1, while differentiated neurons are at the periphery (Curchoe, Russo and Terskikh, 2012) (Figure 12.2 G). Appropriate rosette's cytoarchitecture, morphology and size depend on a fine balance between self-renewal and differentiation which defines the further correct neuronal differentiation/maturation capability (Temple, 2001; Zhang, Schöler and Greber, 2013; Ziv *et al.*, 2015). Being the early-rosette-forming state crucial for neural commitment, we evaluated whether the silencing of MATR3 impacted on rosette cytoarchitecture. Zo-1 $^{+}$ rosettes, as shown by representative images in Figure 12G, have been generated from shMATR3 and shCtrl NPCs and the quantification of their relative number and size is reported in Figure 12.2 H. We observed that shMATR3 NPCs formed about the double of the number of ZO-1^{+}-rosette. Indeed, the number of rosettes in shMATR3 cultures we identified were approximately 8 for every 1000 cells or 10^{10} cell area in compared to 4 rosettes found in control (Temple, 2001). Moreover, concomitant to the increase in rosette number their size resulted altered as well. MATR3-silenced cultures have a 2-fold increase in the percentage of

rosette characterized by a small lumen (area lower then 101µm^2) and a decrement of medium (area between 101 and 350 µm^2) and large (area bigger than 350 µm^2) rosette of approximately 1.5- and 3-fold respectively (Figure 12.2 H). Collectively, our data suggest that the critical role of MATR3 during the early neuronal differentiation could be associated with dramatic consequences in terminal maturation as observed, indeed, in mature neurons formation. shMATR3 mature motor neurons are characterized by a reduction of neurites length and arborization that confirm how the levels of MATR3 impact on differentiation potential and terminal maturation of neurons (Figure 12.2 I).

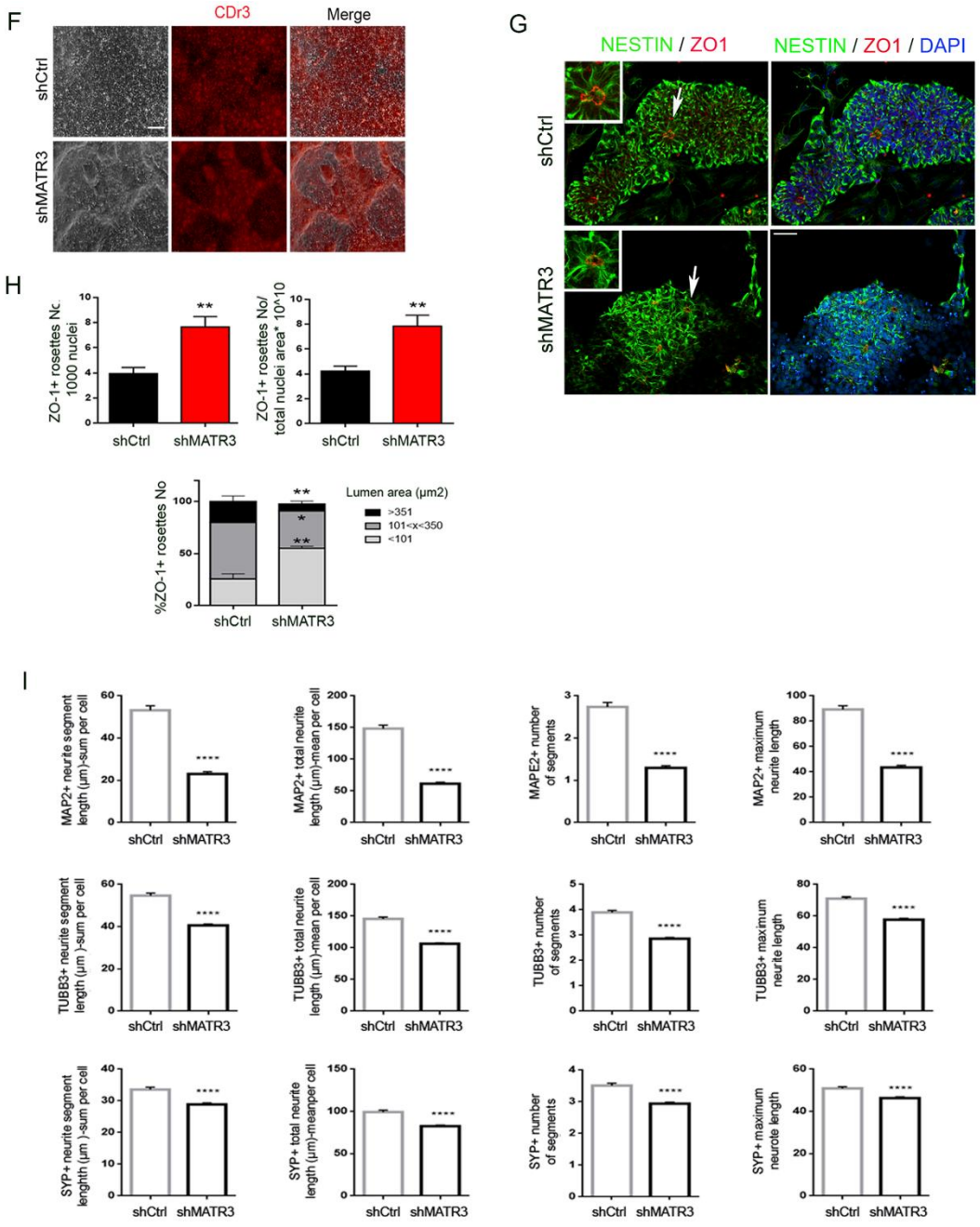

Figure 12.1 MATR3 allows the ability of proper iPSCs differentiation

(F) Differentiation into NPCs was confirmed by staining for FABP7 expression (red). Scale bar 250 µm. **(G)** Characterization of NSCs rosette's structure derived from hiPSCs. NPCs stained for Nestin and ZO-1. Scale bar 10µm. **(H)** Above panel, quantification of ZO-1+ rosettes number (on 1000 nuclei or on total nuclei area (*1010)). Below the panel, the percentage of the number of ZO-1+ rosettes having lumen area > 351, 101 < or < 100 μm^2. Quantification was obtained using Columbus software. Statistical analysis was presented as mean ± S.E.M. of three biological replicates. P-value was calculated by t-test (* P<0.05; ** P<0.01). **(I)** Parameters of neurite morphology of shMATR3 and shCTRL MNs at day 53 of terminal differentiation. The sum per cell or the mean per cell of neurite segments (µm), the number of cell neurites and the maximum neurite length (µm) of neuronal cells labelled with MAP2 (row1), TUBB3 (row2) and SYP (row3) were measured with Columbus software. Single-cell immunofluorescence analyses obtain data (**** *P*<0.0001). *Rosa Loffredo has performed neural and neuron differentiation experiments.*

3.3 Accumulation of DNA damage in the absence of MATR3 expression

PSCs are permanently exposed to endogenous genotoxic stress factors, such as reactive oxygen species (ROS), which may lead to DNA damage. The cell responds to that through the activation of several molecular mechanisms such as DNA damage repair (DDR), trying to avoid mutations and genome instability. Furthermore, it has been even reported that PSCs are hypersensitive to DNA damage, and apoptosis respects the differentiated cells (Desmarais *et al.*, 2016; Inui *et al.*, 2017). We have found that the silencing of MATR3 leads to the alteration of stemness factors which may alter the cellular homeostasis and compensatory response. Moreover, MATR3 has been linked to DDR as part of the complex with SFPQ/NONO in the NHEJ mechanism (Salton *et al.*, 2010). On these bases, we deepen the role of MATR3 in DDR and whether its downregulation had an impact on the cellular response to DNA damage induction.

We induced DDR in shMATR3 (and shCTRL) iPSCs by treating with Camptothecin (CPT) at 0.5 and 1 µM for 3hrs. CPT inhibits DNA topoisomerase I, inducing the accumulation of DNA lesions. We observed shMATR3 iPSCs behaved differently from control cells in response to double-strand breaks induced by the drug. MATR3-downregulated cells have a stronger early response to the stimulus as higher levels of H2AX phosphorylation (yH2AX) (Figure 13 A and B). To better unveil if the absence of MATR3 affects the DDR, we evaluated the expression levels of some of DDR genes, responsible for DNA repair as RAD51, p53, Ku70, and NONO. The RT-qPCR analysis was then performed, and an upregulation of p53 of 40% was observed in shMATR3 cells respect to control cells upon CPT treatment, supporting the involvement of MATR3 in DDR (Figure 13C) confirming an increased predisposition to apoptosis under a rapid accumulation of DNA damage

(Jain and Barton, 2018). More pieces of information about the apoptosis will be investigated in the next future.

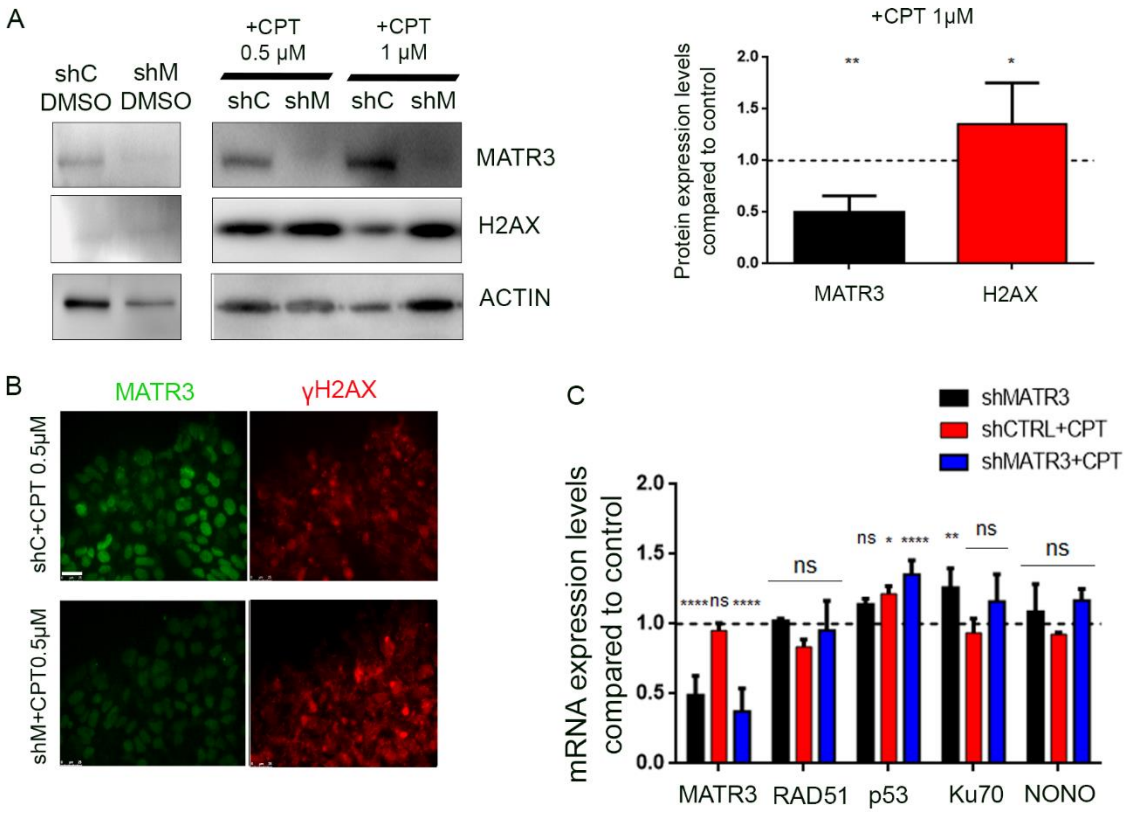

Figure 13. DDR upon CPT treatment in shMATR3 iPSCs

Evaluation of DDR in MATR3-silenced iPSCs. **(A)** DNA damage was evaluated measuring the γH2AX abundance. shMATR3 (shM) and shCTRL (shC) iPCs were incubated with 0.5, 1uM CPT or for 3 hours. Phosphorylated H2AX level was analysed by Western Blot using the specific antibody; ACTIN used as the loading control. The bar plots show the mean values of three independent experiments (right panel) Bar represents ± S.E.M. **(B)** Immunofluorescence staining of γH2AX and MATR3 in shMATR3 and shCTRL iPSCs. Cell nuclei were stained with DAPI in blue. Scale bar: 25µm. **(C)** RNA expression for the DNA damages actors as p53 and actors in the in double-strand breaks response such as RAD51 (HR) and Ku70 and NONO (NHEJ) was measured in shMATR3 and shCtrl cell lines. Data are presented as the mean ± S.E.M. P-value was calculated by One-way ANOVA (* P<0.05; ** P<0.01; **** P<0.0001).

3.4 MATR3 downregulation affects pluripotency

As shown, shMATR3 iPSCs phenotypically behaved differently from control cells in terms of growth and differentiation. We reasoned that this could be the consequence of dysregulated pluripotency circuits. Downregulation of MATR3 induced a decrease in the expression levels (both mRNA and protein) of essential self-renewal genes, such as OCT4, NANOG, and KLF4 (Figures 14 A and B). We observed a significant decrease of LIN28A mRNA levels but only a faint reduction of the protein amount. The involvement of MATR3 in the regulation of self-renewal is determined by its ability to downregulate both OCT4 and NANOG (Liao et al., 2018). Interestingly, despite the downregulation of OCT4 and NANOG expression, the stemness potential was not abolished, as shown in EBs assay (Figures 14 A and C) and immunofluorescences analysis (Figure 14F). In order to understand whether the downregulation of the above gene expression was directly correlated to MATR3 silencing, we rescued MATR3 expression. MATR3 overexpression re-established OCT4, NANOG and KLF4 expression levels (Figures 14 C and D), suggesting a direct contribution of MATR3 to their regulation. Moreover, as OCT4 suppresses neural ectodermal differentiation and promotes mesendodermal differentiation (Thomson et al., 2011), the decrease of OCT4 expression due to MATR3 silencing may explain the alteration in the differentiation commitment we have observed previously (Figure 12E). Data collected so far and the evidence of MATR3 involvement during the differentiation, especially in neuro-differentiation as reported by Niimori-Kita (Niimori-kita et al., 2018), led us to speculate on the role of MATR3 on pluripotency/differentiation balance.

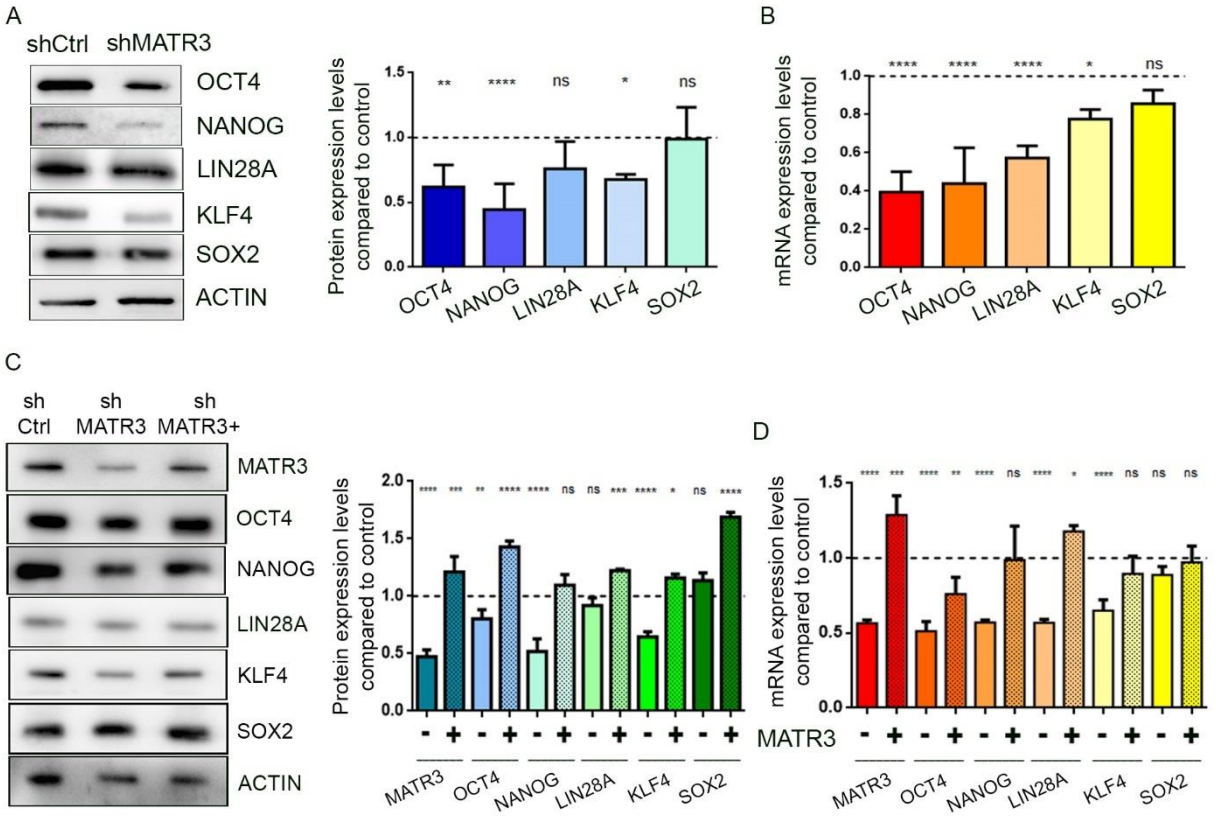

Figure 14. MATR3 downregulation affects pluripotency

(A-B) WB and RT-qPCR analyses for OCT4, NANOG, KLF4 and LIN28A performed on shMATR3- and shCtrl-hiPSC cultures. WB and RT-qPCR results were normalized on the internal housekeeping (β-ACTIN) and reported in comparison to the shCtrl samples (reported as value 1 in the graph). Both analyses were presented as the mean ± S.E.M. of three biological replicates. P-value was calculated by One-way ANOVA (* *P*<0.05; ** *P*<0.01; *** *P*<0.001; **** P<0.0001). **(C-D)** WB and RT-qPCR analyses for OCT4, NANOG, KLF4 and LIN28A performed on shCtrl-, shMATR3- (-), shMATR3- and on MATR3 rescued shMATR3- (+) cultures. WB and RT-qPCR analyses were normalized on the internal housekeeping (β-ACTIN) and reported in comparison to the shCtrl values (reported as value 1 in the graph). Values as reported as mean ± S.E.M. *P*-value was calculated by One-way ANOVA (* *P*<0.05; ** *P*<0.01; *** *P*<0.001; **** *P*<0.0001).

3.5 MATR3-interacting proteins show strong association with RNA processing

In order to study how MATR3 could fine-tune pluripotency, we explored MATR3 interactome, investigating its binding partners in iPS cell line A18945. Cell lysates were immunoprecipitated using MATR3 antibody, and MATR3-associated proteins were identified through tandem mass spectrometry (IP-MS), as schematically shown in Figure 15A. Immunoblot analysis of the immunoprecipitated fractions confirmed MATR3 enrichment in the pulldown. In contrast, no MATR3 was detected in the IgG pulldown (Figure 15B), pointing out the specificity of the test. Notably, we found 151 interactor proteins that were at least 1.5-fold more enriched over IgG ($p \leq 0.05$) (Figure 15C and Table 2).

IP-MS dataset included some already known MATR3-interacting proteins such as PTBP1, which play a role in alternative splicing (Coelho et al., 2015; Processing et al., 2018), and DHX9 and HNRNPK, which have been proposed to interact with MATR3 to regulate RNA processing (Salton *et al.*, 2011). In addition, several key genes of the translational machinery were enriched, such as eIF4A1, eIF4A3, eIF3CL, eIF3D and eIF3F (Table 2). Indeed, a functional enrichment analysis of Gene Ontology categories within this dataset showed significant enrichment in translation-, mRNA surveillance-, and ribosome- related components (Figure 15D Table3). Accordingly, proteomic network analysis revealed that MATR3 interactors congregate into a distinct Cytoplasmic/Translation cluster, which includes ribosomal subunits and translation initiation factors (Figure 15E). Our analyses of the MATR3 protein interactome suggests a pleiotropic role of MATR3 in RNA metabolism in iPSCs for both nuclear and cytoplasmatic activities. Accordingly, we dissected the MATR3-dependent molecular mechanism of stemness regulation, taking into consideration both nuclear and cytoplasmic functions of the protein.

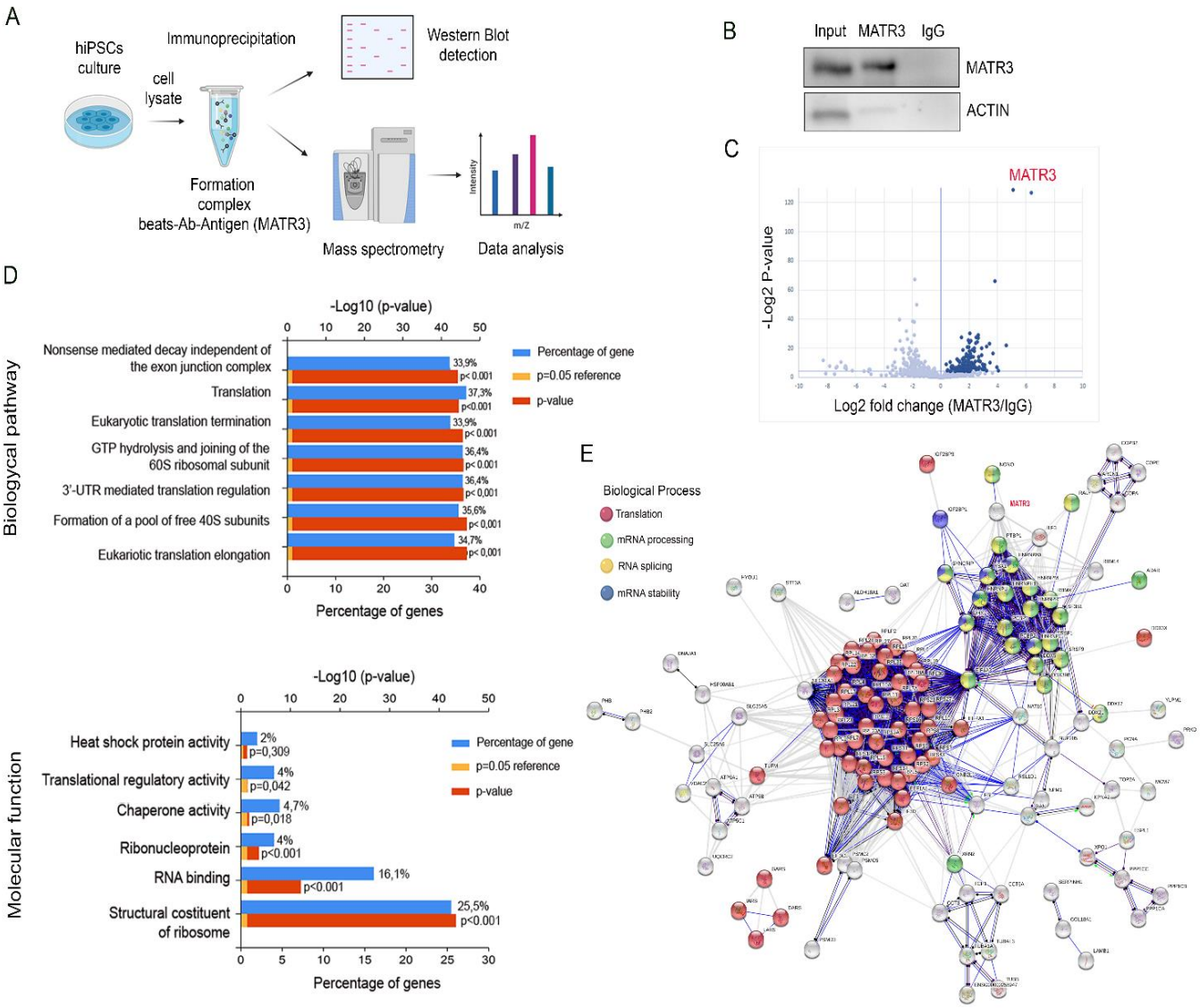

Figure 15. MATR3-interacting proteins show strong association with RNA processing

(A) Schematic representation of the strategy used for identifying MATR3 interactors **(B)** WB performed on parental hiPSC cell lysates co-immunoprecipitated with MATR3 antibodies (ab) and IgG control pull down. Pre-IP lysates are also shown (Input). The presence of β-ACTIN only in input sample in WB analysis confirmed the specificity of MATR3 antibody. **(C)** Volcano-Plot representation of MS analysis results. The Dot-Plot showed 156 proteins significantly enriched in MATR3 (right of the graph) versus IgG pulldown (left part of the graph). *Daniele Peroni performed mass spectrometry at the MS facility.* **(D)** GO chart reporting MATR3 protein-protein interactions results from MS data analysed by FunRich software. Two different GO biological processes analyses, Biological pathway and Molecular function, were used. A red histogram represents the significance of the interactions, *P*<0.001 (orange with minimum *P*<0.05) and the percentage of overrepresentation of the genes is represented by a blue bar. **(E)** Protein-protein interactions calculated by STRING interaction database. Only high confidence interactions, as determined by the STRING database, were accepted. Proteins are represented as nodes. In the graph, proteins

involved in translation (red plot), mRNA processing (green plot), RNA splicing (yellow plot) and mRNA stabilization (blue plot) are reported.

3.6 MATR3 stabilizes NANOG and LIN28A mRNAs

Guided by the GO analyses and from our previous results, we demonstrated that MATR3 depletion affects OCT4 expression, we next investigated more deeply MATR3 in the RNA metabolism. We verified whether MATR3 was able to bind the mRNAs of targets investigated above encoding OCT4, NANOG, LIN28A, SOX2, and KLF4. RNA-Immunoprecipitation (RIP) experiments were carried out immunoprecipitating endogenous MATR3 in A18945 cells and assessing the abundance of transcripts by RT-qPCR analyses. Data analyses revealed MATR3 significantly binds NANOG and LIN28A mRNAs (Figure 16A), as their expression was highly enriched in the anti-MATR3 immunoprecipitated RNA when compared to the IgG control, suggesting its active role in their mRNA metabolism. In order to dissect whether MATR3 affected the stability of those pluripotency genes, we determined their mRNA half-lives by arresting *de novo* RNA synthesis in shMATR3- and control iPSCs. The silencing of MATR3 led to a significant reduction of NANOG ($P<0.05$ at 1h time point) and LIN28A ($P<0.05$ at 1h time point) mRNA half-lives (Figure 16B). The role of MATR3 in post-transcriptional regulation had already been observed by Salton et al., which reported its ability to stabilize a set of mRNA (Salton *et al.*, 2011). In summary, our data show MATR3 to regulate the expression of pluripotency key genes, essential for pluripotency maintenance, since as the depletion of MATR3 was able to modulate the stability of directly bound mRNAs (NANOG and LIN28A), but not affecting the half-life of not directly bounded half-lives of mRNAs (i.e. OCT4, SOX2, and KLF4).

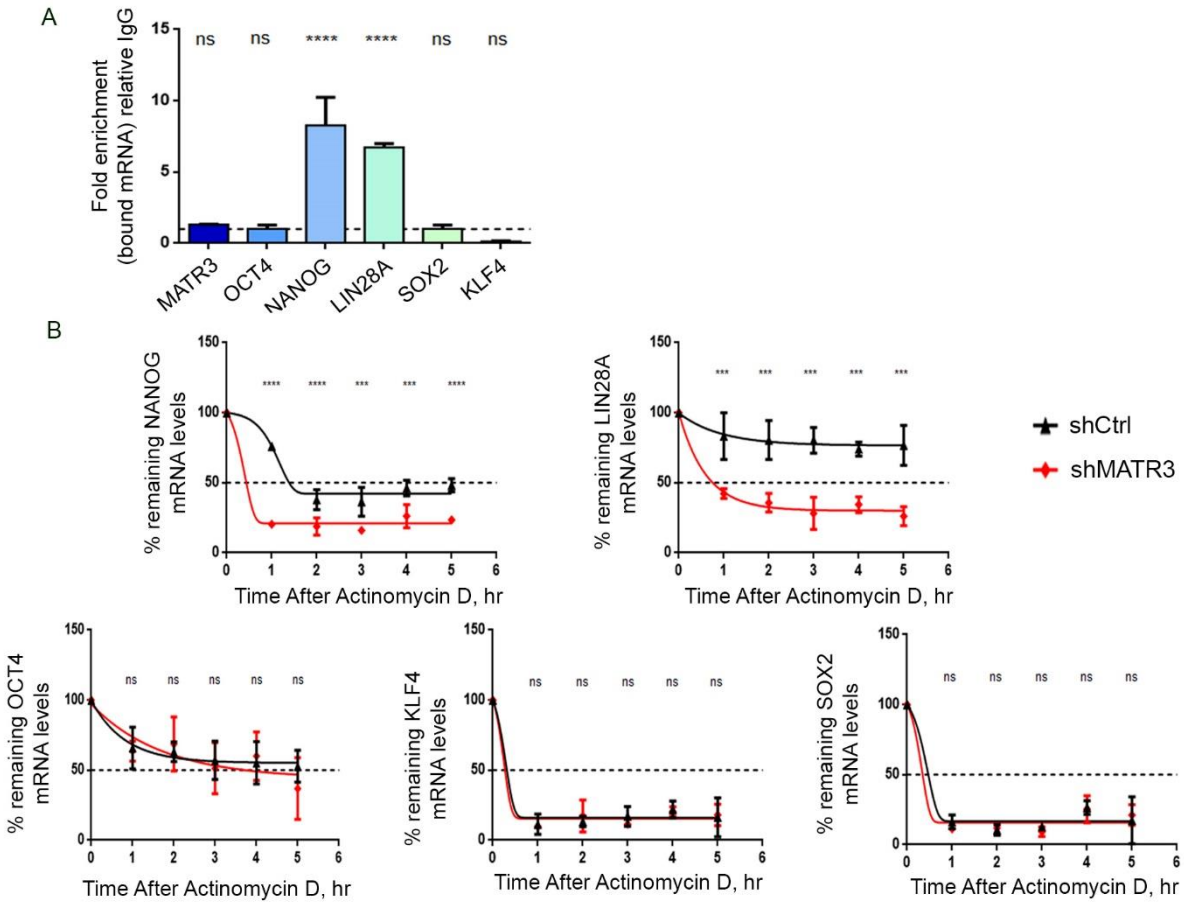

Figure 16. MATR3 stabilizes *NANOG* and *LIN28A* mRNAs

(A) RIP carried out with MATR3 antibody in A18945 cell line, followed by qRT-PCR. Fold enrichment was relative to IgG. Values are represented graphically as the mean ± S.E.M. of three biological replicates. One-way ANOVA (**** *P*<0.0001). **(B)** Actinomycin-D experiments to determine mRNA half-lives in shCtrl and shMATR3 cells. Cells were treated with Actinomycin-D for 0, 1, 2, 3, 4 and 5 hours. Total RNA extracted and NANOG, LIN28A, OCT4, KLF4 and SOX2 mRNA levels quantified by RT-qPCR analysis. qRT-PCR values were normalized on β-ACTIN. The results are expressed as percentages of mRNA abundance relative to time 0. The statistical analyses were done on the mean of three biological replicates, two-way ANOVA (* *P*<0.05; ** *P*<0.01; *** *P*<0.001; **** *P*<0.0001).

3.7 MATR3 co-operates with the translational machinery

The result of IP-MS supports a potential new role of MATR3 in the control of protein synthesis of iPSCs. Although MATR3 is predominantly characterised as a nuclear protein, it has been found to redistribute to NCIs in sALS (Tada *et al.*, 2018) or to shuttle to the cytoplasm *in vitro* models of neurodegeneration (Malik *et al.*, 2018). Moreover, ALS-linked MATR3 mutations led to its re-distribution within the cytoplasm (Niimori-kita *et al.*, 2018). Interestingly, other RBPs linked to motor neuron degeneration, such as TDP-43, FUS, ATXN2, TAF15, EWSR1, hnRNPA1, hnRNPA2/B1, MATR3 and TIA1, have been demonstrated to interact with translation machinery regulating global protein synthesis (Freibaum *et al.*, 2010; Tebaldi *et al.*, 2017; Kamelgarn *et al.*, 2018; Zhao *et al.*, 2018).

To investigate this potential role of MATR3, we first verified its sub-cellular localization. Performing confocal imaging, we found out MATR3 localizes into the cytoplasm as well as in the nucleus (Figure 17A). Indeed, about 25% of the total MATR3 spots lie outside the nucleus (Figure 17B). This is a surprising outcome as for the first time cytoplasmic localization of MATR3 in normal iPSCs has been clearly demonstrated. As a matter of fact, we carried out the quantification of the number of spots useful to appreciate the presence of MATR3 in the cytoplasm although the different MATR3 abundance between the two cell compartments is even reflected on the more vigorous intensity of MATR3 staining in the nucleus.

Successively, we investigated if MATR3 could interact with the translation machinery and performed IF analyses to study the co-localization with the eIF3A, marker of the eIF3-complex required for the initiation of protein synthesis (Masutani, Sonenberg and Yokoyama, 2007). The data analysis, performed on 3D (x,y,z) images of single cells, confirmed MATR3-eIF3A co-localization in the cytoplasm (Figure 17C). 4% of cytoplasmic MATR3-spots merges with eIF3A-spots (Figure 17D). This appealing liaison led us to assess whether the downregulation of MATR3 had effects on global translation. We evaluated *de novo* protein synthesis measured by O-propargyl-puromycin (OPP) Alexa Fluor® 488 incorporations quantifying the fluorescence by the Operetta high content screening system. We observed a marginal reduction of nascent protein synthesis in shMATR3 cells compared to control cells (Figure 17E).

To support our findings, we performed polysome profiling to find out MATR3 implication in the active translational machinery mechanisms. We observed that MATR3 co-sediments with the 40S, 60S, 80S and polysome fractions along with the markers of the small (RPS6) and large

(RPL26) subunits of the ribosome (used as controls for sedimentation) as shown by WB analyses of shCtrl proteins after sucrose gradient fractionation (Figure 17G) (Panda, Martindale and Gorospe, 2017). Comparing the spectra peaks of shCtrl and shMATR3 cells' sucrose-fractions, two main interesting differences showed up. Indeed, the ablation of MATR3 drove to a marked decrease in the monosome peak and polysomal peaks which led us to assume MATR3 plays a crucial role in active translation (Figure 6D). Moreover, the requirement of MATR3 in the ribosomal assembly was also supported by the increase of MATR3 amount in the 80S fraction (Figures 17 F and G). Furthermore, among the interactors of MATR3, we identified, through MS analyses, several initiation factors as eIF4A1, eIF4A3, eIF3CL, eIF3D and eIF3F (Table 2). Those factors are known to be required for the binding of mRNAs to 40S ribosomal subunit to form the 43S preinitiation complex and the joining of the 60S subunit (Närvää et al., 2012; Pelletier et al., 2016). Moreover, the malfunction in the 80S assembly complex is connected to the impairment of the global translation as observed in the decrement of polysomal peaks (Figure 17F) and the reduction of nascent protein synthesis (Figure 17E). These data support the hypothesis that MATR3 may act in the formation of the 80S complex. We then extracted the RNA from sucrose gradient fractions to quantify the amount of mRNA of the pluripotency genes by RT-qPCR. We observed a significant impairment in translation efficiency (TE), i.e. a shift from heavy polysomal fractions to lighter fractions, in shMATR3 condition of *LIN28A, NANOG* and *SOX2* mRNAs, irrespective of their total expression level changes (Figure 17H). MATR3 genetic ablation induced a trend in reducing *OCT4* TE, but without reaching statistic validation, and did not affect the TE of *KLF4,* whose mRNA slightly decreased at the total level. Taken all together, these data suggest that the presence of MATR3 on the translation apparatus is necessary to favour the polysomal loading of specific genes.

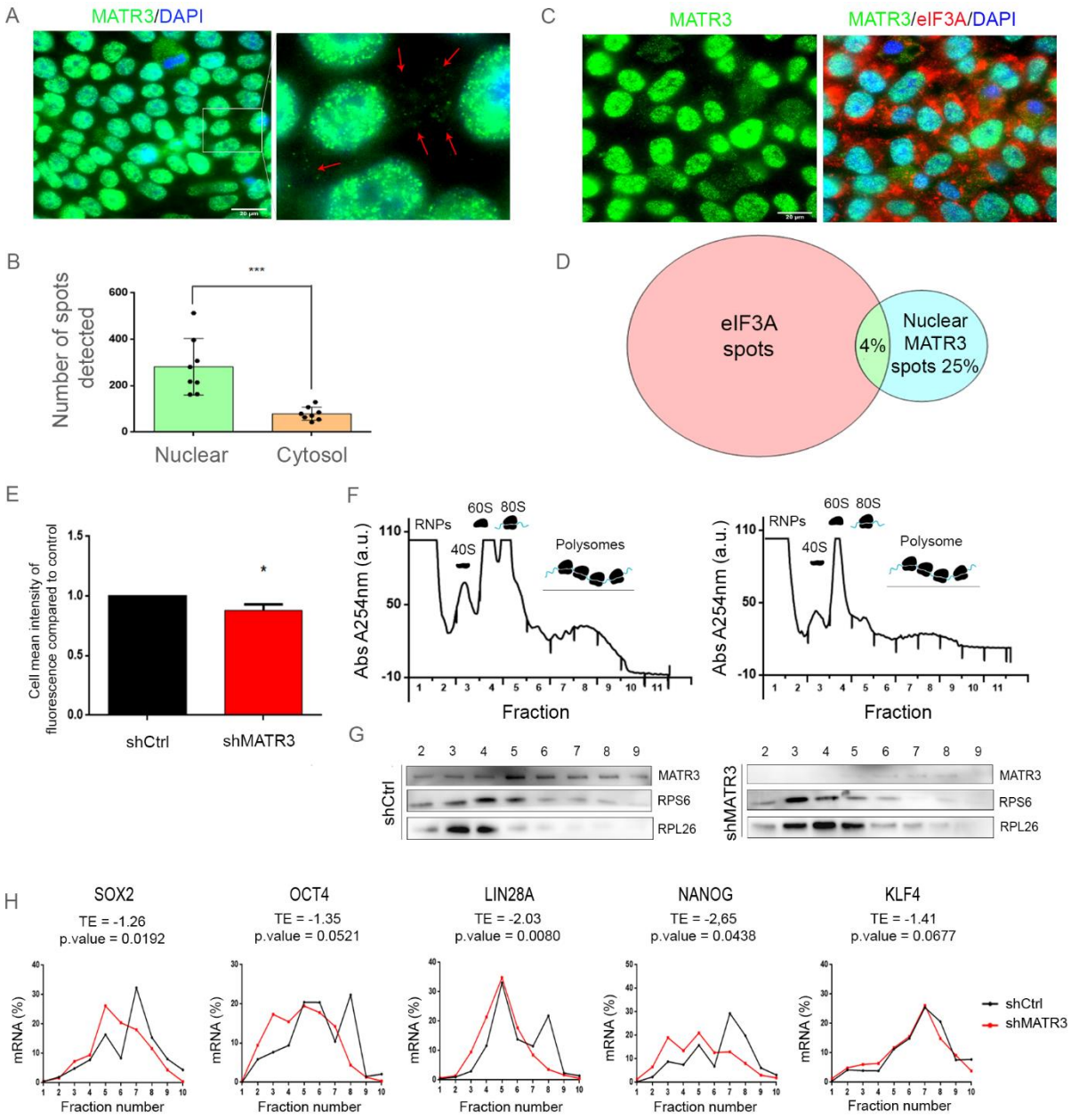

Figure 17. MATR3 co-operates with the translational machinery

(A) IF analyses in iPSCs of MATR3 (green signal). Nuclei stained with DAPI (blue). Arrows indicate cytoplasmatic MATR3-spots. Scale bar: 20µm. **(B)** Quantification of nuclear and cytoplasmic MATR3-spots. The count of spots carried out using the "Find maxima" plugin of ImageJ. Values represented graphically as the mean ± S.E.M. of eight replicates. One-way ANOVA (*** *P*<0.001). **(C)** IF showing the co-localization of MATR3 (green) and eIF3A (red). Nuclei stained with DAPI (blue). Scale bar: 20µm. **(D)** Graphical representation of MATR3 and Eif3A co-localization by Venn diagram. Quantification performed on 3D (x,y,z) images of single cells, considering only the cytoplasmic area of each cell. **(E)** *de novo* protein synthesis measured by O-propargyl-puromycin (OPP) Alexa Fluor® 488 incorporations. Fluorescence was quantified using the Operetta high content screening system. shCtrl was reported at value 1, and shMATR3 was compared to shCtrl. Data are presented as the mean ± S.E.M. of three biological replicates. The statistical data was calculated by t-test. **(F)** Polysome profile analysis, by a sucrose gradient

fractionation, on shMATR3 and shCtrl cell lines. Peaks are showing 40S, 60S, 80S, and polysome fractions. One representative spectrum is reported; all the spectra of biological replicates are reported at the end of the thesis. *Polysome analysis was done in collaboration with Annalisa Rossi.* **(G)** WB analysed proteins obtained from the separation of the fractions. RPS6, RPL26 and MATR3 were detected in each fraction. One representative blot reported. **(H)** qRT-PCR analysis for SOX2, OCT4, LIN28A, NANOG and KLF4 performed on mRNA from fractions obtained from the Polysome profiling.

3.8 MATR3 regulates OCT4 expression by regulating YTHDF1 transcription

We then moved to investigate whether MATR3 could regulate the above factors at the transcriptional level. In rat pituitary cells (GC cells), a ChIP-Seq using a MATR3 antibody, revealed that MATR3 binds to DNA regulatory sequences, by physically interacting with the Pou1f1 transcription factor and contributes to its activity (Skowronska-Krawczyk *et al.*, 2014). Inspection of the Chip-seq data from this dataset revealed that MATR3 binding sites genomic positions corresponded mainly to distal regions from the transcription start sites (Table 4). Still, a fraction was directly associated with promoter regions. Functional analysis performed on this dataset revealed that MATR3 binds sequences of genes involved in the development, stemness and stem cell proliferation processes (Figure 18.1 A). Indeed, we found notable examples of genes regulating embryo development including *Shh* (sonic hedgehog signalling molecule) (Weed, Mundlos and Olsen, 1997; Haraguchi *et al.*, 2001; Blaess *et al.*, 2015; Tickle, Towers and Davey, 2017), Sox factors (*Sox4, Sox5, Sox11*) (Bowles, Schepers and Koopman, 2000; Potzner *et al.*, 2010; Sarkar and Hochedlinger, 2014; She and Yang, 2015) and Wnt signalling (*Sfrp2, Wnt7a*) (Hao *et al.*, 2006; Kele *et al.*, 2012; Miao *et al.*, 2018; Ren *et al.*, 2018). We then shortlisted the first most significant 500 ChIP-seq peak sequences, ordered according to peak score, and obtained the two best putative MATR3 DNA binding motifs by using HOMER (Figure 18.1 B). We examined the *LIN28A*, *NANOG*, *SOX2*, *KLF4* and *OCT4* Transcriptional Start Site (TSS) upstream regions and checked for the presence of the MATR3 DNA-binding consensus sequence. We did not find any consensus sequence on these genes. Indeed, the experimental verification by ChIP assay in iPSCs, using the anti-MATR3 antibody, did confirm no enrichment of DNA sequences of *OCT4, NANOG, LIN28A* upstream TSS regions (Figure 18.1 C) associated to MATR3.

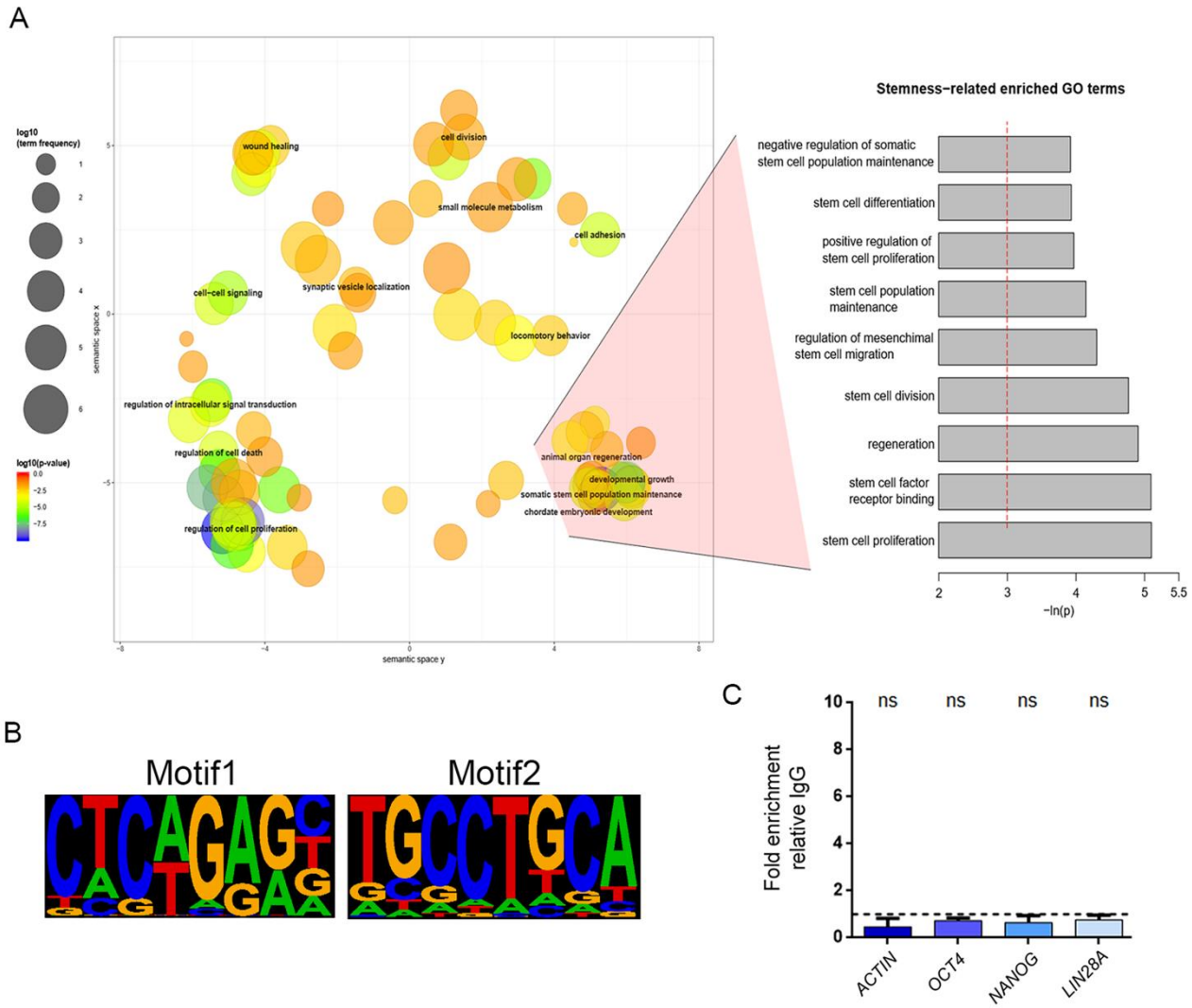

Figure 18.1 MATR3 regulates OCT4 expression by regulating YTHDF1 transcription

(A) Semantic similarity of enriched Gene Ontology terms (biological process branch). Functionally related processes are close to one another, with circle size representing the abundance of genes annotated to that process in the genome. The colour gradient represents the enrichment P-value. Barplot of significantly enriched Gene Ontology terms related to stemness processes, *P*-values are expressed in -log10(*P*-value) and the red line indicates the adjusted *P*-value threshold (0.05). **(B)** Highest-scoring motifs analysis (best motif on the left, and second-best on the right) on the 500 DNA sequences most significantly bound by MATR3 according to the ChIP-seq assay (Skowronska-Krawczyk *et al.*, 2014), obtained with HOMER (Heinz *et al.*, 2011). *Erik Dassi performed bioinformatic analyses.* **(C)** ChIP assay of MATR3 at or near the promoters of *ACTIN, OCT4, NANOG, LIN28A* and *YTHDF1* in iPSCs. ChIP performed using the antibody against MATR3 and IgG as the negative control. Data were normalized to non-immunoprecipitated sample (INPUT) and compared to the IgG sample. Only the *YTHDF1'* promoter showed a region predicted to contain the MATR3 DNA consensus sequence. Values, as reported as mean ± S.E.M. P-value, were calculated using One-way ANOVA (** *P*<0.01).

Chen et al. reported that the transcripts of the stemness regulators, including *OCT4, LIN28A, SOX2* and *NANOG* mRNAs, can be post-transcriptionally modified by methylation in position N^6 of the adenosines (m^6A) (Chen, Y. J. Hao, *et al.*, 2015). By RIP assay, using anti-m^6A antibody (MeRIP), we observed that *OCT4* and *LIN28A* transcripts were methylated with a more than 20- and 6-fold enrichment over the IgG background, respectively (Figure 18.2 D). We, therefore, searched for the MATR3-DNA binding consensus in the promoter regions of the genes involved in the m^6A machinery and found enrichment in the promoters of all the genes involved in m^6A regulation (Table 5). We decided to focus our attention on *YTHDF1* that was the gene with the highest presence of predicted MATR3 biding elements in its promoter (123 significant binding sequences). Indeed, experimental validation of the computational prediction by ChIP, indicated that MATR3 bound to the YTHDF1 promoter region (Figure 18.2 E). Coherently with a transcriptional mediated regulation of *YTH*, we found both YTHDF1 mRNA and protein expression levels in shMATR3 hiPSCs (Figures 18.2 F and G). In addition, YTHDF1 bound to *OCT4* and *LIN28A* methylated transcripts but not to *SOX2, KLF4* and *NANOG*, as assessed by RIP (Figure 18H), suggesting that these two transcripts are under the direct regulation of YTHDF1. Indeed, this RNA-binding protein binds to m^6A-methylated RNAs and regulates their metabolism, generally promoting their translation (Wang *et al.*, 2015). The restoration of YTHDF1 expression in shMATR3 iPSCs rescued both *OCT4* and *LIN28A* transcript levels (Figure 18.2 I), suggesting the presence of a regulatory loop MATR3 triggers the expression of YTHDF1 that, in turn, regulates the metabolism of the *OCT4* and *LIN28A* transcripts.

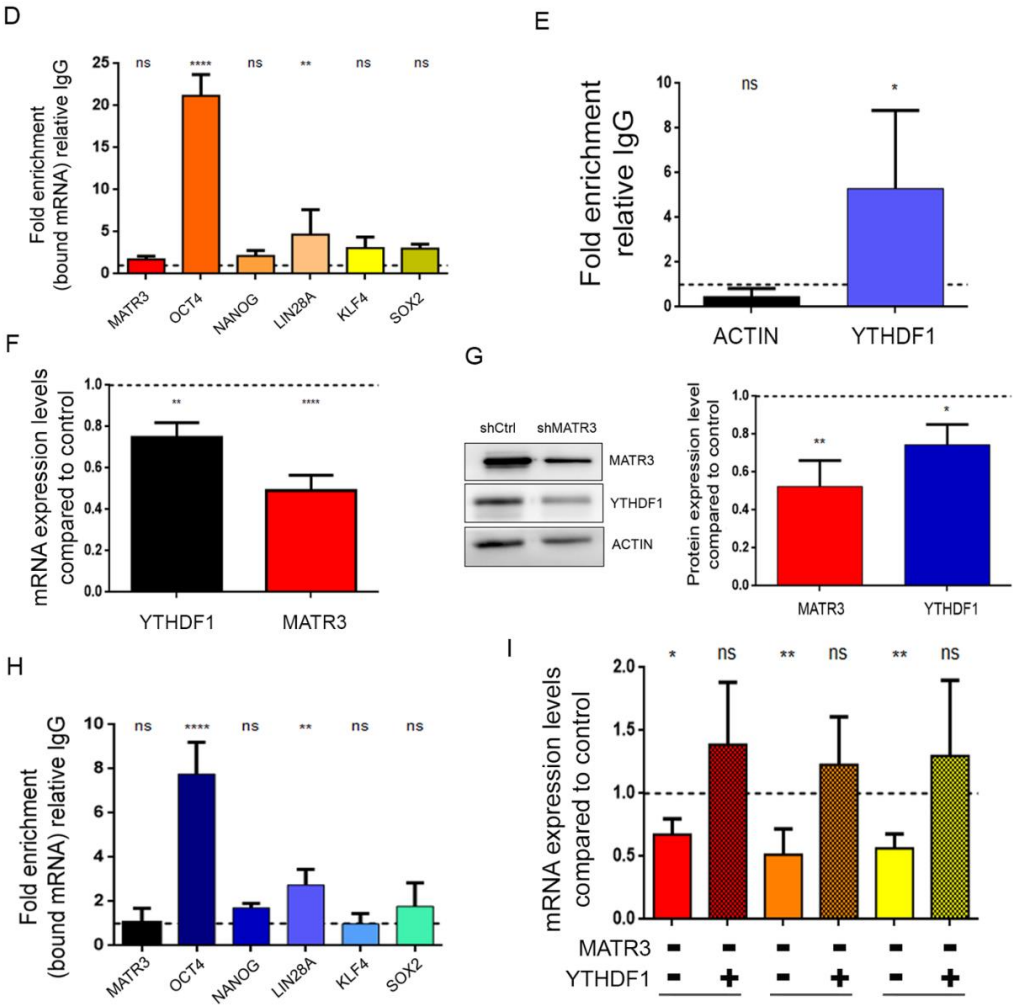

Figure 18.2 MATR3 regulates OCT4 expression by regulating YTHDF1 transcription

(D) RIP using m^{6}A antibody, in iPSCs, followed by RT-qPCR. Fold enrichment was relative to IgG. Values represented graphically as the mean ± S.E.M. of three biological replicates. One-way ANOVA (** *P*<0.01; **** *P*<0.0001). **(E)** ChIP assay of MATR3 at or near the promoters of *YTHDF1* in iPSCs. ChIP performed using the antibody against MATR3 and IgG as the negative control. Data were normalized to non-immunoprecipitated sample (INPUT) and compared to the IgG sample. Values, as reported as mean ± S.E.M. P-value, was calculated by One-way ANOVA (* *P*<0.01). **(F)** WB and **(G)** qRT-PCR analyses for assessing YTHDF1 expression in shMATR3 and shCtrl cells. Values were normalized on the internal housekeeping (β-ACTIN) and reported in comparison to shCtrl values (reported as value 1 in the graph). Both analyses were presented as the mean ± S.E.M. of three biological replicates. P-value was calculated by One-way ANOVA (* *P*<0.05; ** *P*<0.01; *** *P*<0.001; **** P<0.0001). **(H)** RIP using YTHDF1 antibody in iPSCs, followed by RT-qPCR. Fold enrichment was relative to IgG. Values represented graphically as the mean ± S.E.M. of three biological replicates. One-way ANOVA (** *P*<0.01; *** *P*<0.001; **** *P*<0.0001). **(I)** RT-qPCR analyses for YTHDF1, OCT4 and LIN28A, on shCtrl-, shMATR3- (-), and YTHDF1 rescued shMATR3- (+) cultures. RT-qPCR analyses were normalized on the internal housekeeping (β-ACTIN) and reported in comparison to the shCtrl values (reported as value 1 in the graph). Values are reported as mean ± S.E.M. P-value, was calculated by One-way ANOVA (* *P*<0.05).

3.9 Generation and characterization of a human iPSC line from an ALS patient carrying the Q66K-MATR3 mutation

To create a suitable model for our research in order to study the roles of MATR3 deeply have been presented so far, we decided to reprogram ALS patient's fibroblasts in pluripotent stem cells. Fibroblast cells, carrying p.Q66K mutation in the MATR3 gene, were isolated from a 51-years old male ALS patient biopsy. iPSCs were generated by the non-integrating system based on the use of the episomal plasmid mix (System Biosciences SBI) expressing a combination of reprogramming factors OCT4, SOX2, KLF4, Lin28, p53shRNA, L-MYC and miR-302/367 cluster (Takahashi et al., 2007). Moreover, the expression of a GFP-marker allowed monitoring of plasmid delivery and loss. PCR analysis showed that constructs used for reprogramming of primary fibroblasts and EBV-related latency elements (EBNA1) were eliminated from the established fibroblast-derived iPSC (Figure. 19E). iPSC-like colonies appeared after 15 days, with clear margins and compact cells with a high nucleus/cytoplasmic ratio, were picked ten days later (Figure 19B) and the stabilized iPSCs, called Q66K#44 DRM, were expanded over several passages for further characterization. IF (Figure 19B) and qPCR (Figure 19C) analyses were performed in order to confirm the expression of pluripotency markers such as NANOG, OCT4, SOX2 and KFL4. Q66K#44 DRM line displayed a usual diploid 46, XY karyotype, without noticeable abnormalities (Figure 19A) and the presence of missense mutation harboured by parental fibroblasts was confirmed by sequencing in the generated iPSC line (Figure 19D). The corresponding identity of the generated iPSC line to the parental fibroblasts was confirmed by short tandem repeat (STR) analysis, which showed that genomic DNA extracted from Q66K#44 DRM and the parental fibroblasts matched on 19 loci tested (Table 6). To assess the pluripotent competence of Q66K#44 DRM, embryoid bodies were randomly differentiated (Figure 19G). Embryoid bodies expressed all three germ layer markers. NESTIN and βIII-Tubulin (ectodermal); α-SMA (mesodermal) and AFP (endodermal) expression was verified by RT-qPCR (Figure 19F) and β III Tubulin, αSMA and GATA-4 expression were confirmed by immunofluorescence staining (Figure 19G).

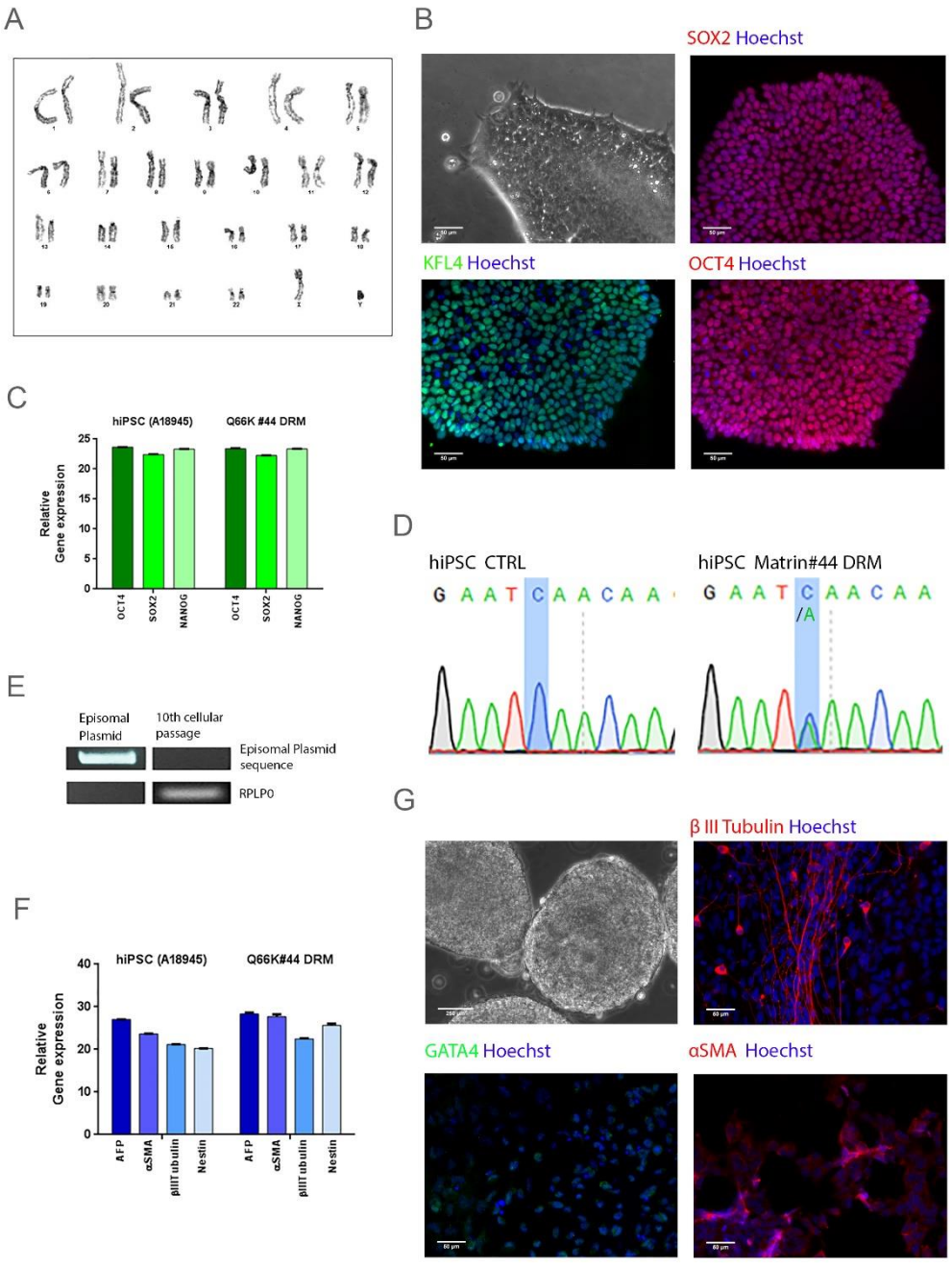

Figure 19. Generation and characterization of a human iPSC line from an ALS patient carrying the Q66K-MATR3 mutation

(A) Karyotype analysis of Q66K#44 after reprogramming showed normal diploidy. **(B)** Immunofluorescent staining showing the expression of the stemness marker proteins, SOX2 (red), KLF4 (green), OCT4 (red), in Q66K#44 DRM cells. **(C)** qPCR evaluating the expression level of the stemness markers genes OCT4, SOX2 and NANOG in Q66K#44 DRM and in A18945. **(D)** Q66K mutation was confirmed by sequencing after the episomal reprogramming of patient-derived fibroblast in Q66K#44 DRM cells and was compared with

iPSCs obtained from a Healthy Volunteer (hiPSC HV). **(E)** PCR was showing the loss of expression of the episomal vector in Q66K#44 DRM cells at the 10th passage. **(F)** qPCR evaluating the expression level of marker genes belonging to the three germ layers in embryoid bodies obtained from Q66K#44 DRM hiPSCs. AFP (Endoderm), αSMA (Mesoderm), βIIITubulin (Ectoderm) and NESTIN (Ectoderm). **(G)** Immunofluorescent staining showing the protein expression of marker genes belonging to the three germ layers in embryoid bodies obtained from Q66K#44 DRM hiPSCs. AFP (Endoderm), αSMA (Mesoderm), βIIITubulin (Ectoderm) and NESTIN (Ectoderm).

3.10 Establishment of an induced pluripotent stem cell (iPSCs) line from a patient with Sporadic Amyotrophic Lateral Sclerosis (sALS).

Similarly, we were interested in seeking if altered mechanisms were common in fALS and sALS models. For this reason, we decided to reprogram fibroblasts derived from one sALS patient. Fibroblast cells derived from a male patient 65-year-old were used for the generation of an iPSC line (sALS#24 DRM). The approach used was the same as the one adopted for Q66K#44 DRM cell line. The loss of reprogramming plasmid during several cell passages was confirmed by RT-qPCR (showed in Table 9) after 10-15 cell divisions (Figure 20B). iPSC-like colonies with a high nucleus/cytoplasmic ratio were picked after 25 days from the nucleofection and propagated. STR analysis confirmed the identical genetic background of iPSC clone with the donor fibroblasts (Table 7). sALS#24 DRM showed a regular diploid 46, XY karyotype, without chromosomal genetic aberrations (Figure 20A). Molecular analyses were performed to assess cell line stemness potential. Stemness was confirmed by both expressions mRNA and protein levels, the expression of stem cell markers such as KLF4, SOX2 and OCT4 proteins evaluated by IF (Figure 20C) and NANOG, SOX2 and OCT4 mRNAs by RT-qPCR analyses (Figure 20D). Pluripotency was further tested with embryoid bodies-based differentiation to all three germ layers. Indeed, after spontaneous differentiation EBs were able to express endodermal (GATA-4 and AFP), mesodermal (αSMA) and ectodermal (NESTIN and βIII Tubulin) markers proved through immunofluorescence (Figure 20E) and RT-qPCR (Figure 20F) analysis.

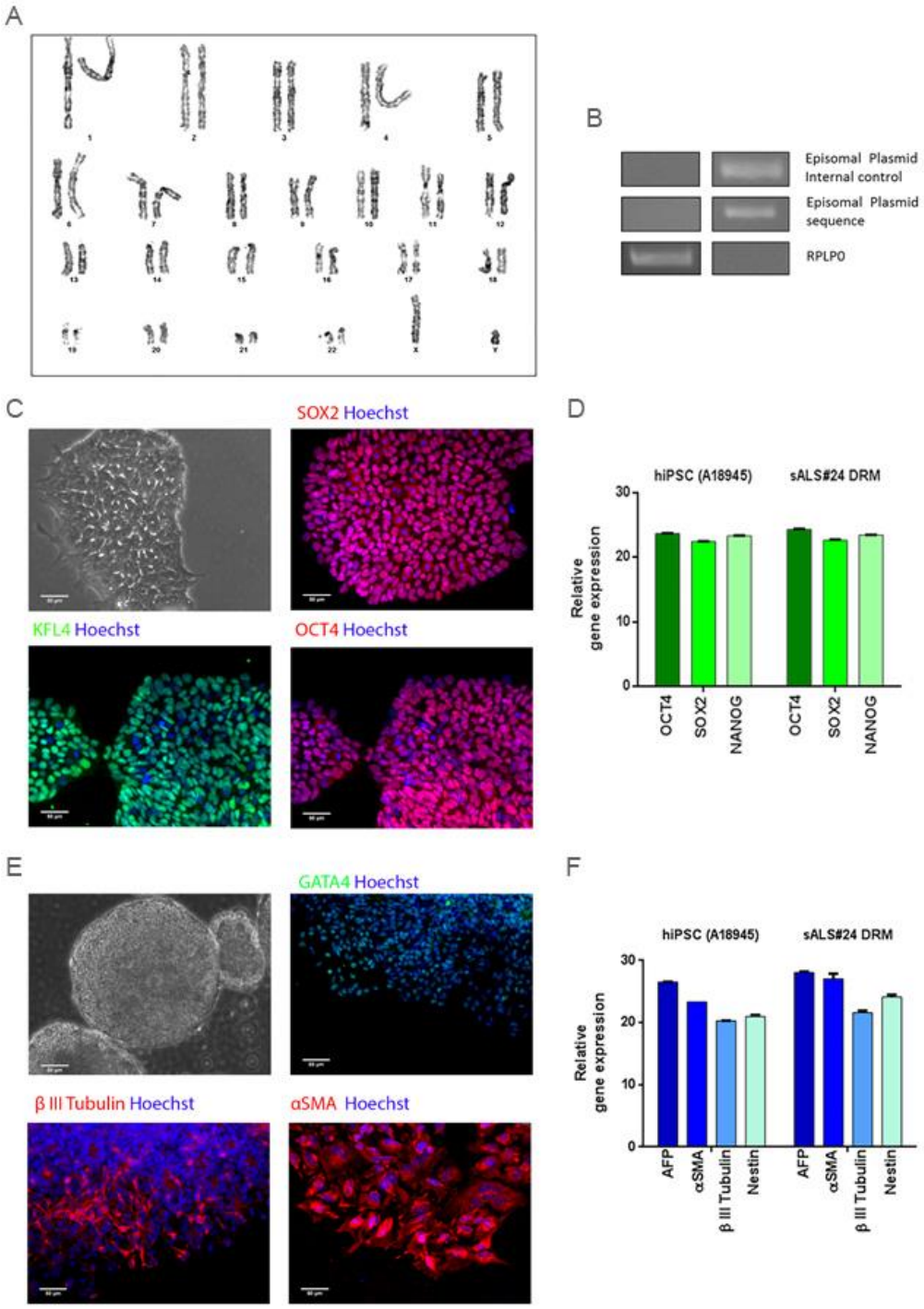

Figure 20. Establishment of an induced pluripotent stem cell (iPSCs) line from a patient with Sporadic Amyotrophic Lateral Sclerosis (sALS).

(A) Karyotype analysis of sALS#24 DRM after reprogramming showed normal diploidy. **(B)** PCR was showing the loss of expression of the episomal vector in sALS#24 DRM cells at the 10th passage. **(C)** Immunofluorescent staining showing the expression of the stemness marker proteins, SOX2 (red), KLF4 (green), OCT4 (red), in sALS#24 DRM cells. *Karyotype was performed in Medical Genetics Unit, IRCCS Casa*

Sollievo della Sofferenza Hospital, I-71013 San Giovanni Rotondo (FG), Italy **(D)** RT-qPCR was evaluating the expression level of the stemness markers genes OCT4, SOX2 and NANOG in sALS#24 DRM and in a commercial hiPSC line named A18945. **(E)** Immunofluorescent staining showing the protein expression of marker genes belonging to the three germ layers in embryoid bodies obtained from sALS#24 DRM hiPSCs. AFP (Endoderm), αSMA (Mesoderm), βIIITubulin (Ectoderm) and NESTIN (Ectoderm). **(F)** RT-qPCR was evaluating the expression level of marker genes belonging to the three germ layers in embryoid bodies obtained from sALS#24 DRM hiPSCs. AFP (Endoderm), αSMA (Mesoderm), βIIITubulin (Ectoderm) and NESTIN (Ectoderm).

3.11 Impact of Q66K mutation on MATR3 in iPSCs

To figure out the functional effect of Q66K MATR3 mutation in hiPSCs, we investigated whether the mutation affected the proliferation rate of Q66K#27 cells compared to cells derived from a healthy donor (CTRL#11) and no differences in proliferation were observed (Figure 21.1 A). These data are not surprising, as we already reported no differences in growth and viability in shMATR3, where even the profound reduction of MATR3 levels of expression had no impact on the viability (Figures 11D and 11E). We then, investigated the effect of the sub-optimal condition of Q66K#27 cells culturing, to study whether the mutation could have a similar effect of what observed in MATR3 downregulation experiments. As described previously, we evaluated cell growth and morphology of hiPSCs upon having seeded them as single cells or small colonies. We observed that Q66K#27 cells have not growth deficit, measured in terms of number and area of the single cells and colonies in comparison to CTRL#11 cells (Figures 21.1 B). This suggests that Q66K MATR3 mutation does not inhibit MATR3 function in hiPSCs and allows the regular rate of growth even in optimal and sub-optimal conditions. It is essential to underline MATR3 Q66K cells carry the mutation in heterozygosis.

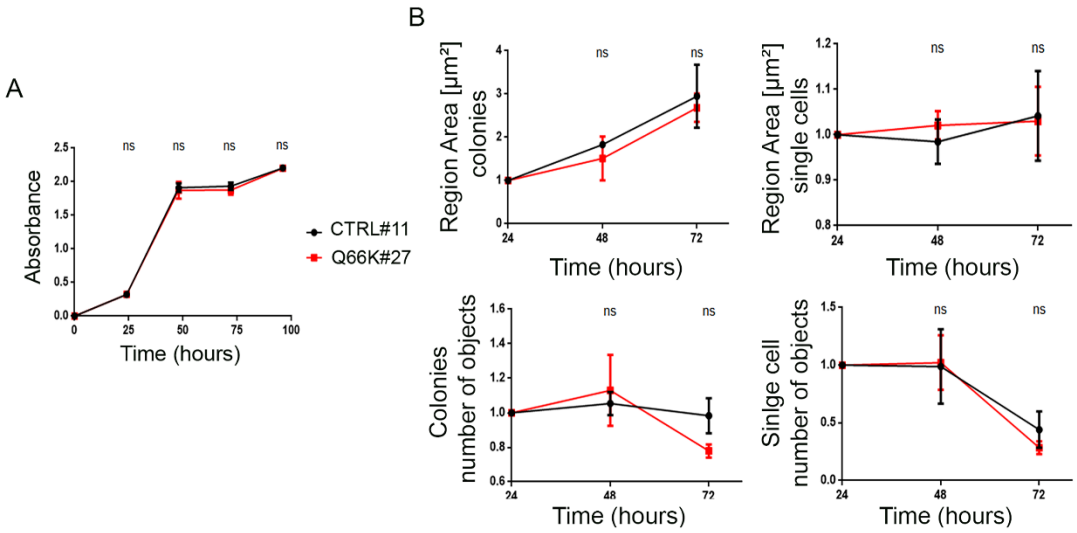

Figure 21.1 Impact of Q66K mutation on MATR3 roles in iPSCs

(A) Growth curve of CTRL#11 and Q66K#27 cell lines was reported by OZBlue method. Data are presented as the mean ± S.E.M. of three biological replicates. One-way ANOVA (*ns*, not significant). **(B)** Analyses of CTRL#11 and Q66K#27 hiPSCs following single-cell seeding. The number and area of cells and colonies were measured by Operetta High Content Screening System using 5X objective 0.08NA for three time points (24, 48 and 72 hours). The region Areas [µm^2] for the single cells and for the colonies are reported for each time point. Data are presented as the mean ± S.E.M. of two biological replicates. One-way ANOVA (*ns*, not significant).

We successively investigated if the mutation could affect the MATR3 role during the spontaneous differentiation of hiPSCs towards the three germ layers. , Q66K#27 EBs were able to differentiate into all three germ layers (Figure 19G), and no significant morphological differences were reported when compared with the CTRL#11 (Figure 21.2 C). Nevertheless, after 14 days of cultivation, an up-regulation of mRNAs expression of neuroectoderm (TUBB3), and endodermal (AFP) markers was observed in the Q66K#27 cells, but no significant expression differences were reported for the mesodermal marker (αSMA) (Figure 21.2 D). Even if no morphological differences between Q66K#27 and CTRL#11 EBs were reported, however an altered expression of early differentiation markers was observed. Unexpectedly Q66K#27 EBs showed a similar expression trend of ectoderm and endoderm markers mRNAs as of shMATR3 cells, suggesting that the mutation affects the molecular function of MATR3 during the three germ layer differentiation.

Conversely, Q66K MATR3 mutation does not affect the control of self-renewal genes expression like its downregulation. Nevertheless, we reported some alteration in iPSCs carrying MATR3

mutation. We observed no significative differences in OCT4, KLF4 and LIN28A expression; however, we observed the downregulation in NANOG mRNA and protein expression levels and the increase of both SOX2 mRNA and protein expression. Interestingly, SOX2 gene expression was not affected by the silencing of MATR3, but we observed a significant increase of SOX2 protein expression levels in shMATR3 when wild type MATR3 was overexpressed (Figure 14C). This suggests a positive control of MATR3 on the protein expression of SOX2, that was not elucidated in our previous work. Moreover, we reported a slight reduction of protein synthesis in Q66K#27 cells, as observed during MATR3 downregulation, with respect to the relative control (Figure 21.2 G) measured as OPP incorporation. These data lead us to speculate that the mutation has a negative effect on the translation of the MATR3 function as a loss of function. These preliminary data may drive to find new interesting dysregulated molecular mechanisms happening in ALS-MNs.

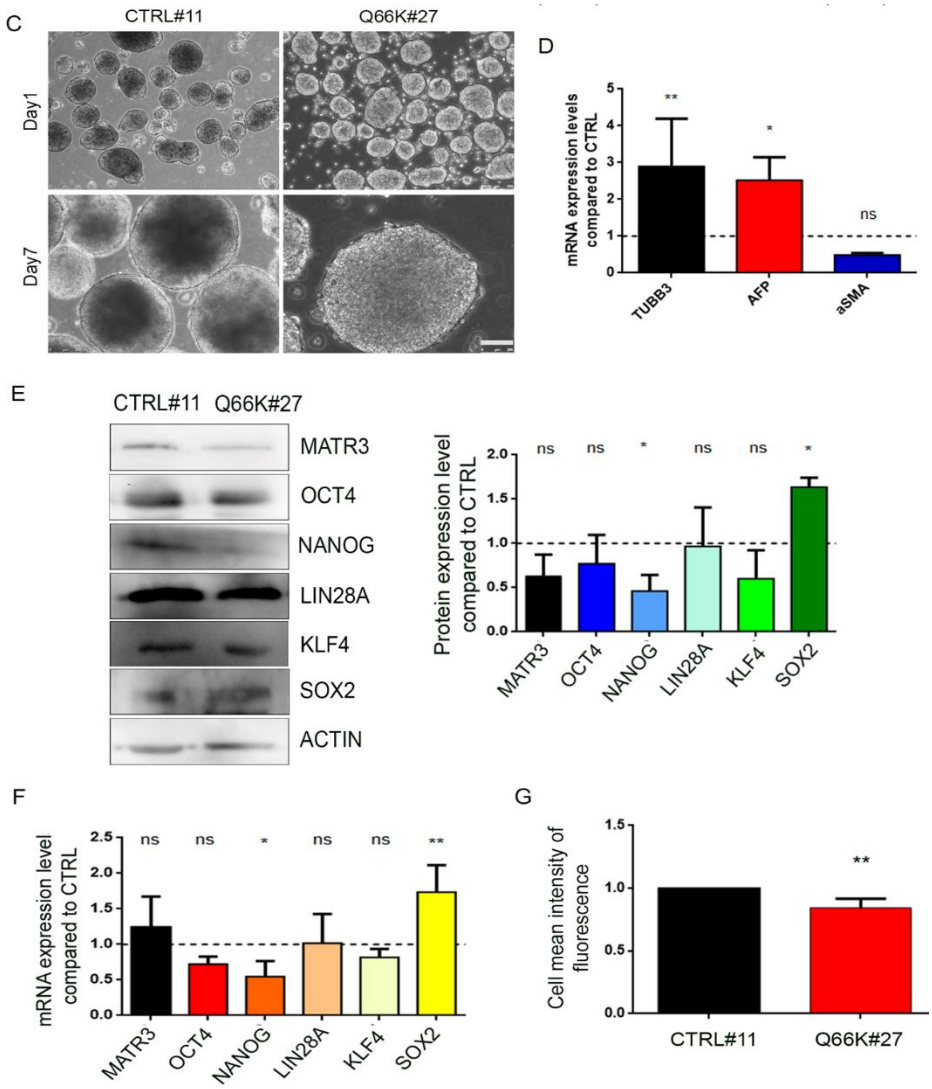

Figure 21.2 Impact of Q66K mutation on MATR3 roles in iPSCs

(C) CTRL#11 and Q66K##27 hiPSCs, were dissociated and transferred to suspension cultures for seven days and then pated on Geltrex-coated culture plate for other 7 days in order to obtain spontaneous differentiation (upper panel). Images reported the first and last time point of the EB assay (Day 1 and Day 14) detected by optical microscope (scale bar 250 µm). **(D)** TUBB3 (Ectoderm), AFP (Endoderm) and α-SMA (Mesoderm) mRNA levels were analysed by RT-qPCR in 14 days differentiating-EBs. RPLP0 used as housekeeping and values normalized on the CTRL#11 reported at value 1 in the graph. Data are presented as the mean ± S.E.M. P-value was calculated by One-way ANOVA (* P<0.05; ** P<0.01). **(E-F)** WB and RT-qPCR analyses for OCT4, NANOG, KLF4, SOX2 and LIN28A performed on Q66K#27 and CTRL#11 hiPSC cultures. WB and RT-qPCR results were normalized on the internal housekeeping (β-ACTIN) and reported in comparison to the CTRL#11 samples (reported as value 1 in the graph). Both analyses were presented as the mean ± S.E.M. of two biological replicates. One-way ANOVA calculated p-value (* *P*<0.05; ** *P*<0.01). **(G)** *de novo* protein synthesis measured by O-propargyl-puromycin (OPP) Alexa Fluor® 488 incorporations. Fluorescence was quantified using the Operetta high content screening system. CTRL#11 was reported at value 1, and Q66K#27 was compared to CTRL#11. Data are presented as the mean ± S.E.M. of two biological replicates. The statistical data was calculated by t-test (** *P*<0.01).

3.12 Generation of patient's brain organoids

We generated hiPSC-derived 3D organoid, from the healthy donor and ALS patients cell lines, obtained from the reprogrammed showed before followed the commercial Cerebral Organoids Kit. The kit is optimized to increase the efficiency and reproducibility of organoid formation based on the formulation published by Lancaster *et al.* (Lancaster *et al.*, 2013) (Figure 22.1 A). Moreover, the new formulation allowed to obtain the development of various interdependent brain regions, including the cerebral cortex. Cerebral organoid setting up has initiated through an intermediate EBs formation, a step followed by the expansion of neuroepithelia. After 7 days since their formation, neuroectodermal tissues were embedded in droplets of matrigel to support the three-dimensional structure for more complex tissue growth. After the expansion period, on the 10^{th} day, the organoids in matrigel droplets were placed on a shaker (at 37°C) to safeguard the correct provision of nutrients supplied by the specific maturation medium inducing the correct growth and maturation of organoids. After 42 days, organoids exhibited dense cores with optically translucent edges (Figure 22.1 B) and the maturation arrested.

During the human brain development, precise patterns of cell division and migration allow transforming the neuroepithelium of the embryonic forebrain in the adult cerebral cortex in a process named neurogenesis. Neurogenesis takes place in two proliferative regions of the embryonic cortical telencephalon, in the VZ where reside the neural stem cell population and the

SVZ a secondary proliferative zone containing neural progenitors and glial cells (in development showed in both zones), both VZ and SVZ give rise to intermediate progenitors and ultimately post-mitotic neurons (Figure 22.1 C) (Noctor *et al.*, 2004). The mature organoids (from six months in culture) can recapitulate the first part of the neurogenesis, with the formation of the basal zone, the VZ composed by neuroepithelial stem cells and ventricular radial glial cells, an intermediate zone, the SVZ with the presence of the outer radial glial cells and cells positive to glia and cortical layer markers, and an external zone, cortical plate, with the presence of mature neurons (Figure 22.1 C). Immature organoids (to 3 months of culture) contain neuroepithelial stem cells and ventricular radial glia cells that dived the VZ from the apical surface, with a no organized intermediate zone SVZ (Di Lullo and Kriegstein, 2017) (Figure 10). Organoids obtained showed the neural identity and the heterogeneous composition defined by different brain regions (Figures 22.1 B and D). We examined by histological analysis the correct formation of the organoids structures. 42-days old organoid is an immature organoid, able to form a VZ, with stem cells expressing SOX2 and intermediate progenitors expressing TBR2. Furthermore, it was possible to appreciate the formation of cortical neurons in the organoid's cortical plate, positive for TBR1, TUBB3, and Reelin (Figure 22.1 D). All three organoid cultures have been induced and matured correctly as expressing all the markers of characteristics of different functional sub-areas. Moreover, it was tested the immature organoid ability to form a regional specification. Forebrain was identified through FOXG1 staining, which assesses the typical cerebral cortical morphology. Nevertheless, in immature organoids, it was not possible to appreciate the classical morphology of the structures formed by the cells positive for FOXG1. We successfully compared the CTRL organoid's ability to generate the VZ/cortical plate with the patient's derived organoids, Q66K, and sALS cell lines (Figure 22.1 D). It has been interesting to investigate the morphology of organoids we obtained as it is a key parameter for assessing healthy organoids. The morphology of sALS-organoids compared with CTRL and Q66K ones appear to be much different, revealing a struggling ability to grow during the expansion stage. That impacts on the size but not on the ability to differentiate (Figure 22.1 D). Indeed, sALS organoids were able to organize the VZ/cortical structures like the CTRL organoid. Further comparison analysis between the CTRL with Q66K organoids showed no structural differences. This suggests that the mutation Q66K-*MATR3* did not have any impact either on the organoid formation and growth and cell differentiation. The same outcome was observed during the EB's formation of the Q66K#44 cell

line; where we reported a normal EBs formation in the Q66K#44 cell line, in contrast, it was reported to the shMATR3 ability to form the EBs (Figure 12B).

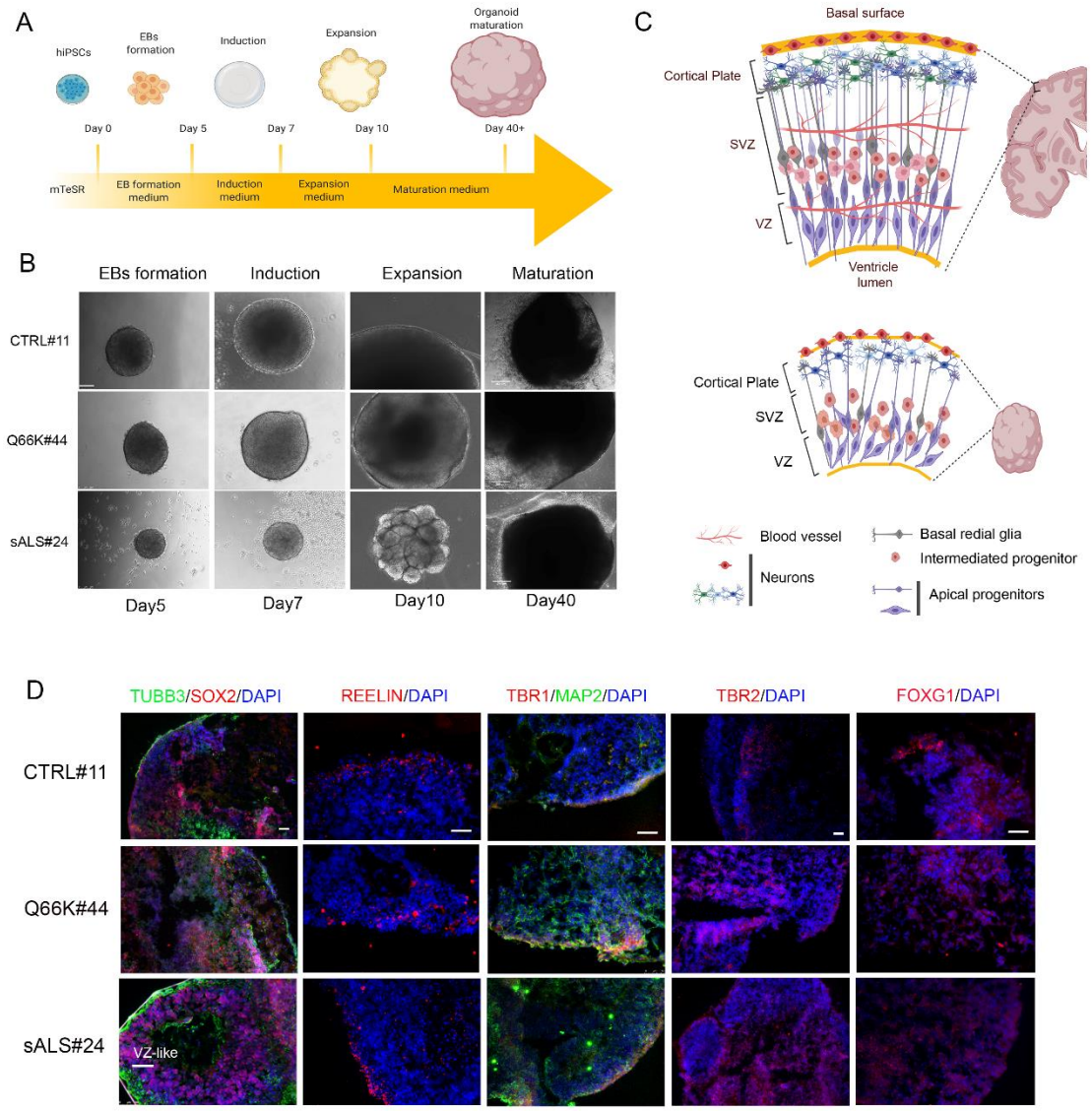

Figure 22.1 Generation of patients brain organoids

(A) Schematic timeline of organoid culture. **(B)** Time-lapse of organoid culture arising from iPSCs deriving from a healthy donor (CTRL#11), fALS (Q66K#44) and sALS (sALS#24) patients. EBs formation, Induction and Expansions pictures scale bar: 100µm; maturation pictures scale bar: 250 µm. **(C)** Schematic representation of a human brain and mature organoids structures (Di Lullo and Kriegstein, 2017; Qian, Song and Ming, 2019). **(D)** Immunohistochemistry revealed the morphology of an immature brain organoid, with the presence of a structured VZ zone and cortical plate. Different markers were used to label the VZ/Cortical plate regions, (SOX2 and TBR2), cortical neurons (TBR1, TUBB3 and Reelin). Scale bar: 50µm.

One of the main aims of setting up 3D organoid models was their suitability for new drug screening (Liu *et al.*, 2016).

We then verify if we could test some drugs under oxidative stress conditions. We hypothesized the involvement of Q66K mutation on MATR3 roles in DNA damage response.

We aimed to set up a system allowing us to study live organoid response to stress with a possible high throughput drug screening approach. We treated the organoids with hydrogen peroxide (H2O2) (1mM) for 24 hours to create oxidative stress, and consequently, we evaluated the viability/mortality of cells (Figure 22.2 E). We observed an increase in the mortality rate under the oxidative stress in both patients' organoids respect to control. sALS organoids may show a significant increase in cell death due to the smaller shape and greater accessibility to the core of the organoid by the drug. Similarly, Q66K organoids have a higher number of cell death in the core of the organoids respect to control organoids. This outcome may indirectly support the *MATR3* mutation could be correlated with the loss of cell capacity to respond to the stress stimuli like oxidative stress.

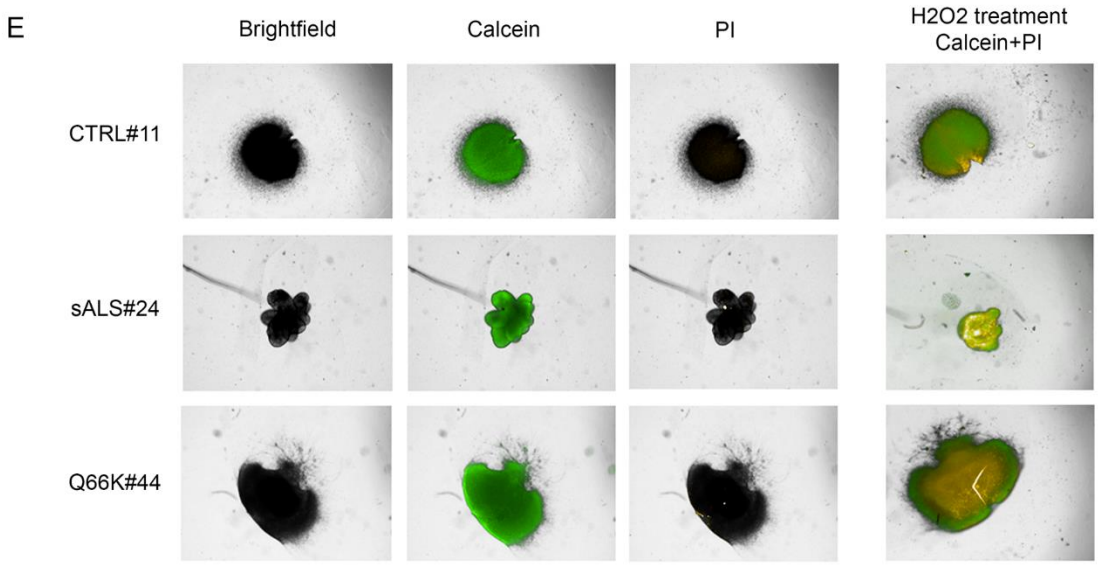

Figure 22.2 Generation of patients brain organoids

(E) LIVE/DEAD Viability/Cytotoxicity assay performed on CTRL#11, sALS#24 and Q66L#44 organoids. In the right of the panel, organoids were treated with two mM of hydrogen peroxide for 24 hours. The images were acquired with the Operetta High Content Screening System using 2X objective 0.08NA.

4 DISCUSSION

Despite some MATR3 mutations, i.e. S85C, F115C, Q66K, have been reported to be associated with ALS (Johnson et al., 2014; Boehringer et al., 2017; Leblond et al., 2016; Xu et al., 2016; Marangi, Lattante, Niccolò, et al., 2017) the molecular mechanism(s) responsible or co-responsible for the neuropathology is still unknown. In this work, we took efforts to characterize better the cellular role of MATR3, evaluating the effects of its silencing on iPS cells, a powerful resource that could provide great insights into MATR3 functions in the early stages of development and pluripotency state. Indeed, we first found out that developmental and self-renewal abilities appear to be altered by the downregulation of MATR3 in iPS cells. First of all, we showed how MATR3 silencing does not affect viability or proliferation in normal culture conditions (Figures 11D and 11E) while it is fatal in suboptimal culture conditions (Figure 11G). That suggests MATR3 may be crucial for iPS cells survival capacity.

Surprisingly, our data show that the downregulation of MATR3 had a significant impact on the correct mRNA and protein expression levels of the master stemness factors, i.e. OCT4 and NANOG but not SOX2 (Figure 14). SOX2 independence from MATR3 expression would ensure stemness maintenance even if OCT4 and NANOG were deregulated. Recent studies report that transcription factors rarely act alone, but rather transcription activity is finely orchestrated by several other factors (Wong, Chambers and Mullin, 2016). By the way, the improper stemness status could have significant implications in a loss of the physiological cell balance. The balance between self-renewal and differentiation states in PSCs could be critical for tissue homeostasis, and it was demonstrated how ROS regulate this balance (Mohyeldin, N-Muvdi and Quin˜ones-Hinojosa, 2010; Bigarella, Liang and Ghaffari, 2014a; Cie *et al.*, 2017). The redox state is essential for stem cells because it can influence the fate decision of stem cells (Lee *et al.*, 2018). Low level of double-strand breaks DNA damage due to stress conditions, must be repaired by NHEJ or HR but otherwise, a rapid accumulation of DNA damage could lead the cell to differentiate or undertake an activation of the apoptosis pathways (TeSlaa, Setoguchi and Teitell, 2016). MATR3 was found to be a target for ATM in the DNA damage response pathway and was found to interact with SFPQ/NONO complex that has a role in DNA strand break rejoining (Salton *et al.*, 2010; Nishida *et al.*, 2017). Our MS data (Table2) reported the interaction between MATR3 and RBM14, which is crucial for the recruitment of Ku70/80. Moreover, we observed that the cellular response to the camptothecin treatment was different between control and shMATR3 iPSCs.

Indeed, we observed an increase in response to DNA damage in shMATR3 cells measured as H2AX phosphorylation levels (Figure 13). That can suggest an interaction between MATR3 and RBM14 to activate the NHEJ response.

Furthermore, we wanted to assess whether the alteration of the tuning of stemness potential could have significant implications during spontaneous and induced differentiation, and we evaluated whether MATR3-silenced cultures behaved differently respect to control cells. We observed profound differences between shCtrl and shMATR3 iPS cells during the EBs formation, in both morphology and expression of specific trilineage markers (Figures 12A, B, C, D and E). We hypothesized that shMATR3 cells were not able to aggregate well to form regular EBs due to the initial EBs low number. Indeed, shMATR3-EBs formation was induced starting from smaller and less healthy colonies of shMATR3 iPS cells in comparison with shCtrl cells because of sub-optimal conditions to which iPS cells have to been subjected for the correct attainment assay (Figure 11G) (Lin et al., 2014). Moreover, the irregular shape could be responsible for altered axis formation in EBs changing germ layers specification (Fuchs and Pasteiner, 2012). Our data show that the silencing of MATR3 could also affect neural commitment. In shMATR3-silenced cultures, we found a higher number of the rosette, peculiar structures formed by NPCs during neural induction, which are also characterized by bigger lumens (Figures 12G and H). In several works, neuroepithelial rosettes are used as a model for early neurulation events underlying the implications of their cytoarchitecture in their differentiative potential (Curchoe, Russo and Terskikh, 2012). In addition to this, we also evaluated the effect of MATR3 depletion during the maturation of the neurons. Reduced numbers of neurites and neurite arborization were present in shMATR3 hiPSC-derived neurons following the long-term neuronal culture of 41 days (Figure 12I). Changes in morphology, arborization and synapse formation have been observed in association with ALS/FTD in patients, animal models, and *in vitro* models (Starr and Sattler, 2018). Moreover, in accordance with our data, affection of regular differentiative capacity by silencing of MATR3 was also demonstrated by Niimori-Kita in as much as the knockdown of MATR3 caused neuronal differentiation of NSCs in vitro and altered the cerebral layer structure of the fetal brain in vivo (Niimori-kita et al., 2018). These outcomes suggested an unexplored role of MATR3 in cell development, and so we decided to examine in-depth MATR3 cruciality in pluripotency maintenance mechanisms. We found that MATR3 regulated expression levels of some of the pluripotency master factors, i.e. OCT4, KLF4, NANOG and LIN28A (Figure 14). We investigated molecular mechanisms with which that regulation is determined. Here, we reported an active

role of MATR3 in post-transcriptional regulation of NANOG and LIN28A. MATR3 binds NANOG and LIN28A mRNAs changing their stability. Silencing of MATR3 decreases NANOG and LIN28A mRNAs stability (Figure 16). Furthermore, in PSCs, the mechanism of alternative splicing is quite common and increases proteomic diversity with a huge impact on lineage commitment and differentiation (Pritsker et al., 2005; Salomonis et al., 2010). Indeed, the regulation of isoforms synthesis significantly impacts on self-renewal-differentiation states balance by altering protein interaction networks or changing the cellular localization. MATR3 has been described as a splicing regulator (Coelho et al., 2015; Uemura et al., 2017) and to bind NANOG mRNA (Figure 16), we hypothesized a MATR3 acting on NANOG alternative splicing. Indeed, NANOG mRNA is reported to be regulated by alternative splicing, resulting in three different products: two codings (with different capacities for self-renewal and pluripotency) and one non-coding protein (Das, Jena and Levasseur, 2011). Unfortunately, our investigation does not report reliable data (Data not showed). The involvement of MATR3 in the control of pluripotency circuitry emerged after GO analyses were conducted on MATR3 interactors identified by MS (Figure 15). Data confirmed that MATR3 has a critical role in RNA metabolism and but even in translation. First of all, we verified that partially MATR3 also localizes into the cytoplasm and not only in the nucleus as it has been reported in the literature so far (Salton *et al.*, 2011; Gallego-iradi *et al.*, 2015; Iradi *et al.*, 2018) (Figures 17A, B, C and D). We suppose that MATR3 is able to translocate from the nucleus to the cytoplasm through nucleopores. In fact, in accordance with MS analysis we performed, MATR3 physically interacts with nucleopore proteins (NUP 205, NUP 93), suggesting a probable shuttling. In addition to this, MS data reveal as MATR3 binds proteins like eIF4A1, eIF4A3, eIF3CL, eIF3D and eIF3F (Table2), which are required for loading mRNAs to 40S ribosomal subunits to form a 43S preinitiation complex (Marchione, Leibovitch and Lenormand, 2013) underlying the possibility of its role in translation mechanism. We also found interactions between MATR3 and NAT1, a protein involved in translation (Sugiyama et al., 2017), DHX9, which forms a complex with HNRNPK acting in RNA splicing and translation (Hartman et al., 2006; Salton, Elkon, Borodina, Davydov, Yaspo, et al., 2011) and L1TD1, a protein that is highly expressed in PSCs under the control of OCT4, NANOG and SOX2 with a role in pluripotency state maintenance through a wide variety of cellular processes including translation (Närvä et al., 2012; Stubb et al., 2015). All these indications led us to hypothesize a function of MATR3 in translation (Figures 17E, F, G and H). Our polysome profiling showed that MATR3 is mainly associated with the monosome fraction, and MATR3 silencing led to a marked decrease in the monosome and

polysomal peaks, suggesting a possible critical role in the assembly of the 80S complex. The mild reduction of nascent protein synthesis and the decrease of translational efficiency of specific, but not all, genes suggest that MATR3 is involved in the translation of a relevant subset of transcripts but not of the entire transcriptome. Coherently, mRNAs directly bound by MATR3 as *NANOG* and *LIN28A* showed a decrease of *NANOG* and *LIN28A* transcripts stability that can be explained by a MATR3-dependent reduction in polysomal loading. However, transcripts not bound by MATR3 underwent a decrease in polysomal loading, suggesting the indirect effects of MATR3 on translation. For example, the *SOX2* expression level was not dependent on MATR3, and MATR3 did not bound its transcript, but *SOX2* mRNA experienced impairment of translation efficiency. On the other side, *KLF4* changed expression level, was not bound by MATR3, and did not change its translation efficiency.

A different scenario emerged for OCT4, one of the essential stemness factors for the maintenance of self-renewal (Shi and Jin, 2010). OCT4 expression and translation were dependent on MATR3, but the *OCT4* transcript was not bound, nor its stability was affected by MATR3. Envisioning an indirect regulation by MATR3 and exploiting a MATR3 ChIP-seq performed in rat cells (Skowronska-Krawczyk *et al.*, 2014), we identified a new gene regulatory network, in which MATR3 transcriptionally regulates *YTHDF1* expression binding to its promoter and, the encoded protein binds to the m^{6}A methylated *OCT4* transcript. YTHDF1 is a member of YTH domain proteins, a protein family defined as readers of N6-methyl-adenosine (m^{6}A) and plays a crucial role in mediating the translation of m^{6}A-RNAs (Liao, Sun and Xu, 2018; Bai *et al.*, 2019; R. Wu *et al.*, 2019; Zhuang *et al.*, 2019). m^{6}A RNA modification by METTL3 is required for maintaining the ground state of human ESCs (Batista *et al.*, 2015; Geula *et al.*, 2015) and METTL3 overexpression improves reprogramming efficiency. Therefore, the m^{6}A modification may play pivotal physiological functions in regulating RNA metabolism in pluripotency, leading to changes in the expression of key factors such as OCT4 (Chen *et al.*, 2015). YTHDF1 and YTHDF3 binding to m^{6}A modifications enhance mRNA translation, while YTHDF2 mediates degradation of m^{6}A transcripts (Chen *et al.*, 2015; Paris *et al.*, 2019). Moreover, YTHDF1 interacts with eIF3 and facilitates translation initiation (Wang *et al.*, 2015). In our model, YTHDF1 recognizes m^{6}A modifications on *OCT4* mRNA, and the downregulation of MATR3 affects negatively YTHDF1 expression, which suggests the indirect regulation of OCT4 expression by MATR3. In summary, our findings show the complex role of MATR3 in maintaining the pluripotency circuitry and introduces translation as a new layer of regulation functionally ruled by this pleiotropic protein.

To increase the reliability of our models, we decided to reprogram ALS patients' fibroblast cells, to recapitulate our findings in that more powerful cell model. The group of Mario Sabatelli, Institute of Genomic Medicine, Catholic University School of Medicine, kindly provided us with three fibroblast primary cell cultures derived from two different ALS patients and one healthy donor. One of the ALS patient-derived fibroblast lines was carrying the Q66K -MATR3 mutation (fALS), the other one was not carrying any known mutation (sALS). We got iPSCs arising from the above primary cell lines by using the non-integrating system and checked their quality (Figures 19 and 20). Successively, we have aimed to study the impact of Q66K mutation on iPSCs viability and their ability to differentiate randomly. Even in growth sub-optimal conditions, we did not report any anomalies in the viability and cell growth capacity (Figures 21A and B). This suggests MATR3 Q66K is not a crucial mutation for iPSCs survival capacity as not affecting wholly MATR3 functions, especially those associated with viability, as demonstrated in its downregulation. Moreover, we reported as MATR3 Q66K determines some aberrations during the differentiation of EBs carrying that mutation. Indeed, despite Q66K#27 cells were able to differentiate towards all three germ layer (Figure 19G), and no significant morphological differences were reported when compared with the CTRL#11 (Figure 21C), the expression of some mRNAs was found altered. We reported an increase of ectoderm (TUBB3) and endoderm (AFP) mRNAs expression markers, which was similar to the trend of expression observed in shMATR3 cells. This outcome supports our hypothesis about shMATR3 EBs formation difficulties. This was due to the deficit of shMATR3 cells to be as single cells/small colonies. The above deficit was not observed in Q66K#27 cells; furthermore, the mutation had an impact on the role played by MATR3 to allow the correct differentiation of iPSCs into the three germ layers (Figure 21D). This functional alteration of MATR3 caused by the Q66K mutation leads us to investigate the state of pluripotency maintenance factors. We did not report substantial differences in stemness pathways found in shMATR3 cells; however, it was found in Q66K#27 cells the downregulation of both mRNA and protein expression levels of NANOG, one of them the mRNA target of MATR3 previously identified, but no changs in LIN28A mRNA expression level. Furthermore, we reported an increase of mRNA and protein expression of SOX2, which was not reported in shMATR3 (Figures 21E and F). More investigations about the role of Q66K mutation are ongoing, such as its affection on target mRNA stability, even if the mutation is not in the RRM domains. Nevertheless, we reported an exciting aspect, the global translation efficiency in the Q66K#27 cell line resulted in decreased when compared with the CTRL#11 cells (Figure 21G). This outcome suggests the

involvement of Q66K mutation on the ability of MATR3 to play its role during translation, as already presented above. One of our studies aims to determine and characterize the impact of the mutation on cell phenotype. Like the cells, we used for the study carry heterozygous MATR3 mutation; we observed a peculiar phenotype associated with interest mutation. Our data suggest Q66K is a recessive mutation as it does not affect the morphology of iPSCs and EBs and their viability as contrarily observed in MATR3-silenced cells; the wild-type allele can overtake the mutant protein and to be sufficient for the normal cellular physiology. Nevertheless, the mutation has a significant impact on some other molecular mechanisms involving MATR3 protein as differentiation and self-renewal and protein translation. Since this impact has a trend similar to what observed in MATR3-silenced cells, Q66K MATR3 acts as a recessive mutation inactivating the gene and leading to a *loss of function*. So far, we do not have all the pieces yet to put together the all jigsaw puzzle, but we can speculate the different effects of Q66K MATR3 mutation could be explained as the protein functional domains (and their associated functions) differently are affected by the mutation.

The main advantage of using the iPS derived from the patients is not just the possibility of investigating the MATR3 role during the early stages, but also the possibility of having a reliable picture of events happening during the differentiation. To investigate the affection of the MATR3 Q66K mutation during the neuralization and neuron formation processes, we decided to differentiate the Q66K#44 cells into motor neurons (ongoing) and into brain organoids (Lancaster *et al.*, 2013). The 3D model offered us the possibility to obtain the brain "in a dish" is a compelling and informative model (Figure 22). We successfully obtained the immature 42 days-old brain organoids from the hiPSCs derived from health donor, and ALS patients. All organoids were able to generate organized structures, with an internal stemness zone, VZ, and an external cortical plate zone with mature neurons (Figure 22D). Moreover, it was possible to compare the morphological shape of 3D structures derived from the three different hiPSCs lines. We observed morphological abnormalities in the sALS#24 organoids to form good size organoids (Figure 22B). However, the small size did not impact on the ability to form the specific areas of the brain (Figure 22D). Indeed, sALS#24 organoids were able to organize the VZ/cortical structures like the CTRL organoids. Further comparison analysis between the CTRL#19 with Q66K#44 organoids showed no evident structural and morphological differences. This suggests that the mutation MATR3 Q66K does not have any impact on the differentiation ability. The same outcome was observed

during EBs formation process of Q66K#44 cells (Figure 19); in contrast to what reported for the shMATR3 cells ability to aggregate in EB structures (Figure 12B).

Then, with the aim to generate a 3D model able to be used for a potential drug screening, we set up a model of stress *in live*. We treated organoids with hydrogen peroxide (H_2O_2) (1mM) for 24 hours to create oxidative stress, and consequently, we used the LIVE/DEAD Viability/Cytotoxicity assay to evaluate the response of organoids. We observed an increase in the number of cell death upon the stress induction in both patients-deriving organoids (Figure 22E). sALS organoids may be showing a significant increase in death due to their smaller size and the consequent greater accessibility to the core by the drug. On the contrary Q66K MATR3 organoids higher rate of mortality may be due to the effect of the mutation. This outcome supports our hypothesis for which the oxidative stress condition in ALS patients have a significant impact on cell viability as reported in some studies (Hand and Rouleau, 2002; Coppedè and Migliore, 2015; Hall *et al.*, 2017; Xiao *et al.*, 2018). Moreover, this data could open a new window to link MATR3 and DNA damage response in neurodegeneration and also highlight the usefulness of this model for a drug screening.

4.1 Future perspectives

This work elucidated the role of MATR3 in hiPSCs, bringing to light for the first time cytoplasmatic functions of MATR3 outside of the nucleus in healthy condition. Its involvement in translation could elucidate and help to understand the cases of fALS carrying mutations on MATR3. Indeed, the most critical aspect to understand in the future is the roles of mutations that affect MATR3. The next step will be to consolidate the data obtained, to understand if the Q66K mutation is involved in the RNA binding role of MATR3 and, consequently, affect its role in the stability of mRNAs. We have to elucidate how Q66K MATR3 modulates the expression of SOX2 positively. We reported in part how the Q66K mutation might influence the role of MATR3 in translation; this outcome open interesting perspectives, in the immediate future we will study by polysome assay if the Q66K affects the ability of MATR3 to form the 80S complex reported previously, and this experiment could elucidate better if the mutation is involved in MATR3 translation roles. Moreover, it remains interesting to understand how the mutations reported at the beginning of the MATR3 (Q66K, A72T, S85C, F115C, R147W, G153C, and P154S) affects its roles. This mutation afflicts the protein outside its active domains, such as the RRMs and ZF domains; this can suggest

a structure modification, that in Q66K can bother the MATR3 interactions with proteins involved in translations such as DHX9, DDX3X, and RPS25. Moreover, these last proteins cited were found to play an essential role in the translation of C9ORF72 (Cheng *et al.*, 2019; Yamada *et al.*, 2019). If this hypothesis could be proven, it will be possible to expand the cases of fALS that are possible to cure with a drug that can help the function of MATR3 in translation. Nevertheless, it remains interesting to investigate the localization of Q66K MATR3 in MNs and its role during the differentiation. Furthermore, we will able to investigate it also in 3D models, with an interesting perspective to design a drug screening on it. Moreover, it remains to be seen the involvement of MATR3 in the DNA damage and how it can affect the MNs.

5 EXPERIMENTAL PROCEDURES

Cell Culture and generation of stable cell line

Human Episomal Pluripotent Stem Cell (hiPSC) line (Gibco, A18945) was cultivated on Geltrex (Thermo Fisher Scientific) coated plates in TeSR-E8 Medium (STEMCELL) according to the manufacturer's indications. Cultures were passaged by using 0.5 mM EDTA as the detaching agent. To establish the MATR3-silenced line, cells were infected with MATR3 shRNA or control shRNA lentivirus (MISSION shRNA NM_018834 and PLKO.1-puro respectively, Sigma-Aldrich) and selected with 1ug/mL puromycin. Lentiviral particles were generated in HEK293T cells by co-transfecting the Δ891 and VSV-G encoding vectors along with the shRNA transfer lentiviral plasmid PLKO and shMATR3 plasmid (Thongon *et al.*, 2018). Patient-derived and healthy volunteer (HV)-derived fibroblasts were provided by the ALS Center of the NEMO Clinical Center (Rome, Italy). Fibroblasts were cultured in DMEM (Sigma-Aldrich) medium containing 20% of Fetal Bovine Serum (FBS), penicillin/streptomycin and Glutamax (Sigma-Aldrich). The human episomal iPSC line A18945 is a commercially available strain derived from CD34+ cord blood using a three-plasmid, seven-factor (SOKMNLT; SOX2, OCT4 (POU5F1), KLF4, MYC, NANOG, LIN28, and SV40L T antigen) EBNA-based episomal system (Thermo Fisher catalogue number A18945). Reprogrammed iPSCs and A18495 iPSCs were grown in TeSR-E8 (STEMCELL) medium on Geltrex (Thermo Fisher Scientific)-coated plates (Costar).

Reprogramming procedures

iPSC reprogramming Patient's and HV's fibroblasts were reprogrammed using the Episomal iPSC Reprogramming Plasmids (SBI System Biosciences), following manufacturer's indications. Cells were electroporated with the Amaxa Nucleofector 2D (Lonza), using the P-022 program and seeded on Geltrex-coated wells in complete DMEM medium. The following day, fibroblast medium was replaced with N2B27 medium (DMEM/F12 with Hepes, N2 1%, B27 2%, MEM Non-Essential Aminoacids, Glutamax, β-mercaptoethanol 55 µM), supplemented with FGF-2 (100 ng/ml, STEMCELL). The medium was refreshed every other day for two weeks. When colonies with iPSC-like phenotype started to appear, N2B27 medium was replaced with TeSR-E8. After 28 days from the nucleofection, colonies with a clear hiPSCs morphology were picked and expanded. Q66K#44DRM clone and HV clone had been selected for further characterization.

Cell assays

Viability assay was performed on cells cultured for 96h. Every 24h, OZBlue assay (OZbiosciences) was performed by incubating the plates at 37°C for 4h following the manufacturer's protocol. Absorbance was detected at 570nm by Infinite M200 (Tecan) plate reader. Cell proliferation of hiPSCs was measured using a Click-iT EdU Imaging Kit (Thermo Fisher Scientific) according to the manufacture's indications. For EdU incorporation, cells were labelled by incubation with 1µM EdU for 2h at 37°C. Labelled cells were immediately fixed with 3.7% formaldehyde in PBS and permeabilized by 0.5% Triton X-100 for 30 min at RT, followed by EdU detection using 10µM Alexa Fluor-488 for 45 min at RT. Standard flow cytometry method was used then to determine the percentage of S-phase cells in the population. Alkaline Phosphatase Live Stain (AP) (Thermo Fisher Scientific), was assessed following the manufacturer's protocol by incubating cell cultures at 37°C for 30 min. Images were acquired with the Operetta High Content Screening System (Perkin Elmer) using 2X objective 0.08NA and analysed using the software Harmony 4.1 (Perkin Elmer). The number of cell colonies and the number of single cells were counted, and the intensity of the fluorescent signal was measured for both populations. LIVE/DEAD Viability/Cytotoxicity Kit (Invitrogen) was performed according to the manufacturer's specifications. Briefly, was incubated 1h of LIVE/DEAD solution (1:1) with a singular organoid before to acquisition with the Operetta High Content Screening System (Perkin Elmer). To verify the DNA damage response in organoids was used the LIVE/DEAD Viability/Cytotoxicity Kit, as specificated, after the treatment of hydrogen peroxide (H_2O_2) 1mM for 24 hours.

EB formation and morphometric parameters

EBs assay was performed by plating hiPSC clumps in ultralow attachment plates (Voden) in TeSR-E8 Medium supplemented with 2 mg/mL of PVA (polyvinyl alcohol, Sigma-Aldrich) and 10 µg/ml of Y-27632 ROCK inhibitor (MACS, Miltenyi Biotec) for one day. Then, cell aggregates were shifted to a 1:1 mix of Essential 6 medium (E6 medium, Thermo Fisher Scientific) and TeSR-E8 Medium supplemented with 2 mg/mL of PVA for two days. After two days, the medium was replaced with Essential 6 medium. After one week, Embryoid Bodies were collected and plated on Geltrex-coated plastic 6-well plates and let to differentiate for further 7 days in Essential 6 medium. The medium was renewed entirely every other day. Brightfield cultures' images were captured with a Leica DM IL LED microscope equipped with a DFC450C digital camera (Leica Microsystem). EBs Images were also acquired with the Operetta High Content Screening System (Perkin Elmer) using 2X objective 0.08NA, and EBs count and morphometric properties were calculated using the software Harmony 4.1 (Perkin Elmer). Elongation distortion index (EDI) expressed the extent of axial elongation and was calculated as (1/[circularity]-1) using ImageJ software, as previously reported (Warkus *et al.*, 2016).

Neuronal differentiation (2D)

Motor neuron differentiation was performed as previously described (Jha, Rao and Malik, 2015). Briefly, hiPSCs were seeded on Geltrex-coated 6-well plate in TeSR-E8 Medium supplemented with 10 µM Y27632. The following day, cells were exposed to PSC Neuronal Induction Medium (NIM, Thermo Fisher Scientific). At day 7, cultures were dissociated and replated in NIM supplemented with 10 µM Y27632. The following day, the medium was replaced by the fresh medium without Y27632. From day 10, the presence of Neural Progenitors cells (NPCs) was checked by live membrane-permeable fluorescent probe NeuroFluor CDr3 (STEMCELL). When NPCs reached the 80% of confluence, the medium was shifted to StemPro ESC SFM (Thermo Fisher Scientific) supplemented with 1µM Purmorphamin (Pur) (MACS, MilenyiBiotec), 50µM Retinoic Acid (RA) (Sigma-Aldrich), 8 ng/mL FGF-2 (Voden) and 10 ng/mL Activin (Voden). At 100% confluency, cultures dissociated by using Accutase (Thermo Fisher Scientific) and replated on polyornthine/laminin-coated plastic in StemProhESC SFM medium supplemented with 10 ng/mL BDNF (Miltenyi Biotec) and 10 ng/mL GDNF (Voden). The medium was replaced every other day.

Generation of brain organoids (3D)

General brain organoids were performed by using the commercial kit STEMdiff™ Cerebral Organoid Kit (STEMCELL Technologies), derived by the Lancaster's protocol (Lancaster *et al.*, 2013). Briefly, the protocol is dived in 4 steps; 1) EB formation (0-5 days), 9.000 hiPSCs were semed in 96 U-bottom well in 100 µL of media. After 2 days was added 100 µL of new media. 2) Induction (5-7 days), the EBs were moved in 24 wells with a new media, the induction media in 0,5 of final volume per well. 3) Expansion (7-10 days), the organoids were inserted to drops of Matrigel (SACCO) and left for 30 minutes at 37°C. After were collected in 6 well in Expansion Medium. 4) Organoid Maturation (10-40+ days), the Expansion Medium was changed with the Maturation Medium, and the plate was placed on the orbital shaker in the incubator. Every four days, the medium was replaced for 42 days.

Cell extracts and Western Blot Analysis

Samples were lysed in RIPA lysis buffer supplemented with Protease Inhibitor Cocktail (Thermo Scientific). Equal amounts of proteins were separated on 10% SDS-PAGE and blotted onto PVDF membrane (GE Healthcare). Primary and secondary antibodies used are reported in Table2. The immunoreactive signals were detected by incubation with Amersham ECL Selected (GE) and acquisition with the Chemidoc Imaging System (BioRad).

RNA extraction and real-time PCR

Total RNA was extracted by Trizol Reagent (Thermo Fisher Scientific) according to the manufacturer's protocol and then retro-transcribed with RevertAid RT Reverse Transcription Kit (Thermo Fisher Scientific). cDNAs were used to verify the expression of specific target genes by RT-PCR (primer sequences are reported in Table3) by using the KAPA SYBR FAST qPCR Master Mix (2X) kit (Kapa Biosystems) according to the manufacturer's specifications. qRT-PCR data were analysed according to the comparative ΔΔCt method and normalized by using β-ACTIN and/or RPLP0 housekeeping gene.

Immunocytochemistry and fluorescence microscopy

Cultures were gently washed in pre-warmed PBS and then fixed in 4% PFA (Sigma-Aldrich) in PBS pH 7.4 for 15 min at room temperature, permeabilized with 0.3% Triton X-100 in PBS for 10 min, and then incubated in blocking solution (PBS, 5% FBS, 0.2% Triton X-100) for 90 min. Incubation

with primary antibodies was performed overnight at 4°C in antibody solution (Ab dilutions indicated in Table2). Incubation with the appropriate Alexa Fluor secondary antibodies (Thermo Fisher Scientific) was performed at room temperature for 1h followed by nuclei were counterstained with 1 µg/ml Hoechst 33258 or DAPI (Thermo Fisher Scientific) for 10 min at room temperature. Fluorescent signals were acquired using different instruments: i) Leica DM IL Led Fluo microscope and Leica DFC450 C (Leica Microsystem) camera, ii) Operetta High Content Screening System (PerkinElmer) using 20x 0.75NA and 40x 0.95NA objectives, iii) Zeiss Axio Observer Z1 equipped with Colibri 1, ApoTome 1 and Cell Observer modules, iv) Nikon Eclipse Ti2-E equipped with spinning disc unit and VCS. Neural rosettes analysis was carried out by plating $1.8*10^4$ NPCs in CellCarrier-96 Black plate (PerkinElmer). Rosettes and neurites outgrowth was calculated by analysing the images with Columbus 3.5.2 software (PerkinElmer). MAP-2/βIII-TUBULIN/SYNAPTHOSIN-positive cells were selected and analysed for neurites morphology by using the neurite tracing algorithm (CSIRO Neurite Analysis). Localization and co-localization analysis were performed by ImageJ Fiji software. The count of MATR3 green-positive dots in the nuclear and cytoplasmic regions was performed by using the ImageJ "Find maxima" plugin, on maximum intensity projection. Images' pre-processing before the dots count analysis only involved uniform denoising and background subtraction steps. The total number of nuclear or cytoplasmic dots was then divided by the number of nuclei present in each field of view. The colocalization analysis between eIF3A and MATR3 was performed on 3D (x,y,z) images of single cells, considering only the cytoplasmic area of each cell. Images' pre-processing before colocalization analysis only involved uniform denoising and background subtraction steps. The total number of eLF3A and MATR3 dots, as well as the total number of MATR3 dots touching eLF3A dots, was evaluated by using the ImageJ "DiAna v.1.47" plugin (Gilles *et al.*, 2016). DiAna plug-in settings were optimized for successful detection and segmentation of the spot-like structures corresponding to eLF3A or MATR3 fluorescent signals and were kept constant for all the analysed images. Data obtained from the colocalization analysis were represented by the Venn diagram obtained from the "Venn Diagram Plotter Integrative Omics" software (https://omics.pnl.gov/software/venn-diagram-plotter).

Cerebral organoids were collected after 42 days and fixed in 4% PFA overnight at 4°C, followed by three wash in PBS 1x and incubation in 20% sucrose solutions overnight at 4°C. Tissue sections were stained with eosin before to collect in optimal cutting temperature compound, (OTC) (Leica). Tissue sections were sectioned with a cryostat (Leica) into 20 µm thick sections. For the

immunohistochemistry, sections were permeabilized in 0.3% of Triton-X solution in PBS and blocked with blocking solution and immunolabeled overnight at 4°C using primary antibodies: SOX2 (GeneTex), TUBB3 (Invitrogen), TBR1, TBR2, Reelin and FOXG1 (GeneTex) and MAP2 (SantaCruz). Secondary antibodies Alexa Fluor 488 and Alexa Fluor 594 were used.

Immunoprecipitation assay and Mass Spectrometry analyses

Immunoprecipitation (IP) was performed as previously described (Bonifacino, Gershlick and Angelica, 2016). Briefly, hiPSCs were lysed in Lysis Buffer (20 mM Tris–HCl at pH 7.5, 100 mM KCl, 5 mM $MgCl_2$, and 0.5% NP-40) and subjected to IP by using anti-MATR3 IgG-IP control with a mixture of Dynabeads® Protein A and protein G (Thermo Fisher). These were incubated with MATR3 antibodies or normal IgG at 4°C for 1h, and then incubated with lysate overnight at 4°C. Beads were washed three times with washing buffer (0.05% Tween20 and 50 mM ammonium bicarbonate pH 8) and additional three times with 50 mM ammonium bicarbonate, to remove any residual detergent. Bound protein complexes were eluted with urea buffer (8M Urea, 100 mM ammonium bicarbonate pH 8), reduced using 10 mM DTT for 1 hour and alkylated with 20 mM iodoacetamide (IAA) in the dark for 30 minutes at room temperature. Subsequently, the proteins were digested with 0.5 µg Lys-C (Promega) for 4h and then diluted in 50mM ammonium bicarbonate in water before being further digested with 1 µg trypsin overnight at room temperature. Resulting peptide solution was desalted on C18 stage-tips and vacuum dried before being resuspended in 20 µl of 0.1% formic acid buffer for LC-MS/MS analysis. Samples were analyzed using an Easy-nLC 1200 system coupled online with an Orbitrap Fusion Tribrid mass spectrometer (both Thermo Fisher Scientific, San Jose, CA, USA). A reversed-phase column (Thermo Fisher Scientific, Acclaim PepMap RSLC C18 column, 2µm particle size, 100Å pore size, id 75 µm) with a two-component mobile phase system of 0.1% formic acid in water (buffer A) and 0.1% formic acid in acetonitrile (buffer B) was used for separating the digested peptides. Peptides were eluted using a gradient of 5% to 25% over 52 minutes, followed by 25% to 40% over 8 minutes and 40% to 98% over 10 minutes at a flow rate of 400 nL/min. The data-dependent acquisition (DDA) method is based on full scans performed at 120.000 fwhm resolving power (at 200 m/z) and an AGC target of $1x10^6$. Full scans were followed by a set of (HCD) MS/MS scans over 3 sec cycle time, at a collision energy of 30%, 150 ms of maximum injection time (ion trap) and AGC target of $5x10^3$. A mass range of 350-1100 m/z was surveyed for precursors, with

first mass set at 140 m/z for fragments. The DDA data files were searched in Proteome Discoverer 2.2 software (Thermo Fisher Scientific). Peptides searches were performed using Human protein FASTA file (UniProt, reviewed, downloaded July 2019). Proteins were identified using the SEQUEST HT search engine using precursor mass tolerance of 10 ppm and product mass tolerance of 0.6 Da. Trypsin was chosen as the enzyme with 3 missed cleavages, and static modification of carbamidomethyl (C) with variable modification of oxidation (M) was incorporated in the search. PSMs and protein false discovery rate were filtered for <0.01. Peak intensities were log2 transformed. Data were then normalized by the average of the protein abundance with each sample to account for variation in sampling volumes. The significant abundance of differences between conditions was determined using a t-test. The Gene Ontology enrichment analysis was performed with FunRich software (http://www.funrich.org) (Pathan *et al.*, 2015). Protein-protein interactions were also calculated by STRING interaction database (https://string-db.org/) (Mering *et al.*, 2003). Only high confidence interactions, as determined by the STRING database, were accepted. Proteins are represented as nodes.

RNA Immunoprecipitation Assay

RNA Immunoprecipitation (RIP) assay was performed as described (Keene, Komisarow and Friedersdorf, 2006). Briefly, 1,2 x 10^7 hiPSCs were lysed in 20 mM Tris–HCl at pH 7.5, 100 mM KCl, 5 mM $MgCl_2$, and 0.5% NP-40 for 10 min on ice and centrifuged at 15 000 × g for 10 min at 4°C. A mixture of Dynabeads Protein A and protein G (Thermo Fisher) were incubated with YTHDF1 or MATR3 antibodies or normal IgG at 4°C for 1h, and then incubated with lysate overnight at 4°C. The beads were washed with NT2 buffer (50 mM Tris–HCl [pH 7.5], 150 mM NaCl, 1 mM $MgCl_2$, 0.05% NP-40). RNA was purified from the supernatant using TRIzol Reagent following the procedure described before and used for RT-qPCR validation.

ChIP-seq analysis and ChIP

Bedgraph-format data were obtained from GEO with ID GSM1399416 (Skowronska-Krawczyk *et al.*, 2014), and peaks were called with MACS2 (Zhang *et al.*, 2008), using the *bdgpeakcall* command with default parameters. HOMER (Heinz *et al.*, 2011) was then used to annotate the closest gene to each peak (*annotatePeaks* command) and to detect consensus motifs (*find Motifs* command with scrambled input sequences obtained with the *scramble Fasta* command as background) from the 100 nucleotides surrounding the peak centre of the 500 most significant

peaks obtained, ranked by their peak score (-10*log10p-value). The two most significant motifs, as ranked by their p-value, were retained. Gene Ontology enrichment analysis was performed with HOMER (Heinz *et al.*, 2011) (*annotatePeaks* command with *-go* option) on all three branches (BP, MF, CC), using a 0.05 threshold on Benjamini-Hochberg adjusted p-value. The Gene Ontology enrichment results were plotted with REVIGO (Supek *et al.*, 2011) (XY plot with 0.7 similarity threshold). Chromatin Immunoprecipitation (ChIP) was performed as described previously (Ciribilli *et al.*, 2010; Bisio *et al.*, 2013; Thongon *et al.*, 2015).

Click-it and Polysome analysis

The global protein synthesis was evaluated by the Click-iT™ Plus OPP Alexa Fluor™ Protein Synthesis Assay Kit (Thermo Fisher), according to the manufacturer's specifications. Polysome analysis was performed as described in (Provenzani *et al.*, 2006; Viero *et al.*, 2015). Briefly, shCtrl and shMATR3 cell lines were grown on 10 cm Petri dishes with TeSR™-E8™medium. Cells were incubated in medium supplemented with cycloheximide (0.01 mg/ml) for 10 min. Then cells were washed three times with cold PBS plus cycloheximide (0.01 mg/ml) and lysed with the lysis buffer (10 mM NaCl, 10 mM $MgCl_2$, 10 mM Tris–HCl pH 7.5, 1% Triton X-100, 100 U/ml of RNase inhibitors from human placenta (NEB), 1 mM DTT, 0.01 mg/ml cycloheximide, 0.1% NaDeoxycholate, proteinase inhibitor mixture (Roche)). Samples were ultracentrifuged at 180 000 × g for 100 min at 4°C. The sedimentation profiles were monitored by absorbance at 254 nm using an ISCO UA-6 UV detector, and 1 ml of each fraction was collected. For Western blot analysis, proteins precipitated with TCA and acetone, and the pellets were solubilized directly in pH 8 Laemmli buffer.

mRNA stability analysis

The mRNA stability analysis was performed to determinate mRNA half-life in shMATR3 and shCtrl cultures. Cells were treated with 5 µg/mL of Actinomycin D (Thermo Fisher) for 1 to 5h. After RNA extraction, described previously, an RT-qPCR was performed with β-ACTIN used as housekeeping to normalize. The results are expressed as percentages of mRNA abundance relative to time 0.

STR analysis

Microsatellites amplification was carried out by amplifying DNA with two multiplexes (one for chromosomes 13, 18 and 21 and the other for the X and Y chromosomes; Devyser Compact v3). PCR products were separated in ABI3100 capillary genetic analyser, and results were analysed by ABI Genotyper software.

Sequencing

The presence of p.Q66K mutation in the MATR3 gene in the Q66K#44DRM hiPSC, parental fibroblast and HV hiPSC genomes were confirmed by sequencing (Eurofins Genomics) of exon 1. Total RNA was extracted from both cell types and retro-transcribed as described above. The sequence was amplified by PCR using specific primers (Table 2). Amplicons were electrophoretically separated into 1% agarose gel and purified with QIAquik Gel Extraction Kit (Qiagen)

Karyotyping

hiPSCs were incubated overnight with Colcemid (0.05 mg/ml, Invitrogen) and then dispersed with 0.5% trypsin- 0.02% EDTA (Invitrogen). Cells were subsequentially washed with PBS and treated with 0.075 M KCl hypotonic solution and FBS for 20 min at 37 °C. The cells were then fixed with methanol: acetic acid (3:1, v/v) solution and stored for one h at −20 °C. The cell suspension was dropped on ice glass slides and stained in Giemsa stain after banding with GAG-acid solution at 55 °C. Karyotyping was performed at the resolution of 450 bandings by use of the Genikon software (Nikon Italia) and described in accordance to the ISCN 2016: An International System for Human Cytogenomic Nomenclature (2016) ISBN: 978-3-318-05857-4

Mycoplasma test

Mycoplasma contamination was checked by colourimetric mycoplasma detection assay (Invivogen) following the manufacturer's indications.

Statistical analysis

All statistical analyses were performed using GraphPad Prism 6 software (GraphPad Software Inc.). Tested used were: One-way ANOVA, Two-way ANOVA and t-test. Data were presented as

mean ± standard deviation (SD) or statistical error of the mean (SEM), as indicated for the specific experiment, indicated in the figure legend, P<0.05 was considered statistically significant.

6 TABLES

Master Protein Accessions	Prot. Fold change	p-value	Protein name
P43243	6,385420171	126,8568149	MATR3
P49750	5,10813107	128,7504999	YLPM1
P62136	4,599753054	21,93945622	PPP1CA
P36873	4,068648105	4,761787966	PPP1CC
P11166	3,940222428	6,916295447	SLC2A1
P53621	3,824889405	66,11922469	COPA
O14579	3,680314188	16,57754269	COPE
P50914	3,463430288	10,11816695	RPL14
P26599	3,432186349	23,2150442	PTBP1
Q5T8P6	3,220351138	21,38640402	RBM26
P46778	3,217896454	4,878452263	RPL21
P62140	3,097554344	6,779215136	PPP1CB
O95758	3,077931941	8,473611238	PTBP3
Q8NE65	3,027057491	5,399267087	ZNF738
Q96PK6	3,024088293	7,835599756	RBM14
P05141	2,961797847	8,890783104	SLC25A5
P11169	2,914285122	6,010646366	SLC2A3
P31943	2,87804725	20,23355441	HNRNPH1
P17844	2,864053456	15,3255438	DDX5
P12236	2,757882016	10,97832528	SLC25A6
P61313	2,704605694	6,954772445	RPL15
P62424	2,674798571	11,40695617	RPL7A
Q9UBC3	2,673711568	11,96255212	DNMT3B
P62280	2,661338745	14,0174627	RPS11
P62829	2,658434033	5,861470197	RPL23
P36578	2,63265714	27,28334811	RPL4
O00571	2,626014401	29,02739817	DDX3X
O15226	2,615267615	6,224881681	NKRF
P35606	2,555462493	24,33165719	COPB2
Q9H0A0	2,493269564	5,341412858	NAT10
P60842	2,483583903	27,65468418	EIF4A1
P62913	2,473980786	6,500998002	RPL11
P62241	2,472766868	23,7713726	RPS8
P46781	2,434638474	10,93824831	RPS9
P61353	2,367615668	8,011617784	RPL27
P33993	2,360012906	20,00183428	MCM7
Q9NR30	2,344338584	17,90328391	DDX21
Q07020	2,33071128	6,825082865	RPL18
P62910	2,321658538	9,511466001	RPL32
Q92841	2,319369824	19,72963909	DDX17
Q13838	2,306583165	7,96898671	DDX39B
P04181	2,303461076	7,331106427	OAT

P39023	2,292141808	14,21624444	RPL3
P27635	2,273914179	9,256199901	RPL10
P55265	2,224898245	18,85294258	ADAR
Q9H0D6	2,219670954	9,598867947	XRN2
Q9Y295	2,18517303	6,583070322	DRG1
P62906	2,180249741	10,24872111	RPL10A
P23396	2,128502064	15,06628478	RPS3

Table 2. Mass Spectrometry analysis. 151 proteins that were at least 1.5-fold enriched over IgG ($p \leq 0.05$)

Dataset item (Gene symbol)	Entrez ID	Gene symbol	Chromosome	Map location
MATR3	9782	MATR3	5	5q31.2
YLPM1	56252	YLPM1	14	14q24.3
PPP1CA	5499	PPP1CA	11	11q13
PPP1CC	5501	PPP1CC	12	12q24.1-q24.2
SLC2A1	6513	SLC2A1	1	1p34.2
COPA	1314	COPA	1	1q23.2
COPE	11316	COPE	19	19p13.11
RPL14	9045	RPL14	3	3p22-p21.2
PTBP1	5725	PTBP1	19	19p13.3
RBM26	64062	RBM26	13	13q31.1
RPL21	6144	RPL21	13	13q12.2
PPP1CB	5500	PPP1CB	2	2p23
PTBP3	9991	PTBP3	9	9q32
RBM14	10432	RBM14	11	11q13.2
SLC25A5	292	SLC25A5	X	Xq24
SLC2A3	6515	SLC2A3	12	12p13.3
HNRNPH1	3187	HNRNPH1	5	5q35.3
DDX5	1655	DDX5	17	17q21
SLC25A6	293	SLC25A6	X|Y	Xp22.32/Yp11.3
RPL15	6138	RPL15	3	3p24.2
RPL7A	6130	RPL7A	9	9q34
DNMT3B	1789	DNMT3B	20	20q11.2
RPS11	6205	RPS11	19	19q13.3
RPL23	9349	RPL23	17	17q
RPL4	6124	RPL4	15	15q22
DDX3X	1654	DDX3X	X	Xp11.3-p11.23
NKRF	55922	NKRF	X	Xq24
COPB2	9276	COPB2	3	3q23
NAT10	55226	NAT10	11	11p13
EIF4A1	1973	EIF4A1	17	17p13
RPL11	6135	RPL11	1	1p36.1-p35
RPS8	6202	RPS8	1	1p34.1-p32
RPS9	6203	RPS9	19	19q13.4
RPL27	6155	RPL27	17	17q21
MCM7	4176	MCM7	7	7q21.3-q22.1
DDX21	9188	DDX21	10	10q21

RPL18	6141	RPL18	19	19q13
RPL32	6161	RPL32	3	3p25-p24
DDX17	10521	DDX17	22	22q13.1
DDX39B	7919	DDX39B	6	6p21.3
OAT	4942	OAT	10	10q26
RPL3	6122	RPL3	22	22q13
RPL10	6134	RPL10	X	Xq28
ADAR	103	ADAR	1	1q21.3
XRN2	22803	XRN2	20	20p11.2-p11.1
DRG1	4733	DRG1	22	22q12.2
RPL10A	4736	RPL10A	6	6p21.31
RPS3	6188	RPS3	11	11q13.3-q13.5
RPL22	6146	RPL22	1	1p36.31

Table 3. Functional enrichment analysis of Gene Ontology categories from MS data analysed by FunRich software.

Sequence (Gene|chr|TSSpos|strand| ntsUpstreamTSS|ntsDownstreamTSS)	start	end	score	attributes
Actb|5|142906754|-1|30000|1000	7298	7305	0,956599	sequence=TGCCTTCA;pvalue=1.525879e-05
Actb|5|142906754|-1|30000|1000	8804	8811	0,956599	sequence=TGCCTTCA;pvalue=1.525879e-05
Actb|5|142906754|-1|30000|1000	14998	15005	0,956599	sequence=TGCCTTCA;pvalue=1.525879e-05
Actb|5|142906754|-1|30000|1000	10624	10631	0,951918	sequence=TCCCTGCA;pvalue=3.051758e-05
Alkbh5|11|60536381|1|30000|1000	14363	14370	0,951918	sequence=TCCCTGCA;pvalue=3.051758e-05
Fto|8|91313525|1|30000|1000	5045	5052	1	sequence=TGCCTGCA;pvalue=0.000000e+00
Fto|8|91313525|1|30000|1000	14472	14479	1	sequence=TGCCTGCA;pvalue=0.000000e+00
Gapdh|6|125166467|-1|30000|1000	19438	19445	1	sequence=TGCCTGCA;pvalue=0.000000e+00
Gapdh|6|125166467|-1|30000|1000	22343	22350	1	sequence=TGCCTGCA;pvalue=0.000000e+00
Gapdh|6|125166467|-1|30000|1000	21137	21144	0,956599	sequence=TGCCTTCA;pvalue=1.525879e-05
Igf2bp1|11|96005940|-1|30000|1000	19756	19763	1	sequence=TGCCTGCA;pvalue=0.000000e+00
Igf2bp1|11|96005940|-1|30000|1000	7564	7571	0,956599	sequence=TGCCTTCA;pvalue=1.525879e-05
Igf2bp1|11|96005940|-1|30000|1000	20285	20292	0,956599	sequence=TGCCTTCA;pvalue=1.525879e-05
Igf2bp1|11|96005940|-1|30000|1000	29880	29887	0,951918	sequence=TCCCTGCA;pvalue=3.051758e-05
Igf2bp2|16|22163299|-1|30000|1000	17924	17931	1	sequence=TGCCTGCA;pvalue=0.000000e+00
Igf2bp2|16|22163299|-1|30000|1000	6130	6137	0,956599	sequence=TGCCTTCA;pvalue=1.525879e-05
Igf2bp2|16|22163299|-1|30000|1000	19394	19401	0,956599	sequence=TGCCTTCA;pvalue=1.525879e-05
Igf2bp2|16|22163299|-1|30000|1000	23720	23727	0,956599	sequence=TGCCTTCA;pvalue=1.525879e-05
Igf2bp2|16|22163299|-1|30000|1000	15378	15385	0,951918	sequence=TCCCTGCA;pvalue=3.051758e-05
Igf2bp3|6|49214957|-1|30000|1000	8308	8315	1	sequence=TGCCTGCA;pvalue=0.000000e+00
Igf2bp3|6|49214957|-1|30000|1000	22624	22631	1	sequence=TGCCTGCA;pvalue=0.000000e+00
Mettl14|3|123386108|-1|30000|1000	12181	12188	1	sequence=TGCCTGCA;pvalue=0.000000e+00
Mettl14|3|123386108|-1|30000|1000	13956	13963	0,951918	sequence=TCCCTGCA;pvalue=3.051758e-05
Pou5f1|17|35506018|1|30000|1000	8384	8391	0,956599	sequence=TGCCTTCA;pvalue=1.525879e-05
Pou5f1|17|35506018|1|30000|1000	14789	14796	0,956599	sequence=TGCCTTCA;pvalue=1.525879e-05
Virma|4|11485958|1|30000|1000	11702	11709	1	sequence=TGCCTGCA;pvalue=0.000000e+00

Virma|4|11485958|1|30000|1000	15792	15799	1	sequence=TGCCTGCA;pvalue=0.000000e+00
Virma|4|11485958|1|30000|1000	22676	22683	1	sequence=TGCCTGCA;pvalue=0.000000e+00
Wtap|17|12994169|-1|30000|1000	2635	2642	1	sequence=TGCCTGCA;pvalue=0.000000e+00
Wtap|17|12994169|-1|30000|1000	23650	23657	0,956599	sequence=TGCCTTCA;pvalue=1.525879e-05
Wtap|17|12994169|-1|30000|1000	9221	9228	0,951918	sequence=TCCCTGCA;pvalue=3.051758e-05
Ythdc2|18|44827746|1|30000|1000	7883	7890	1	sequence=TGCCTGCA;pvalue=0.000000e+00
Ythdc2|18|44827746|1|30000|1000	21822	21829	1	sequence=TGCCTGCA;pvalue=0.000000e+00
Ythdc2|18|44827746|1|30000|1000	20126	20133	0,956599	sequence=TGCCTTCA;pvalue=1.525879e-05
Ythdc2|18|44827746|1|30000|1000	22121	22128	0,956599	sequence=TGCCTTCA;pvalue=1.525879e-05
Ythdc2|18|44827746|1|30000|1000	18142	18149	0,951918	sequence=TCCCTGCA;pvalue=3.051758e-05
Ythdf1|2|180920949|-1|30000|1000	2226	2233	1	sequence=TGCCTGCA;pvalue=0.000000e+00
Ythdf1|2|180920949|-1|30000|1000	27781	27788	1	sequence=TGCCTGCA;pvalue=0.000000e+00
Ythdf1|2|180920949|-1|30000|1000	2226	2233	1	sequence=TGCCTGCA;pvalue=0.000000e+00
Ythdf1|2|180920949|-1|30000|1000	27781	27788	1	sequence=TGCCTGCA;pvalue=0.000000e+00
Ythdf1|2|180920949|-1|30000|1000	14247	14254	0,951918	sequence=TCCCTGCA;pvalue=3.051758e-05
Ythdf1|2|180920949|-1|30000|1000	21003	21010	0,951918	sequence=TCCCTGCA;pvalue=3.051758e-05
Ythdf1|2|180920949|-1|30000|1000	21479	21486	0,951918	sequence=TCCCTGCA;pvalue=3.051758e-05
Ythdf1|2|180920949|-1|30000|1000	14247	14254	0,951918	sequence=TCCCTGCA;pvalue=3.051758e-05
Ythdf1|2|180920949|-1|30000|1000	21003	21010	0,951918	sequence=TCCCTGCA;pvalue=3.051758e-05
Ythdf1|2|180920949|-1|30000|1000	21479	21486	0,951918	sequence=TCCCTGCA;pvalue=3.051758e-05
Ythdf2|4|132212303|-1|30000|1000	18163	18170	1	sequence=TGCCTGCA;pvalue=0.000000e+00
Ythdf2|4|132212303|-1|30000|1000	17650	17657	0,956599	sequence=TGCCTTCA;pvalue=1.525879e-05
Ythdf2|4|132212303|-1|30000|1000	2806	2813	0,951918	sequence=TCCCTGCA;pvalue=3.051758e-05
Ythdf2|4|132212303|-1|30000|1000	12337	12344	0,951918	sequence=TCCCTGCA;pvalue=3.051758e-05
Ythdf2|4|132212303|-1|30000|1000	23041	23048	0,951918	sequence=TCCCTGCA;pvalue=3.051758e-05
Ythdf3|3|16183212|1|30000|1000	6769	6776	1	sequence=TGCCTGCA;pvalue=0.000000e+00

Table 4. Number of MATR3 significant binding sequences in the promoter regions of epitranscriptrome genes

Gene name	Match predicted
Ythdf1	123
Alkbh5	105
Mettl3	94
Igf2bp1	91
Igf2bp2	88
Ythdf2	83
Wtap	73
Igf2bp3	68
Virma	59
Mettl14	57
Ythdc1	57
Ythdc2	57

Fto	55
Ythdf3	54

Table 5. The number of MATR3 significant binding sequences in the promoter regions of epitranscriptrome genes involved in the m^6A machinery.

ID marker	marker	Q66K#44		FIBROBLASTS	
		1st allele	2nd allele	1st allele	2nd allele
13A	**D13S742**	257	257	257	257
13B	**D13S634**	395	416	395	416
13D	**D13S305**	460	471	460	471
13K	**D13S1492**	124	153	124	153
18B	**D18S978**	212	216	212	216
18C	**D18S535**	322	326	322	326
18D	**D18S386**	356	385	356	385
18J	**D18S976**	461	461	461	461
18M	**GATA178F11**	381	381	381	381
21A	**D21S1435**	180	188	180	188
21B	**D21S11**	253	257	253	257
21C	**D21S1411**	305	322	305	322
21D	**D21S1444**	463	470	463	470
21H	**D21S1442**	373	388	373	388
21I	**D21S1437**	120	135	120	135
X1	**DXS1187**	147		147	
X3	**XHPRT**	290		290	
X9	**DXS2390**	335		335	

Table6 STR analysis for the Q66K#44 cell line

ID marker	marker	sALS#24		FIBROBLASTS	
		1st allele	2nd allele	1st allele	2nd allele
13A	**D13S742**	282	286	282	286
13B	**D13S634**	391	399	391	399
13C	**D13S628**	432	459	432	459
13D	**D13S305**	463	463	463	463
13K	**D13S1492**	132	152	132	152
18B	**D18S978**	208	216	208	216
18C	**D18S535**	326	330	326	330
18D	**D18S386**	385	401	385	401
18J	**D18S976**	460	461	460	461

18M	**GATA178F11**	369	377	369	377
21A	**D21S1435**	184	188	184	188
21B	**D21S11**	243	247	243	247
21C	**D21S1411**	301	313	301	313
21D	**D21S1444**	465	470	465	470
21H	**D21S1442**	384	392	384	392
21I	**D21S1437**	132	139	132	139
X1	**DXS1187**	147		147	
X3	**XHPRT**	286		286	
X9	**DXS2390**	335		335	

ID marker	**marker**	**CTRL#11**		**FIBROBLASTS**	
		1st allele	2nd allele	1st allele	2nd allele
13A	**D13S742**	282	286	282	286
13B	**D13S634**	392	399	392	399
13C	**D13S628**	432	459	432	459
13D	**D13S305**	463	463	463	463
13K	**D13S1492**	132	152	132	152
18B	**D18S978**	208	216	208	216
18C	**D18S535**	326	330	326	330
18D	**D18S386**	384	401	384	401
18J	**D18S976**	461	460	461	460
18M	**GATA178F11**	368	337	368	337
21A	**D21S1435**	184	188	184	188
21B	**D21S11**	243	247	243	247
21C	**D21S1411**	301	313	301	313
21D	**D21S1444**	465	470	465	470
21H	**D21S1442**	384	392	384	392
21I	**D21S1437**	132	139	132	139
X1	**DXS1187**	148		148	
X3	**XHPRT**	286		286	
X9	**DXS2390**	335		335	

Table 7. STR analysis for the CRTL#11 and sALS#24 cell lines

Primary Antibody	Source	Company	Code
MATR3	Ms	Santa Cruz Biotechnology	sc-81318
B ACTIN	Ms	Santa Cruz Biotechnology	sc-47778
OCT4	Rb	Invitrogen	PA527438
NANOG	Ms	EMD Millipore	MABD24
KLF4	Rb	Genetex	GTX101508
SOX2	Rb	Genetex	GTX101507
LIN28A	Rb	Sigma Aldrich	SAB2702125
TUBB3	Ms	Invitrogen	MAI-118X
αSMA	Ms	Sigma Aldrich	A2547
GATA4	Rb	Genetex	GTX113194

NESTIN	Ms	eBioscience	14-9843-82
ZO-1	Rb	Genetex	GTX108613
eIF3A	Rb	Cell Signaling	#3411S
YTHDF1	Rb	Sigma Aldrich	SAB4502274
RPL26	Rb	Cell Signaling	#2065
RPS6	Rb	Cell Signaling	#2211
$_{\gamma}$H2AX	Rb	Cell Signaling	#9718S
REELIN	Rb	Genetex	GTX37552
TBR1	Rb	Abcam	Ab31940
TBR2	Rb	Genetex	GTX134088
MAP2	Ms	SantaCRuz	Sc-74421
FOXG1	Rb	Genetex	GTX134018

Secondary Antibody		**Company**	**Code**
Donkey anti-Goat IgG H+L (HRP)		AbcamLtd	AB97110
Donkey anti-Rabbit IgG H+L (HRP)		AbcamLtd	AB6802
Donkey anti-Mouse IgG H+L (HRP)		AbcamLtd	AB6820
Donkey anti-Mouse IgG (H+L), Alexa Fluor 488		Invitrogen	A21202
Donkey anti-Rabbit IgG (H+L), Alexa Fluor 546		Invitrogen	A10040
Donkey anti-Mouse IgG (H+L), Alexa Fluor 546		Invitrogen	A10036
Donkey anti-Rabbit IgG (H+L), Alexa Fluor Plus 488		Invitrogen	A32790

Table 8. Antibodies used in this work

Human Gene		**Sequence**
MATR3	fw rev	5'-GGAGAACTGAAGAAGGCCCT-3' 5'-GCACTGGGTTGAGACTAGGA-3'
OCT4	fw rev	5'-AGGATCACCCTGGGATATGCAC-3' 5'-ATGTTCTTGAAGCTAAGCTGTTGA-3'
LIN28A	fw rev	5'-GGAAAGAGCATGCAGAAGCG-3' 5'-TTCAGCGGACATGAGGCTAC-3'
NANOG	fw rev	5'-TACCTCAGCCTCCAGCAGAT-3' 5'-CTGGGGTAGGTAGGTGCTGA-3'
SOX2	fw rev	5'-GCTACAGCATGATGCAGGACCA-3' 5'-TCTGCGAGCTGGTCATGGAGTT-3'
KLF4	fw rev	5'-GCGAATTTCCATCCACAGCC-3' 5'-TTCCCATCTCAAGGCACACC-3'
TUBB3	fw rev	5'-GACACAGGCGTCCACAGTTC-3' 5'-GCCCCACTCTGACCAAAGAT-3'
NESTIN	fw rev	5'-GCCACGTACAGGACCCTC-3' 5'-CCTCTGGGGTCCTAGGGAAT-3'
αSMA	fw	5'-AATGCAGAAGGAGATCACGG-3'

	rev	5'-TCCTGTTTGCTGATCCACATC-3'
GATA4	fw	5'-CTCCTACTCCAGCCCCTACC-3'
	rev	5'-CACAGGAGAGGCCCACTC-3'
AFP	fw	5'-GCAGAGGAGATGTGCTGGATTG-3'
	rev	5'- CGTGGTCAGTTTGCAGCATTCTG-3'
YTHDF1	fw	5'-CCAGAGAACAAAAGGACAAG-3'
	rev	5'-TTTGACTGTCCAGTAAGGTAG-3'
ACTIN	fw	5'-ACAGAGCCTCGCCTTTGC-3'
	rev	5'-CCACCATCACGCCCTGG-3'
RPLP0	fw	5'-CATTCTCGCTTCCTGGAG-3'
	rev	5'-CTTGACCTTTTCAGCAAGTGG-3'
GAPDH	fw	5'-AGAAGGCTGGGGCTCATTT-3'
	rev	5'-CAGGAGGCATTGCTGATGAT-3'
P53	fw	5'-TGCTCAAGACTGGCGCTAAA-3'
	rev	5'-CTAGGATCTGACTGCGGCTC-3'
RAD51	fw	5'-GAAGTGGAGCGTAAGCCAGG-3'
	rev	5'-GCTGCATCTGCATTGCCATT-3'
KU70	fw	5'-GCGTTGATTGGGACCGAGTA-3'
	rev	5'-CTTCTTCATCGCCCTCGGTT-3'
NONO	fw	5'-CGCCATTTTGTACCCCTTGG-3'
	rev	5'-TGCCTCCCAGTTCCCTCTAA-3'
Episomal plasmid Detection plasmid	fw rev	5′-AGGTCCCTCGAAGAGGTTCA-3′ 5′-TTCCAACGCGAG AAGGTGTT-3′

Table 9. Primers used in RT-qPCR and PCR

Human Gene		**Sequence**
OCT4	fw	5'-TCC TGG AGG GCC AGG AAT C-3'
	rev	5'-CCA CAG AAC TCA TAC GGC GG-3'
OCT4	fw	5'-TTG GCA TGA CCT CTA ATC CTC TG-3'
	rev	5'-TCT TGG GGC CAT CTC TTG TG-3'
OCT4	fw	5'-AGA GGG ATG CAC AGC CAT AG-3'
	rev	5'-CAA ACC ATC TAC CAC GCT GC-3'
OCT4	fw	5'-GGA GAT TCC AGC CAA ATC CCA-3'
	rev	5'-CCC AGG ACA GAA CCA TCA CG-3'
OCT4	fw	5'-TCC TGG AGG GCC AGG AAT C-3'
	rev	5'-CCA CAG AAC TCA TAC GGC GG-3'
OCT4	fw	5'-CTC TCC CGT GTG TTG ACC C-3'
	rev	5'-GAA CAA AAA GGC TCA CAG ACC A-3'
OCT4	fw	5'-GGT TGC AAG ATA AGG TCA GGC-3'
	rev	5'-CTT CAA GTG GGA GAC ATG GGA-3'
OCT4	fw	5'-CAA GGG TTG AGC ACT TGT TTA GG-3'
	rev	5'-CCT TGG CTG GAC AAT CCC G-3'

OCT4	fw	5'-CTT CTG GCC TTC GAA GCT GT-3'
	rev	5'-TGA TCT CAG TGG AGG GCC TG-3'
GAPDH	fw	5'-GGC TCT CCA GAA CAT CAT CCC-3'
	rev	5'-CCA GTG AGC TTC CCG TTC AG-3'
GAPDH	fw	5'-GAT TCC ACC CAT GGC AAA TTC C-3'
	rev	5'-TCC ATT CTG TCT TCC ACT CAC TC-3'
ACTIN	fw	5'-GTG TCC CGT TGG GTA CAC T-3'
	rev	5'-TCC ATC CTG TCC TGT CTT GTC-3'
ACTIN	fw	5'-GGG GGC TGC ACA CTA CAT TT-3'
	rev	5'-CCT ATT GGT CCA GCC TAG CAG-3'
ACTIN	fw	5'-TCA CGT GTC CCC CAT ATC AGA-3'
	rev	5'-CAG CCT CAG TCT CCC TTG TTC-3'
YTHDF1	fw	5'-ACC TCT GTG AGC TCC TCA CTT-3'
	rev	5'-AGC ACA CGA AAT GGA GCA CT-3'
YTHDF1	fw	5'-TCC AAG TCT GTT AGC ATC TCC TG -3'
	rev	5'-AGT GCG CTC TGA GGG TTT AT-3'
YTHDF1	fw	5'-CAC GCC CCA CGT GAC TT-3'
	rev	5'-CGC TCT CAG GTC CCA GTC T-3'
YTHDF1	fw	5'-CGA CCT GGA ACA CGC GG-3'
	rev	5'-GTC CGA CAG CTG GGC TAC-3'
YTHDF1	fw	5'-GGT TGC CTT CTG AGA ATC TGC-3'
	rev	5'-AGG CCC ATC ACT AAA GTC AAG T-3'
YTHDF1	fw	5'-AAG GAA CTT GGT AAC CCT CCC-3'
	rev	5'-CAT ATG GGC CCA GAG TTC TCC-3'
NANOG	fw	5'-GCA CCT GCC CTT TGA ACT ATG-3'
	rev	5'-ACT GCC GAA TTC TGT GTC CT-3'
NANOG	fw	5'-GCC TAA ACT AGC CAG ATT TTG AGA C-3'
	rev	5'-TGC ATG CAC CTT AAA TTC CTG AG-3'
NANOG	fw	5'-TGT GGA TGT TAC TGG GCA GC-3'
	rev	5'-CAA CGC TTC CCA GGA CTT AGG-3'
NANOG	fw	5'-CTG ATG CCT TGG CTT CAT GC-3'
	rev	5'-GGC AGA AAT TTC AAC TAG CTC CA-3'
LIN28A	fw	5'-CCA TCT CCA GTT GTG CGT GT-3'
	rev	5'-ACC TCT GGG GTG TCC CTT C -3'
LIN28A	fw	5'-TGT CAA GTT GGT GGT GCA GTA-3'
	rev	5'-TTC TGT AGC AAA GCC AGG GTC-3'

Table 10. Primers used for the ChIP detection of DNA bound by MATR3 in RT-qPCR

REFERENCES

Aaronson, Y. and Meshorer, E. (2013) 'Regulation by alternative splicing', *Nature*, 498(7453), pp. 176–177. doi: 10.1038/nature12253.

Abhinav, K. *et al.* (2007) 'Amyotrophic Lateral Sclerosis in South-East England: A Population-Based Study', *Neuroepidemiology*, 29(1–2), pp. 44–48. doi: 10.1159/000108917.

Ajroud-driss, S. and Siddique, T. (2015) 'Sporadic and hereditary amyotrophic lateral sclerosis (ALS)', *BBA - Molecular Basis of Disease*. Elsevier B.V., 1852(4), pp. 679–684. doi: 10.1016/j.bbadis.2014.08.010.

Akberdin, I. R. *et al.* (2018) 'Pluripotency gene network dynamics : System views from parametric analysis', *PLoS ONE*, pp. 1–24.

Allouba, M. H. *et al.* (2015) 'NaNog : A pluripotency homeobox (master) molecule', *Global cardiology science e practice*, pp. 1–9. doi: http://dx.doi.org/10.5339/gcsp.2015.36.

Bai, Y. *et al.* (2019) 'YTHDF1 Regulates Tumorigenicity and Cancer Stem Cell-Like Activity in Human Colorectal Carcinoma', *frontiers in oncology*, 9(May), pp. 1–12. doi: 10.3389/fonc.2019.00332.

Balzer, E. and Moss, E. G. (2007) 'Localization of the Developmental Timing Regulator Lin28 to mRNP Complexes, P-bodies and Stress Granules', *RNA Biology*. Taylor & Francis, 4(1), pp. 16–25. doi: 10.4161/rna.4.1.4364.

Banerjee, A. *et al.* (2017) 'Nuclear poly (A) binding protein 1 (PABPN1) and Matrin3 interact in muscle cells and regulate RNA processing', *Nucleic Acids Research*. Oxford University Press, 45(18), pp. 10706–10725. doi: 10.1093/nar/gkx786.

Barkan, C. L. and Zornik, E. (2019) 'Feedback to the future : motor neuron contributions to central pattern generator function', *The Company of Biologists*. doi: 10.1242/jeb.193318.

Batista, P. J. *et al.* (2014) 'm 6 A RNA Modification Controls Cell Fate Transition in Mammalian Embryonic Stem Cells Article m 6 A RNA Modification Controls Cell Fate Transition in Mammalian Embryonic Stem Cells', *Stem Cell*. Elsevier Inc., 15(6), pp. 707–719. doi: 10.1016/j.stem.2014.09.019.

Batista, P. J. *et al.* (2015) 'm6A RNA modification controls cell fate transition in mammalian embryonic stem cells', *Cell Stem Cell*, 15(6), pp. 707–719. doi: 10.1016/j.stem.2014.09.019.m.

Belgrader, P., Dey, R. and Berezneyg, R. (1991) 'Molecular Cloning of Matrin 3', *THE JOURNAL OF BIOLOGICAL CHEMISTRY*, 266(15).

Ben-shushan, E. *et al.* (1993) 'Extinction of Oct-3 / 4 Gene Expression in Embryonal Carcinoma x Fibroblast Somatic Cell Hybrids Is Accompanied by Changes in the Methylation Status , Chromatin Structure , and Transcriptional Activity of the Oct-3 / 4 Upstream Region', *Molecular and Cellular Biology*, pp. 891–901.

Ben-Shushan, E. *et al.* (1998) 'Rex-1, a gene encoding a transcription factor expressed in the early embryo, is regulated via Oct-3/4 and Oct-6 binding to an octamer site and a novel protein, Rox-1, binding to an adjacent site.', *Molecular and cellular biology*, 18(4), pp. 1866–1878. doi: 10.1128/mcb.18.4.1866.

Berdasco, M. and Esteller, M. (2011) 'DNA methylation in stem cell renewal and multipotency', *stem cell research e therapy*, pp. 1–9.

Berg, D. L. C. Van Den *et al.* (2010) 'An Oct4-Centered Protein Interaction Network in Embryonic Stem Cells', *Stem Cell*. Elsevier Ltd, 6(4), pp. 369–381. doi: 10.1016/j.stem.2010.02.014.

Bhartiya, D. and Nagvenkar, P. (2013) 'An Overview of Pluripotent Stem Cells', *INTECH open science*, pp. 3–24.

Bialkowska, A. B., Yang, V. W. and Mallipattu, S. K. (2017) 'Kruppel-like factors in mammalian stem cells and development', *Development*, pp. 737–754. doi: 10.1242/dev.145441.

Bigarella, C. L., Liang, R. and Ghaffari, S. (2014a) 'Stem cells and the impact of ROS signaling', *Development*, pp. 4206–4218. doi: 10.1242/dev.107086.

Bigarella, C. L., Liang, R. and Ghaffari, S. (2014b) 'Stem cells and the impact of ROS signaling', *Development*, 141(22), pp. 4206 LP – 4218. doi: 10.1242/dev.107086.

Blackshear, P. J. and Lai, W. S. (2003) *Regulation of mRNA Turnover*, *Handbook of Cell Signaling*. Elsevier Science (USA). doi: 10.1016/B978-0-12-124546-7.50679-3.

Blaess, S. *et al.* (2015) 'Sonic hedgehog signaling in the development of the mouse hypothalamus', *Frontiers in Neuroanatomy*, 8(January), pp. 1–6. doi: 10.3389/fnana.2014.00156.

Blanco, S. *et al.* (2016) 'Stem cell function and stress response are controlled by protein synthesis', *Nature*, 534(7607), pp. 335–340. doi: 10.1038/nature18282.Stem.

Boehringer, A. *et al.* (2017) 'ALS Associated Mutations in Matrin 3 Alter Protein-Protein Interactions and Impede mRNA Nuclear Export', *Scientific Reports*, 7(1), pp. 1–14. doi: 10.1038/s41598-017-14924-6.

Boer, B. *et al.* (2007) 'Elevating the levels of Sox2 in embryonal carcinoma cells and embryonic stem cells inhibits the expression of Sox2 : Oct-3 / 4 target genes y', *Nucleid Acids Research*, 35(6), pp. 1773–1786. doi: 10.1093/nar/gkm059.

Bowles, J., Schepers, G. and Koopman, P. (2000) 'Phylogeny of the SOX family of developmental transcription factors based on sequence and structural indicators.', *Developmental biology*. United States, 227(2), pp. 239–255. doi: 10.1006/dbio.2000.9883.

Boyer, L. A. *et al.* (2005) 'Core Transcriptional Regulatory Circuitry in Human Embryonic Stem Cells', *Cell*, 122(Icm), pp. 947–956. doi: 10.1016/j.cell.2005.08.020.

Brandsma, I. and van Gent, D. C. (2012) 'Pathway choice in DNA double strand break repair: observations of a balancing act', *Genome Integrity*, 3(1), p. 9. doi: 10.1186/2041-9414-3-9.

Brehm, A. *et al.* (1997) 'The Carboxy-Terminal Transactivation Domain of Oct-4 Acquires Cell Specificity through the POU Domain', *Molecular and Cellular Biology*, 17(1), pp. 154–162.

Cai, Y. *et al.* (2015) 'Gene expression of OCT4 , SOX2 , KLF4 and MYC (OSKM) induced pluripotent stem cells : identification for potential mechanisms', *BioMedCentral*. ???, pp. 1–8. doi: 10.1186/s13000-015-0263-7.

Cakir, B. *et al.* (2019) 'Engineering of human brain organoids with a functional vascular-like system', *Nature Methods*. Springer US. doi: 10.1038/s41592-019-0586-5.

Carvalho, K. A. T. (2017) '14 - Mesenchymal Stem Cells Seeded on Biofunctionalized Scaffold for Tissue Engineering', in Thomaz-Soccol, V., Pandey, A., and Resende, R. R. B. T.-C. D. in B. and B. (eds). Elsevier, pp. 349–367. doi: https://doi.org/10.1016/B978-0-444-63660-7.00014-0.

Chagastelles, P. C. and Nardi, N. B. (2011) 'Biology of stem cells: an overview', *Kidney International Supplements*, 1(3), pp. 63–67. doi: https://doi.org/10.1038/kisup.2011.15.

Chambers, I. *et al.* (2003) 'Functional Expression Cloning of Nanog , a Pluripotency Sustaining Factor in Embryonic Stem Cells', *Cell*, 113, pp. 643–655.

Chang, L. and Karin, M. (2001) 'Mammalian MAP kinase signalling cascades', *Nature*, pp. 37–40.

Chapman, J. R., Taylor, M. R. G. and Boulton, S. J. (2012) 'Playing the end game: DNA double-strand break repair pathway choice.', *Molecular cell*. United States, 47(4), pp. 497–510. doi: 10.1016/j.molcel.2012.07.029.

Chattopadhyay, M. and Valentine, J. S. (2009) 'Aggregation of Copper–Zinc Superoxide Dismutase in Familial and Sporadic ALS', *Antioxidants & Redox Signaling*. Mary Ann Liebert, Inc., publishers, 11(7), pp. 1603–1614. doi: 10.1089/ars.2009.2536.

Chaudhary, R. *et al.* (2017) 'Prosurvival long noncoding RNA PINCR regulates a subset of p53 targets in human colorectal cancer cells by binding to Matrin 3', pp. 1–32. doi: 10.7554/eLife.23244.

Chen, H., Qian, K., Du, Z., Cao, J., Petersen, A., Liu, H., Blackbourn IV, L. W., *et al.* (2014) 'Modeling ALS with iPSCs Reveals that Mutant SOD1 Misregulates Neurofilament Balance in Motor Neurons', *Cell Stem Cell*. Elsevier, 14(6), pp. 796–809. doi: 10.1016/j.stem.2014.02.004.

Chen, H., Qian, K., Du, Z., Cao, J., Petersen, A., Liu, H., Iv, L. W. B., *et al.* (2014) 'NIH Public Access', 14(6), pp. 796–809. doi: 10.1016/j.stem.2014.02.004.Modeling.

Chen, T., Hao, Y., *et al.* (2015) 'm 6 A RNA Methylation Is Regulated by MicroRNAs and Promotes Reprogramming to Pluripotency Article m 6 A RNA Methylation Is Regulated by MicroRNAs and Promotes Reprogramming to Pluripotency', *Stem Cell*. Elsevier Inc., 16(3), pp. 289–301. doi: 10.1016/j.stem.2015.01.016.

Chen, T., Hao, Y. J., *et al.* (2015) 'M6A RNA methylation is regulated by microRNAs and promotes reprogramming to pluripotency', *Cell Stem Cell*. Elsevier Inc., 16(3), pp. 289–301. doi: 10.1016/j.stem.2015.01.016.

Chen, Xi *et al.* (2008) 'Integration of External Signaling Pathways with the Core Transcriptional Network in Embryonic Stem Cells', *Cell*, pp. 1106–1117. doi: 10.1016/j.cell.2008.04.043.

Chen, Xinming *et al.* (2008) 'Krüppel-like Factor 4 (Gut-enriched Krüppel-like Factor) Inhibits Cell Proliferation by Blocking G1 /S Progression of the Cell Cycle', *THE JOURNAL OF BIOLOGICAL CHEMISTRY*, 276(32), pp. 30423–30428.

Chepelev, I. and Chen, X. (2013) 'Alternative splicing switching in stem cell lineages', *Front Biol.*, 8(1), pp. 50–59. doi:

10.1007/s11515-012-1198-y.Alternative.

Chew, J. *et al.* (2005) 'Reciprocal Transcriptional Regulation of Pou5f1 and Sox2 via the Oct4 / Sox2 Complex in Embryonic Stem Cells', *Molecular and Cellular Biology*, 25(14), pp. 6031–6046. doi: 10.1128/MCB.25.14.6031.

Chio, A. *et al.* (2012) 'Prognostic factors in ALS : A critical review', *Amyotroph Lateral Scler*, 10(2), pp. 310–323. doi: 10.3109/17482960802566824.Prognostic.

Choi, S. H. *et al.* (2014) 'A three-dimensional human neural cell culture model of Alzheimer's disease.', *Nature*, 515(7526), pp. 274–278. doi: 10.1038/nature13800.

Chukwurah, E. *et al.* (2019) 'All Together Now: Modeling the Interaction of Neural With Non-neural Systems Using Organoid Models', *Frontiers in Neuroscience*, 13, p. 582. doi: 10.3389/fnins.2019.00582.

Cie, A. *et al.* (2017) 'ROS and Oxidative Stress in Stem Cells', *Oxidative Medicine and Cellular Longevity*, 2017, pp. 2–4.

Coelho, M. B. *et al.* (2015) 'Nuclear matrix protein Matrin 3 regulates alternative splicing and forms overlapping regulatory networks with PTB', *The EMBO journal*, 34(5), pp. 653–668.

Cole, M. F. *et al.* (2008) 'Tcf3 is an integral component of the core regulatory circuitry of embryonic stem cells', *Genes and Development*, pp. 746–755. doi: 10.1101/gad.1642408.4.

Conlon, E. G. and Manley, J. L. (2017) 'RNA-binding proteins in neurodegeneration : mechanisms in aggregate', *Cold spring Harbor Labpratory Press*, pp. 1509–1528. doi: 10.1101/gad.304055.117.GENES.

Coppedè, F. and Migliore, L. (2015) 'DNA damage in neurodegenerative diseases', *Mutation Research - Fundamental and Molecular Mechanisms of Mutagenesis*. Elsevier B.V., 776, pp. 84–97. doi: 10.1016/j.mrfmmm.2014.11.010.

Curatola, A. M. and Basilico, C. (1990) 'Expression of the K-fgf Proto-Oncogene Is Controlled by 3 ' Regulatory Elements Which Are Specific for Embryonal Carcinoma Cellst A EI | AEI SC', *Molecular and Cellular Biology*, 10(6), pp. 2475–2484.

Curchoe, C. L., Russo, J. and Terskikh, A. V (2012) 'hESC derived neuro-epithelial rosettes recapitulate early mammalian neurulation events ; an in vitro model', *Stem Cell Research*. Elsevier B.V., 8(2), pp. 239–246. doi: 10.1016/j.scr.2011.11.003.

Damme, P. Van, Robberecht, W. and Bosch, L. Van Den (2017) 'Modelling amyotrophic lateral sclerosis : progress and possibilities', *The Company of Biologists*, 1, pp. 537–549. doi: 10.1242/dmm.029058.

Darnell, R. B. (2014) 'RNA Protein Interaction in Neurons Robert', *Annu Rev Neurosci*, pp. 243–270. doi: 10.1146/annurev-neuro-062912-114322.RNA.

Daviaud, N., Friedel, R. H. and Zou, H. (2018) 'Vascularization and Engraftment of Transplanted Human Cerebral Organoids in Mouse Cortex', *eNeuro*. Society for Neuroscience, 5(6), p. ENEURO.0219-18.2018. doi: 10.1523/ENEURO.0219-18.2018.

DeJesus-Hernandez, M. *et al.* (2011) 'Expanded GGGGCC hexanucleotide repeat in noncoding region of C9ORF72 causes chromosome 9p-linked FTD and ALS.', *Neuron*, 72(2), pp. 245–256. doi: 10.1016/j.neuron.2011.09.011.

Deng, H.-X. *et al.* (2011) 'Mutations in UBQLN2 cause dominant X-linked juvenile and adult-onset ALS and ALS/dementia.', *Nature*, 477(7363), pp. 211–215. doi: 10.1038/nature10353.

Desmarais, J. A. *et al.* (2016) 'Apoptosis and failure of checkpoint kinase 1 activation in human induced pluripotent stem cells under replication stress', *Stem Cell Research & Therapy*. Stem Cell Research & Therapy, pp. 1–7. doi: 10.1186/s13287-016-0279-2.

Elkon, R., Ugalde, A. P. and Agami, R. (2013) 'Alternative cleavage and polyadenylation: extent, regulation and function', *Nature Reviews Genetics*, 14(7), pp. 496–506. doi: 10.1038/nrg3482.

Fecto, F. *et al.* (2011) 'SQSTM1 mutations in familial and sporadic amyotrophic lateral sclerosis.', *Archives of neurology*. United States, 68(11), pp. 1440–1446. doi: 10.1001/archneurol.2011.250.

Feng, R. and Wen, J. (2011) 'Overview of the roles of Sox2 in stem cell and development', *Biological Chemistry*. doi: 10.1515/hsz-2014-0317.

Feng, R. and Wen, J. (2015) 'Overview of the roles of Sox2 in stem cell and development', 396(8), pp. 883–891. doi: 10.1515/hsz-2014-0317.

Ferrara, D. *et al.* (2018) 'Role of Extracellular Vesicles in Amyotrophic Lateral Sclerosis', *Frontiers in neuroscience*, 12(August), pp. 1–9. doi: 10.3389/fnins.2018.00574.

Fidalgo, M. *et al.* (2012) 'Zfp281 mediates Nanog autorepression through recruitment of the NuRD complex and inhibits somatic cell reprogramming', *PNAS*. doi: 10.1073/pnas.1208533109/-/DCSupplemental.www.pnas.org/cgi/doi/10.1073/pnas.1208533109.

Finn, R. D. *et al.* (2010) 'The Pfam protein families database', *Nucleid Acids Research*, 38(November 2009), pp. 211–222. doi: 10.1093/nar/gkp985.

Flemr, M. *et al.* (2014) 'Lin28a Is Dormant , Functional , and Dispensable During Mouse Oocyte-to-Embryo', *Biology of reproduction*, 90(May), pp. 1–9. doi: 10.1095/biolreprod.114.118703.

Freibaum, B. D. *et al.* (2010) 'Global Analysis of TDP-43 Interacting Proteins Reveals Strong Association with RNA Splicing and Translation Machinery research articles', *Journal of Proteome Research*, pp. 1104–1120.

Freischmidt, A. *et al.* (2015) 'Haploinsufficiency of TBK1 causes familial ALS and fronto-temporal dementia.', *Nature neuroscience*. United States, 18(5), pp. 631–636. doi: 10.1038/nn.4000.

Fujimori, K. *et al.* (2018) 'Modeling sporadic ALS in iPSC-derived motor neurons identifies a potential therapeutic agent', *Nature Medicine*, 24(10), pp. 1579–1589. doi: 10.1038/s41591-018-0140-5.

Gallego-iradi, M. C. *et al.* (2015) 'Subcellular Localization of Matrin 3 Containing Mutations Associated with ALS and Distal Myopathy', *PLoS ONE*, pp. 1–15. doi: 10.1371/journal.pone.0142144.

Gardner, R. L. (2013) *Pluripotential Stem Cells from Vertebrate Embryos : Present Perspective and Future Challenges*. Second Edition, *Handbook of Stem Cells, Two-Volume Set*. Second Edition. Elsevier Inc. doi: 10.1016/B978-0-12-385942-6.00003-2.

Gawlik-rzemieniewska, N. and Bednarek, I. (2016) 'The role of NANOG transcriptional factor in the development of malignant phenotype of cancer cells', *Cancer Biology & Therapy*. Taylor & Francis, 17(1), pp. 1–10. doi: 10.1080/15384047.2015.1121348.

Geula, S. *et al.* (2015) 'm6A mRNA methylation facilitates resolution of naïve pluripotency toward differentiation', *Science*, 347(6225), pp. 0–5.

Ghaleb, A. M. *et al.* (2018) 'Krüppel-like factor 4 (KLF4): What we currently know Amr', *Gene*, pp. 27–37. doi: 10.1016/j.gene.2017.02.025.Kr.

Göke, J. *et al.* (2011) 'Combinatorial Binding in Human and Mouse Embryonic Stem Cells Identifies Conserved Enhancers Active in Early Embryonic Development', *PLOS Computational Biology*. Public Library of Science, 7(12), p. e1002304. Available at: https://doi.org/10.1371/journal.pcbi.1002304.

Gong, J. *et al.* (2017) 'RBM45 competes with HDAC1 for binding to FUS in response to DNA damage', *Nucleic acids research*. Oxford University Press, 45(22), pp. 12862–12876. doi: 10.1093/nar/gkx1102.

Grebenyuk, S. and Ranga, A. (2019) 'Engineering Organoid Vascularization', *frontiers in Biogineering and Biotechnology*, 7(March), pp. 1–12. doi: 10.3389/fbioe.2019.00039.

Greenway, M. J. *et al.* (2006) 'ANG mutations segregate with familial and " sporadic " amyotrophic lateral sclerosis', *Nature Genetics*, 38(4), pp. 2005–2007. doi: 10.1038/ng1742.

Grenier, K., Kao, J. and Diamandis, P. (2020) 'Three-dimensional modeling of human neurodegeneration: brain organoids coming of age', *Molecular Psychiatry*, 25(2), pp. 254–274. doi: 10.1038/s41380-019-0500-7.

Guerreiro, R., Brás, J. and Hardy, J. (2015) 'SnapShot: Genetics of ALS and FTD.', *Cell*. United States, 160(4), pp. 798-798.e1. doi: 10.1016/j.cell.2015.01.052.

Gurney, M. E. *et al.* (1994) 'Motor neuron degeneration in mice that express a human Cu,Zn superoxide dismutase mutation', *Science*, 264(5166), pp. 1772 LP – 1775. doi: 10.1126/science.8209258.

Guyett, P., Hendrickson, M. and Laha, K. (2018) 'CNS Drug Discovery Using iPSC-Derived Neurons ', *Genetic Engineering e Biotechnology News*, 38(20), pp. 14–15. doi: 10.1089/gen.38.20.08.

Hackett, J. A. and Surani, M. A. (2014) 'Regulatory Principles of Pluripotency : From the Ground State Up', *Cell Stem Cell*. doi: 10.1016/j.stem.2014.09.015.

Hadjimichael, C. *et al.* (2015) 'Common stemness regulators of embryonic and cancer stem cells', *world journal of stem cells*, 7(9), pp. 1150–1184. doi: 10.4252/wjsc.v7.i9.1150.

Hall, C. E. *et al.* (2017) 'Progressive Motor Neuron Pathology and the Role of Astrocytes in a Human Stem Cell Model of VCP-Related ALS', *Cell Reports*. ElsevierCompany., 19(9), pp. 1739–1749. doi: 10.1016/j.celrep.2017.05.024.

Hall, J. *et al.* (2009) 'Oct4 and LIF/Stat3 Additively Induce Kru¨ppel Factors to Sustain Embryonic Stem Cell Self-Renewal John', *Cell Stem Cell*. Elsevier Ltd, 5(6), pp. 597–609. doi: 10.1016/j.stem.2009.11.003.

Hammachi, F. *et al.* (2012) 'Transcriptional Activation by Oct4 Is Sufficient for the Maintenance and Induction of Pluripotency', *Cell Reports*, 1(2), pp. 99–109. doi: https://doi.org/10.1016/j.celrep.2011.12.002.

Han, G., Wang, H. and Hao, J. (2013) 'Molecular Mechanisms of Embryonic Stem Cell Pluripotency', *Open Science Intech*. doi: http://dx.doi.org/10.5772/54365.

Hand, C. K. and Rouleau, G. A. (2002) 'Familial amyotrophic lateral sclerosis', *Muscle & Nerve*. John Wiley & Sons, Ltd, 25(2), pp. 135–159. doi: 10.1002/mus.10001.

Hanson, K. A., Kim, S. H. and Tibbetts, R. S. (2012) 'RNA-binding proteins in neurodegenerative disease: TDP-43 and beyond', *Wiley interdisciplinary reviews. RNA*. 2011/10/25, 3(2), pp. 265–285. doi: 10.1002/wrna.111.

Hao, J. *et al.* (2006) 'WNT / h -catenin pathway up-regulates Stat3 and converges on LIF to prevent differentiation of mouse embryonic stem cells', *Developmental Biology*. Elsevier Inc., 290(1), pp. 81–91. doi: 10.1016/j.ydbio.2005.11.011.

Haraguchi, R. *et al.* (2001) 'Unique functions of Sonic hedgehog signaling during external genitalia development', *Development*, 128(21), pp. 4241 LP – 4250. Available at: http://dev.biologists.org/content/128/21/4241.abstract.

Hardiman, O. *et al.* (2017) 'Amyotrophic lateral sclerosis', *Nature Reviews Disease Primers*, 3. doi: 10.1038/nrdp.2017.71.

Hashemikhabir, S., Neelamraju, Y. and Janga, S. C. (2015) 'Database of RNA binding protein expression and disease dynamics (READ DB)', *Database*, 2015. doi: 10.1093/database/bav072.

Hattori, Naoko *et al.* (2004) 'Epigenetic Control of Mouse Oct-4 Gene Expression in Embryonic Stem Cells and Trophoblast Stem Cells *', *THE JOURNAL OF BIOLOGICAL CHEMISTRY*, 279(17), pp. 17063–17069. doi: 10.1074/jbc.M309002200.

Hayashi, Y. *et al.* (2015) 'Structure-based discovery of NANOG variant with enhanced properties to promote self-renewal and reprogramming of pluripotent stem cells', *PNAS*, pp. 1–6. doi: 10.1073/pnas.1502855112.

Hill, S. J. *et al.* (2016) 'Two familial ALS proteins function in prevention/repair of transcription-associated DNA damage', *Proceedings of the National Academy of Sciences*, 113(48), pp. E7701–E7709. doi: 10.1073/pnas.1611673113.

Hisada-Ishii, S. *et al.* (2007) 'Bipartite nuclear localization signal of matrin 3 is essential for vertebrate cells', *Biochemical and Biophysical Research Communications*, 354(1), pp. 72–76. doi: https://doi.org/10.1016/j.bbrc.2006.12.191.

Homan, K. A. *et al.* (2019) 'Flow-enhanced vascularization and maturation of kidney organoids in vitro', *Nature Methods*, 16(3), pp. 255–262. doi: 10.1038/s41592-019-0325-y.

Hor, J. H. *et al.* (2018) 'Cell cycle inhibitors protect motor neurons in an organoid model of Spinal Muscular Atrophy.', *Cell death & disease*, 9(11), p. 1100. doi: 10.1038/s41419-018-1081-0.

HR, S. *et al.* (1990) 'New type of POU domain in germ line-specific protein Oct-4', *Nature*, 344, 435–4. doi: 10.1038/344435a0.

Hualin, Z. *et al.* (2014) 'RNA-binding proteins in neurological diseases', *Life Sciences, Science China*, 57(4), pp. 432–444. doi: 10.1007/s11427-014-4647-9.

Hyun, S. *et al.* (2014) 'Biochimica et Biophysica Acta The ubiquitin ligase human TRIM71 regulates let-7 microRNA biogenesis via modulation of Lin28B protein', *BBA - Gene Regulatory Mechanisms*. Elsevier B.V., 1839(5), pp. 374–386. doi: 10.1016/j.bbagrm.2014.02.017.

Ilic, D. *et al.* (2012) 'Basic principles of human embryonic stem cells', *Woodhead*, pp. 29–48. doi: 10.1533/9780857096074.1.29.

Inui, S. *et al.* (2017) 'Irradiation strongly reduces tumorigenesis of human induced pluripotent stem cells', *Journal of Radiation Research*, 58(4), pp. 430–438. doi: 10.1093/jrr/rrw124.

Iradi, M. C. G. *et al.* (2018) 'Characterization of gene regulation and protein interaction networks for Matrin 3 encoding mutations linked to amyotrophic lateral sclerosis and myopathy', *Scientific Reports*. Springer US, (November 2017), pp. 1–15. doi: 10.1038/s41598-018-21371-4.

Jaafar, L. *et al.* (2017) 'SFPQ•NONO and XLF function separately and together to promote DNA double-strand break repair via canonical nonhomologous end joining', *Nucleic acids research*. Oxford University Press, 45(4), pp. 1848–1859. doi: 10.1093/nar/gkw1209.

Jackson, R. J., Hellen, C. U. T. and Pestova, T. V. (2015) 'THE MECHANISM OF EUKARYOTIC TRANSLATION INITIATION', *Nat Rev Mol Cell Biol*, 11(2), pp. 113–127. doi: 10.1038/nrm2838.THE.

Jain, A. K. and Barton, M. C. (2018) 'p53: emerging roles in stem cells, development and beyond', *Development*, 145(8), p. dev158360. doi: 10.1242/dev.158360.

Janga, S. C. and Mittal, N. (2011) 'CONSTRUCTION , STRUCTURE AND DYNAMICS OF POST-TRANSCRIPTIONAL REGULATORY NETWORK DIRECTED BY RNA-BINDING PROTEINS', *RNA infrastructure and Networks*, pp. 103–117.

Jha, B. S., Rao, M. and Malik, N. (2015) 'Motor Neuron Differentiation from Pluripotent Stem Cells and Other Intermediate Proliferative Precursors that can be Discriminated by Lineage Specific Reporters', *Stem Cell Reviews and Reports*, 11(1), pp. 194–204. doi: 10.1007/s12015-014-9541-0.

Johnson, B. V *et al.* (2008) 'Understanding pluripotency—how embryonic stem cells keep their options open', *Molecular Human Reproduction*, 14(9), pp. 513–520. doi: 10.1093/molehr/gan048.

Johnson, J. O. *et al.* (2010) 'Exome sequencing reveals VCP mutations as a cause of familial ALS.', *Neuron*, 68(5), pp. 857–864. doi: 10.1016/j.neuron.2010.11.036.

Johnson, J. O. *et al.* (2014) 'Mutations in the Matrin 3 gene cause familial amyotrophic lateral sclerosis', *Nature Neuroscience*, 17(5), pp. 664–666. doi: 10.1038/nn.3688.

Kafasla, P. *et al.* (2012) 'Defining the roles and interactions of PTB', *Biochem Soc Trans*.

Kamachi, Y. and Kondoh, H. (2013) 'Sox proteins : regulators of cell fate specification and differentiation', *Development*, 4144, pp. 4129–4144. doi: 10.1242/dev.091793.

Kamelgarn, M. *et al.* (2018) 'ALS mutations of FUS suppress protein translation and disrupt the regulation of nonsense-mediated decay', *PNAS*, 115(51). doi: 10.1073/pnas.1810413115.

Karwacki-Neisius, V. *et al.* (2013) 'Reduced Oct4 Expression Directs a Robust Pluripotent State with Distinct Signaling Activity and Increased Enhancer Occupancy by Oct4 and Nanog', *Cell Stem Cell*, pp. 531–545. doi: 10.1016/j.stem.2013.04.023.

Kawada, J. *et al.* (2017) 'Generation of a Motor Nerve Organoid with Human Stem Cell-Derived Neurons', *Stem Cell Reports*, 9(5), pp. 1441–1449. doi: 10.1016/j.stemcr.2017.09.021.

Kele, J. *et al.* (2012) 'SFRP1 and SFRP2 dose-dependently regulate midbrain dopamine neuron development in vivo and in embryonic stem cells.', *Stem cells (Dayton, Ohio)*, 30(5), pp. 865–875. doi: 10.1002/stem.1049.

Kellner, S. and Kikyo, N. (2012) 'Transcriptional regulation of the Oct4 gene, a master gene for pluripotency', *Histol Histopathol*, 25(3), pp. 405–412.

Kim, C. (2015) 'iPSC technology--Powerful hand for disease modeling and therapeutic screen', *BMB reports*. Korean Society for Biochemistry and Molecular Biology, 48(5), pp. 256–265. doi: 10.5483/bmbrep.2015.48.5.100.

Kim, H. J. *et al.* (2013) 'Mutations in prion-like domains in hnRNPA2B1 and hnRNPA1 cause multisystem proteinopathy and ALS.', *Nature*, 495(7442), pp. 467–473. doi: 10.1038/nature11922.

Koo, B. *et al.* (2019) 'Past, Present, and Future of Brain Organoid Technology', *Molecules and cells*. Korean Society for Molecular and Cellular Biology, 42(9), pp. 617–627. doi: 10.14348/molcells.2019.0162.

Kopp, J. L. *et al.* (2008) 'Small Increases in the Level of Sox2 Trigger the Differentiation of Mouse Embryonic Stem Cells', *Stem Cell*. doi: 10.1634/stemcells.2007-0951.

Kurland, L. T. and Mulder, D. W. (1955) 'Epidemiologic investigations of amyotrophic lateral sclerosis. 2. Familial aggregations indicative of dominant inheritance. II.', *Neurology*. United States, 5(4), pp. 249–268. doi: 10.1212/wnl.5.4.249.

Kwiatkowski, T. J. J. *et al.* (2009) 'Mutations in the FUS/TLS gene on chromosome 16 cause familial amyotrophic lateral sclerosis.', *Science (New York, N.Y.)*. United States, 323(5918), pp. 1205–1208. doi: 10.1126/science.1166066.

Lancaster, M. A. *et al.* (2013) 'Cerebral organoids model human brain development and microcephaly', *Nature*. Nature Publishing Group, 501(7467), pp. 373–379. doi: 10.1038/nature12517.

Lancaster, M. A. and Knoblich, J. A. (2014) 'Organogenesisin a dish: Modeling development and disease using organoid technologies', *Science*, 345(6194). doi: 10.1126/science.1247125.

Leblond, C. S. *et al.* (2016) 'Neurobiology of Aging Replication study of MATR3 in familial and sporadic amyotrophic lateral sclerosis', *Neurobiology of Aging*. Elsevier Inc, 37, pp. 209.e17-209.e21. doi: 10.1016/j.neurobiolaging.2015.09.013.

Lee, J. *et al.* (2018) 'Pharmacological Regulation of Oxidative Stress in Stem Cells', *Oxidative Medicine and Cellular Longevity*, 2018.

Lemmens, R. *et al.* (2010) 'RNA metabolism and the pathogenesis of motor neuron diseases', *Cell Neurosciences*. Elsevier Ltd, 33(5), pp. 249–258. doi: 10.1016/j.tins.2010.02.003.

Leong, C. *et al.* (2013) 'ScienceDirect Neural stem cell isolation from the whole mouse brain using the novel FABP7-binding fluorescent dye , CDr3', *Stem Cell Research*. Elsevier B.V., 11(3), pp. 1314–1322. doi: 10.1016/j.scr.2013.09.002.

Li, L., Chao, J. and Shi, Y. (2018) 'Modeling neurological diseases using iPSC-derived neural cells : iPSC modeling of neurological

diseases', *Cell and tissue research*. 2017/10/28, 371(1), pp. 143–151. doi: 10.1007/s00441-017-2713-x.

Li, M., Carlos, J. and Belmonte, I. (2018) 'Deconstructing the pluripotency gene regulatory network', *Nature Cell Biology*, 20(April). doi: 10.1038/s41556-018-0067-6.

Li, Z. *et al.* (2010) 'KLF4 promotes hydrogen-peroxide-induced apoptosis of chronic myeloid leukemia cells involving the bcl-2/bax pathway.', *Cell stress & chaperones*, 15(6), pp. 905–912. doi: 10.1007/s12192-010-0199-5.

Liang, J. *et al.* (2008) 'Nanog and Oct4 associate with unique transcriptional repression complexes in embryonic stem cells', *Nature Cell Biology*, 10(6). doi: 10.1038/ncb1736.

Liao, S., Sun, H. and Xu, C. (2018) 'YTH Domain : A Family of N 6 -methyladenosine (m 6 A) Readers', *Genomics, Proteomics & Bioinformatics*. Beijing Institute of Genomics, Chinese Academy of Sciences and Genetics Society of China, 16(2), pp. 99–107. doi: 10.1016/j.gpb.2018.04.002.

Liao, Y. *et al.* (2018) 'Effects of Klf4 and c-Myc Knockdown on Pluripotency Maintenance in Porcine Induced Pluripotent Stem Cell', *Cell*, 19(4), pp. 640–646. doi: 10.22074/cellj.2018.4428.Introduction.

Lin, K.-P. *et al.* (2015) 'Mutational analysis of MATR3 in Taiwanese patients with amyotrophic lateral sclerosis.', *Neurobiology of aging*. United States, 36(5), pp. 2005.e1–4. doi: 10.1016/j.neurobiolaging.2015.02.008.

Lin, K. *et al.* (2015) 'Neurobiology of Aging Mutational analysis of MATR3 in Taiwanese patients with amyotrophic lateral sclerosis', *Neurobiology of Aging*. Elsevier Inc, 36(5), pp. 2005.e1-2005.e4. doi: 10.1016/j.neurobiolaging.2015.02.008.

Lin, Y. *et al.* (2014) 'Embryoid body formation from human pluripotent stem cells in chemically defined E8 media', *stembook*, pp. 1–4. doi: 10.3824/stembook.1.98.1.1.

Liu, L. and Roberts, R. M. (1996) 'Silencing of the Gene for the Beta Subunit of Human Chorionic Gonadotropin by the Embryonic Transcription Factor Oct-3 / 4 *', *THE JOURNAL OF BIOLOGICAL CHEMISTRY*, 271(28), pp. 16683–16689.

Liu, Q. *et al.* (2014) 'Effect of potent γ-secretase modulator in human neurons derived from multiple presenilin 1-induced pluripotent stem cell mutant carriers.', *JAMA neurology*, 71(12), pp. 1481–1489. doi: 10.1001/jamaneurol.2014.2482.

Logan, S. *et al.* (2019) 'Studying Human Neurological Disorders Using Induced Pluripotent Stem Cells: from 2D Monolayer to 3D Organoid and Blood Brain Barrier Models', *Compr Physiol*, 9(2), pp. 565–611. doi: 10.1002/cphy.c180025.Studying.

Loh, Y. *et al.* (2006) 'The Oct4 and Nanog transcription network regulates pluripotency in mouse embryonic stem cells', *Nature Genetics*, 38(4), pp. 431–440. doi: 10.1038/ng1760.

Lui, J. H., Hansen, D. V and Kriegstein, A. R. (2011) 'Development and evolution of the human neocortex.', *Cell*, 146(1), pp. 18–36. doi: 10.1016/j.cell.2011.06.030.

Di Lullo, E. and Kriegstein, A. R. (2017) 'The use of brain organoids to investigate neural development and disease', *Nature Reviews Neuroscience*, 18(10), pp. 573–584. doi: 10.1038/nrn.2017.107.

Madabhushi, R., Pan, L. and Tsai, L.-H. (2014) 'DNA damage and its links to neurodegeneration.', *Neuron*, 83(2), pp. 266–282. doi: 10.1016/j.neuron.2014.06.034.

Malik, A. M. *et al.* (2018) 'Matrin 3-dependent neurotoxicity is modified by nucleic acid binding and nucleocytoplasmic localization', *eLife*, pp. 1–30.

Mansour, A. A. *et al.* (2018) 'An in vivo model of functional and vascularized human brain organoids.', *Nature biotechnology*, 36(5), pp. 432–441. doi: 10.1038/nbt.4127.

Mao, Z. *et al.* (2008) 'Comparison of nonhomologous end joining and homologous recombination in human cells', *DNA repair*. 2008/08/20, 7(10), pp. 1765–1771. doi: 10.1016/j.dnarep.2008.06.018.

Marangi, G., Lattante, S., Doronzio, P. N., *et al.* (2017) 'Matrin 3 variants are frequent in Italian ALS patients', *Neurobiology of Aging*. Elsevier Inc, 49, p. 218. doi: 10.1016/j.neurobiolaging.2016.09.023.

Marangi, G., Lattante, S., Niccolò, P., *et al.* (2017) 'Neurobiology of Aging Matrin 3 variants are frequent in Italian ALS patients', *Neurobiology of Aging*. Elsevier Inc, 49, pp. 218.e1-218.e7. doi: 10.1016/j.neurobiolaging.2016.09.023.

Maruyama, H. *et al.* (2010) 'Mutations of optineurin in amyotrophic lateral sclerosis.', *Nature*. England, 465(7295), pp. 223–226. doi: 10.1038/nature08971.

Masutani, M., Sonenberg, N. and Yokoyama, S. (2007) 'Reconstitution reveals the functional core of mammalian eIF3', *The EMBO journal*, 26(14), pp. 3373–3383. doi: 10.1038/sj.emboj.7601765.

Mateen, F. J., Carone, M. and Sorenson, E. J. (2010) 'Patients who survive 5 years or more with ALS in Olmsted County, 1925-2004', *Journal of neurology, neurosurgery, and psychiatry*. 2010/07/13, 81(10), pp. 1144–1146. doi: 10.1136/jnnp.2009.201251.

Matus, S., Medinas, D. B. and Hetz, C. (2014) 'Common Ground: Stem Cell Approaches Find Shared Pathways Underlying ALS', *Cell Stem Cell*. Elsevier, 14(6), pp. 697–699. doi: 10.1016/j.stem.2014.05.001.

Mayr, F. and Heinemann, U. (2013) 'Mechanisms of Lin28-Mediated miRNA and mRNA Regulation — A Structural and Functional Perspective', *international journal of molecular medicine*, pp. 16532–16553. doi: 10.3390/ijms140816532.

McKinnon, P. J. (2009) 'DNA repair deficiency and neurological disease', *Nature Reviews Neuroscience*, 10(2), pp. 100–112. doi: 10.1038/nrn2559.

McKinnon, P. J. (2013) 'Maintaining genome stability in the nervous system', *Nature neuroscience*. 2013/10/28, 16(11), pp. 1523–1529. doi: 10.1038/nn.3537.

Medvedev, S. P., Shevchenko, A. I. and Zakian, S. M. (2010) 'Induced Pluripotent Stem Cells : Problems and Advantages when Applying them in Regenerative Medicine', *Acta naturae*, 2(5), pp. 18–27.

Miao, N. *et al.* (2018) 'Opposite Roles of Wnt7a and Sfrp1 in Modulating Proper Development of Neural Progenitors in the Mouse Cerebral Cortex', *Frontiers in Molecular Neuroscience*, 11(July), pp. 1–14. doi: 10.3389/fnmol.2018.00247.

Mitsui, K. *et al.* (2003) 'The Homeoprotein Nanog Is Required for Maintenance of Pluripotency in Mouse Epiblast and ES Cells', *Cell*, 113, pp. 631–642.

Mohamed, N.-V. *et al.* (2019) 'One Step Into the Future: New iPSC Tools to Advance Research in Parkinson's Disease and Neurological Disorders', *Journal of Parkinson's disease*. IOS Press, 9(2), pp. 265–281. doi: 10.3233/JPD-181515.

Mohyeldin, A., N-Muvdi, T. s G. and Quin˜ones-Hinojosa, A. (2010) 'Oxygen in Stem Cell Biology : A Critical Component of the Stem Cell Niche', *Cell Stem Cell*, (Figure 1). doi: 10.1016/j.stem.2010.07.007.

Molenaar, J. J. *et al.* (2012) 'LIN28B induces neuroblastoma and enhances MYCN levels via let-7 suppression', *Nature Genetics*, 44(11), pp. 1199–1206. doi: 10.1038/ng.2436.

Musunuru, K. (2003) 'Cell-Specific RNA-Binding Proteins in Human Disease', *TCM*, 13(5), pp. 188–195.

Nakayasu, H. and Berezneyt, R. (1991) 'Nuclear matrins : Identification of the major nuclear matrix proteins', *PNAS*, 88(November), pp. 10312–10316. doi: 10.1371/journal.pone.0142144.

Närväa, E. *et al.* (2012) 'RNA-Binding Protein L1TD1 Interacts with LIN28 via RNA and is Required for Human Embryonic Stem Cell Self-Renewal and Cancer Cell Proliferation', *Stem Cells*, 30(3), pp. 452–460. doi: 10.1002/stem.1013.RNA-Binding.

Naumann, M. *et al.* (2018) 'Impaired DNA damage response signaling by FUS-NLS mutations leads to neurodegeneration and FUS aggregate formation', *Nature Communications*. Nature Publishing Group, 9(1), p. 335. doi: 10.1038/s41467-017-02299-1.

Neff, A. T. *et al.* (2012) 'Global analysis reveals multiple pathways for unique regulation of mRNA decay in induced pluripotent stem cells', *Genome Research*, pp. 1457–1467. doi: 10.1101/gr.134312.111.one.

Ng, H. and Surani, M. A. (2011) 'The transcriptional and signalling networks of pluripotency', *Nature Publishing Group*. Nature Publishing Group, 13(5), pp. 490–496. doi: 10.1038/ncb0511-490.

Nguyen, H. P., Van Broeckhoven, C. and van der Zee, J. (2018) 'ALS Genes in the Genomic Era and their Implications for FTD.', *Trends in genetics : TIG*. England, 34(6), pp. 404–423. doi: 10.1016/j.tig.2018.03.001.

Nichols, J. *et al.* (1998) 'Formation of Pluripotent Stem Cells in the Mammalian Embryo Depends on the POU Transcription Factor Oct4', *Cell*, 95, pp. 379–391.

Niimori-kita, K. *et al.* (2018) 'Matrin-3 is essential for fibroblast growth factor 2-dependent maintenance of neural stem cells', *Scientific Reports*. Springer US, pp. 1–10. doi: 10.1038/s41598-018-31597-x.

Nishida, K. *et al.* (2017) 'RNA Binding Proteins and Genome Integrity', *Molecular Sciences MDPI*, pp. 3–5. doi: 10.3390/ijms18071341.

Niwa, H. (2007) 'How is pluripotency determined and maintained ?', *Development*, 646, pp. 635–646. doi: 10.1242/dev.02787.

Niwa, H. *et al.* (2009) 'A parallel circuit of LIF signalling pathways maintains pluripotency of mouse ES cells', *Nature*. Nature Publishing Group, 460(July), pp. 1–5. doi: 10.1038/nature08113.

Niwa, H., Miyazaki, J. and Smith, A. G. (2000) 'Quantitative expression of Oct-3 / 4 defines differentiation , dedifferentiation or self-renewal of ES cells', *Nature Genetics*, 24(april), pp. 2–6.

Noctor, S. C. *et al.* (2004) 'Cortical neurons arise in symmetric and asymmetric division zones and migrate through specific phases',

Nature Neuroscience, 7(2), pp. 136–144. doi: 10.1038/nn1172.

Oliveira, C. *et al.* (2017) 'RNA-binding proteins and their role in the regulation of gene expression in Trypanosoma cruzi and Saccharomyces cerevisiae', *Genetics and Molecular Biology*, 30, pp. 22–30.

Olney, N. T., Spina, S. and Miller, B. L. (2017) 'Frontotemporal Dementia', *Neurologic clinics*, 35(2), pp. 339–374. doi: 10.1016/j.ncl.2017.01.008.

Onos, K. D. *et al.* (2016) 'Toward more predictive genetic mouse models of Alzheimer's disease', *Brain Res Bull.*, pp. 1–11. doi: 10.1016/j.brainresbull.2015.12.003.Toward.

Oosthuyse, B. *et al.* (2001) 'Deletion of the hypoxia-response element in the vascular endothelial growth factor promoter causes motor neuron degeneration', *Nature Genetics*, 28(2), pp. 131–138. doi: 10.1038/88842.

Origone, P. *et al.* (2015) 'A novel Arg147Trp MATR3 missense mutation in a slowly progressive ALS Italian patient A novel Arg147Trp MATR3 missense mutation in a slowly progressive ALS Italian patient', 8421, pp. 3–5. doi: 10.3109/21678421.2015.1058397.

Orkin, S. H. *et al.* (2008) 'The Transcriptional Network Controlling Pluripotency in ES Cells', *Cold spring Harbor Labpratory Press*, LXXIII, pp. 195–202.

Oskarsson, B., Gendron, T. F. and Staff, N. P. (2018) 'Amyotrophic Lateral Sclerosis : An Update', *Mayo Clinic Proceedings*. Mayo Foundation for Medical Education and Research, 93(11), pp. 1617–1628. doi: 10.1016/j.mayocp.2018.04.007.

Pan, G. *et al.* (2001) 'A negative feedback loop of transcription factors that controls stem cell pluripotency and self-renewal', *The FASEB Journal*. doi: 10.1096/fj.05-5543fje.

Pan, G. J. *et al.* (2002) 'Stem cell pluripotency and transcription factor Oct4', *Nature*, 12, pp. 321–329.

Pan, G. and Thomson, J. A. (2007) 'Nanog and transcriptional networks in embryonic stem cell pluripotency', *Nature*, pp. 42–49. doi: 10.1038/sj.cr.7310125.

Pan, L., Penney, J. and Tsai, L.-H. (2014) 'Chromatin regulation of DNA damage repair and genome integrity in the central nervous system', *Journal of molecular biology*. 2014/08/14, 426(20), pp. 3376–3388. doi: 10.1016/j.jmb.2014.08.001.

Panda, A. C., Martindale, J. L. and Gorospe, M. (2017) 'Polysome Fractionation to Analyze mRNA Distribution Profiles Amaresh', *Bio Protocol*, 7(3). doi: 10.21769/BioProtoc.2126.Polysome.

Paris, J. *et al.* (2019) 'Short Article Targeting the RNA m 6 A Reader YTHDF2 Selectively Compromises Cancer Stem Cells in Acute Myeloid Short Article Targeting the RNA m 6 A Reader YTHDF2 Selectively Compromises Cancer Stem Cells in Acute Myeloid Leukemia', pp. 137–148. doi: 10.1016/j.stem.2019.03.021.

Park, C. S. *et al.* (2019) 'Regulation of Self-Renewal in Normal and Malignant Hematopoietic Stem Cells by Krüppel-Like Factor 4', *Stem Cell Translational Medicine*, pp. 568–574. doi: 10.1002/sctm.18-0249.

Pelletier, J. *et al.* (2016) 'TARGETING THE eIF4F TRANSLATION INITIATION COMPLEX: A CRITICAL NEXUS FOR CANCER DEVELOPMENT', *Cancer Res.*, 75(2), pp. 250–263. doi: 10.1158/0008-5472.CAN-14-2789.TARGETING.

PENG, S. *et al.* (2011) 'Genome-Wide Studies Reveal That Lin28 Enhances the Translation of Genes Important for Growth and Survival of Human Embryonic Stem', *Stem Cell*, pp. 496–504. doi: 10.1002/stem.591.

Penndorf, D., Witte, O. and Kretz, A. (2018) 'DNA plasticity and damage in amyotrophic lateral sclerosis', *Neural Regeneration Research*, 13(2), p. 0. doi: 10.4103/1673-5374.226377.

Pesce, M. and Scholer, H. (2001) 'Oct-4: Gatekeeper in the Beginnings of Mammalian Development', *Stem Cells*, pp. 271–278.

Pham, M. T. *et al.* (2019) 'Generation of human vascularized brain organoids Missy', *Neuroreport*, 29(7), pp. 588–593. doi: 10.1097/WNR.0000000000001014.Generation.

Philips, T. and Robberecht, W. (2011) 'Neuroinflammation in amyotrophic lateral sclerosis: role of glial activation in motor neuron disease', *The Lancet Neurology*. Elsevier, 10(3), pp. 253–263. doi: 10.1016/S1474-4422(11)70015-1.

Pickar-Oliver, A. and Gersbach, C. A. (2019) 'The next generation of CRISPR–Cas technologies and applications', *Nature Reviews Molecular Cell Biology*, 20(8), pp. 490–507. doi: 10.1038/s41580-019-0131-5.

Pilié, P. G. *et al.* (2019) 'State-of-the-art strategies for targeting the DNA damage response in cancer', *Nature Reviews Clinical Oncology*, 16(2), pp. 81–104. doi: 10.1038/s41571-018-0114-z.

Piskounova, E. *et al.* (2008) 'Determinants of MicroRNA Processing Inhibition by the Developmentally Regulated', *THE JOURNAL OF BIOLOGICAL CHEMISTRY*, 283(31), pp. 21310–21314. doi: 10.1074/jbc.C800108200.

Piskounova, E. *et al.* (2011) 'Oncogenic Lin28A and Lin28B inhibit let-7 microRNA biogenesis by distinct mechanisms', *Cell*, 147(5), pp. 730–748. doi: 10.1016/j.cell.2011.10.039.Oncogenic.

Pollari, E. *et al.* (2014) 'The role of oxidative stress in degeneration of the neuromuscular junction in amyotrophic lateral sclerosis', *Frontiers in neuroscience*, 8(May), pp. 1–8. doi: 10.3389/fncel.2014.00131.

Pollini, D. *et al.* (2018) 'Generation and characterization of a human iPSC line from an ALS patient carrying the Q66K-MATR3 mutation', *Stem Cell Research*. Elsevier, 33(October), pp. 146–150. doi: 10.1016/j.scr.2018.10.011.

Potzner, M. R. *et al.* (2010) 'Sequential requirement of Sox4 and Sox11 during development of the sympathetic nervous system', *Development*, 137(5), pp. 775 LP – 784. doi: 10.1242/dev.042101.

Processing, L. R. N. A. *et al.* (2018) 'Heteromeric RNP Assembly at LINEs Controls Article Heteromeric RNP Assembly at LINEs Controls Lineage-Specific RNA Processing', *Cell*. Elsevier Inc., 174(5), pp. 1067-1081.e17. doi: 10.1016/j.cell.2018.07.001.

Puzzo, D. *et al.* (2015) 'Rodent models for Alzheimer's disease drug discovery', *Expert Opinion on Drug Discovery*, 10(7), pp. 703–711. doi: 10.1517/17460441.2015.1041913.Rodent.

Qi, H. and Pei, D. (2007) 'The magic of four : induction of pluripotent stem cells from somatic cells by Oct4 , Sox2 , Myc and Klf4', *Cell Research*, pp. 578–580. doi: 10.1038/cr.2007.59.

Qian, J. *et al.* (2010) 'Dynamic transcriptomes during neural differentiation of human embryonic stem cells revealed by short , long , and paired-end sequencing', *PNAS*, 107(11). doi: 10.1073/pnas.0914114107.

Qian, X., Song, H. and Ming, G. (2019) 'Brain organoids: advances, applications and challenges', *Development*, 146(8), p. dev166074. doi: 10.1242/dev.166074.

Qiu, C. *et al.* (2010) 'Lin28-mediated post-transcriptional regulation of Oct4 expression in human embryonic stem cells', *Nucleic Acids Research*, 38(4), pp. 1240–1248. doi: 10.1093/nar/gkp1071.

Radzisheuskaya, A. *et al.* (2013) 'Europe PMC Funders Group Europe PMC Funders Author Manuscripts A defined Oct4 level governs cell state transitions of pluripotency entry and differentiation into all embryonic lineages', 15(6), pp. 579–590. doi: 10.1038/ncb2742.A.

Raquel, D. *et al.* (2019) 'Genome editing : A perspective on the application of CRISPR / Cas9 to study human diseases (Review)', *international journal of molecular medicine*, pp. 1559–1574. doi: 10.3892/ijmm.2019.4112.

Ren, J. I. E. *et al.* (2018) 'Decreased expression of SFRP2 promotes development of the pituitary corticotroph adenoma by upregulating Wnt signaling', *international journal of oncology*, pp. 1934–1946. doi: 10.3892/ijo.2018.4355.

Renton, A. E. *et al.* (2011) 'A hexanucleotide repeat expansion in C9ORF72 is the cause of chromosome 9p21-linked ALS-FTD.', *Neuron*, 72(2), pp. 257–268. doi: 10.1016/j.neuron.2011.09.010.

Rosen, D. R. *et al.* (1993) 'Mutations in Cu/Zn superoxide dismutase gene are associated with familial amyotrophic lateral sclerosis.', *Nature*. England, 362(6415), pp. 59–62. doi: 10.1038/362059a0.

Rowe, R. G. and Daley, G. Q. (2019) 'Induced pluripotent stem cells in disease modelling and drug discovery', *Nature Reviews Genetics*. Springer US. doi: 10.1038/s41576-019-0100-z.

Rowland, B. D., Bernards, R. and Peeper, D. S. (2005) 'The KLF4 tumour suppressor is a transcriptional repressor of p53 that acts as a context-dependent oncogene', *Nature Cell Biology*, 7(11). doi: 10.1038/ncb1314.

Rowland, L. P. and Shneider, N. A. (2001) 'The clinical diagnosis of ALS is probably correct in more than 95 percent of cases. 1 However, because', *The New England Journal of Medicine*, 344(22), pp. 1688–1700.

Salton, M. *et al.* (2010) 'Involvement of Matrin 3 and SFPQ / NONO in the DNA damage response Involvement of Matrin 3 and SFPQ / NONO in the DNA damage response', 4101. doi: 10.4161/cc.9.8.11298.

Salton, M. *et al.* (2011) 'Matrin 3 binds and stabilizes mRNA', *PLoS ONE*, 6(8), pp. 1–9. doi: 10.1371/journal.pone.0023882.

Sampath, P. *et al.* (2008) 'A Hierarchical Network Controls Protein Translation during Murine Embryonic Stem Cell Self-Renewal and Differentiation', *Cell Stem Cell*. doi: 10.1016/j.stem.2008.03.013.

Sarkar, A. and Hochedlinger, K. (2014) 'The Sox Family of Transcription Factors: Versatile Regulators of Stem and Progenitor Cell Fate', *Cell Stem Cell*, 12(1), pp. 15–30. doi: 10.1016/j.stem.2012.12.007.The.

Schaefer, T. and Lengerke, C. (2019) 'SOX2 protein biochemistry in stemness , reprogramming , and cancer : the PI3K / AKT / SOX2 axis and beyond', *Oncogene*. Springer US. doi: 10.1038/s41388-019-0997-x.

Schuh, R. *et al.* (1986) 'A Conserved Family of Nuclear Proteins Containing Structural Elements of the Finger Protein Encoded by Kriippel , a Drosophila Segmentation Gene', *Cell*, 47, pp. 1025–1032.

Scully, R. *et al.* (2019) 'DNA double-strand break repair-pathway choice in somatic mammalian cells', *Nature Reviews Molecular Cell Biology*, 20(11), pp. 698–714. doi: 10.1038/s41580-019-0152-0.

Senderek, J. *et al.* (2009) 'Autosomal-Dominant Distal Myopathy Associated with a Recurrent Missense Mutation in the Gene Encoding the Nuclear Matrix Protein , Matrin 3', *The American Society of Genetics*, pp. 511–518. doi: 10.1016/j.ajhg.2009.03.006.

She, Z.-Y. and Yang, W.-X. (2015) 'SOX family transcription factors involved in diverse cellular events during development', *European Journal of Cell Biology*, 94(12), pp. 547–563. doi: https://doi.org/10.1016/j.ejcb.2015.08.002.

Shi, G. and Jin, Y. (2010) 'Role of Oct4 in maintaining and regaining stem cell pluripotency', *stem cell research e therapy*, pp. 1–9.

Shi, Y. *et al.* (2017) 'Induced pluripotent stem cell technology: a decade of progress', *Nat Rev Drug Discov.*, 16(2), pp. 115–130. doi: 10.1038/nrd.2016.245.Induced.

Shi, Y. *et al.* (no date) 'Induced pluripotent stem cell technology : a decade of progress', *Nature Publishing Group*. Nature Publishing Group. doi: 10.1038/nrd.2016.245.

Shi, Y. and Ai, W. (2013) 'Function of KLF4 in Stem Cell Biology', *INTECH open science*. doi: http://dx.doi.org/10.5772/54370.

Shi, Y. and Massague, J. (2003) 'Mechanisms of TGF- Signaling from Cell Membrane to the Nucleus', *Cell*, 113(Figure 2), pp. 685–700.

Shields, J. M., Christy, R. J. and Yang, V. W. (2008) 'Identification and Characterization of a Gene Encoding a Gut- enriched Krüppel-like Factor Expressed during Growth Arrest', *THE JOURNAL OF BIOLOGICAL CHEMISTRY*, 271(33), pp. 20009–20017.

Shigunov, P. and Dallagiovanna, B. (2015) 'Stem Cell Ribonomics : RNA-Binding Proteins and Gene Networks in Stem Cell Differentiation', *Frontiers in Molecular Biosciences*, 2(December), pp. 1–7. doi: 10.3389/fmolb.2015.00074.

Sibbritt, T. *et al.* (2013) 'Mapping and significance of the mRNA methylome', 4(August). doi: 10.1002/wrna.1166.

Siddique, T. *et al.* (1991) 'Linkage of a Gene Causing Familial Amyotrophic Lateral Sclerosis to Chromosome 21 and Evidence of Genetic-Locus Heterogeneity', *New England Journal of Medicine*. Massachusetts Medical Society, 324(20), pp. 1381–1384. doi: 10.1056/NEJM199105163242001.

Signer, R. A. J. *et al.* (2014) 'Haematopoietic stem cells require a highly regulated protein synthesis rate', *Nature*, 509(7498), pp. 49–54. doi: 10.1038/nature13035.Haematopoietic.

Singh, A. *et al.* (2019) 'Oxidative Stress: A Key Modulator in Neurodegenerative Diseases', *Molecules (Basel, Switzerland)*. MDPI, 24(8), p. 1583. doi: 10.3390/molecules24081583.

Singh, H. and Brivanlou, A. H. (2013) *The Molecular Circuitry Underlying Pluripotency in Embryonic Stem Cells and iPS Cells*. Second Edition, *Handbook of Stem Cells, Two-Volume Set*. Second Edition. Elsevier Inc. doi: 10.1016/B978-0-12-385942-6.00005-6.

Skowronska-Krawczyk, D. *et al.* (2014) 'Required enhancer-matrin-3 network interactions for a homeodomain transcription program', *Nature*, 514(7521), pp. 257–261. doi: 10.1038/nature13573.

Sreedharan, J. *et al.* (2008) 'TDP-43 mutations in familial and sporadic amyotrophic lateral sclerosis.', *Science (New York, N.Y.)*. United States, 319(5870), pp. 1668–1672. doi: 10.1126/science.1154584.

Starr, A. and Sattler, R. (2018) 'Synaptic dysfunction and altered excitability in C9ORF72 ALS / FTD', *Brain Research*. Elsevier B.V., 1693, pp. 98–108. doi: 10.1016/j.brainres.2018.02.011.

Stifani, N. (2014) 'Motor neurons and the generation of spinal motor neuron diversity', *Frontiers in cellular neuroscience*, 8(October), pp. 1–22. doi: 10.3389/fncel.2014.00293.

Suzuki, A. *et al.* (2006) 'Nanog binds to Smad1 and blocks bone morphogenetic protein-induced differentiation of embryonic stem cells', *PNAS*, pp. 1–6.

Tada, M. *et al.* (2018) 'Matrin 3 Is a Component of Neuronal Cytoplasmic Inclusions of Motor Neurons in Sporadic Amyotrophic Lateral Sclerosis', *The American Journal of Pathology*. American Society for Investigative Pathology, 188(2), pp. 507–514. doi: 10.1016/j.ajpath.2017.10.007.

Tahmasebi, S., Amiri, M. and Sonenberg, N. (2019) 'Translational Control in Stem Cells', *Frontiers in Genetics*, 9(January), pp. 1–9. doi: 10.3389/fgene.2018.00709.

Takahashi, K. *et al.* (2007) 'Induction of Pluripotent Stem Cells from Adult Human Fibroblasts by Defined Factors', *Cell*, 131(5), pp.

861–872. doi: 10.1016/j.cell.2007.11.019.

Takahashi, K. and Yamanaka, S. (2006) 'Induction of Pluripotent Stem Cells from Mouse Embryonic and Adult Fibroblast Cultures by Defined Factors', *Cell*, 126(4), pp. 663–676. doi: 10.1016/j.cell.2006.07.024.

Tebaldi, T. *et al.* (2017) 'In Vivo Translatome Profiling in Spinal Muscular Atrophy Reveals a Role for SMN Protein in Ribosome Article In Vivo Translatome Profiling in Spinal Muscular Atrophy Reveals a Role for SMN Protein in Ribosome Biology', *Cell Reports*, pp. 953–965. doi: 10.1016/j.celrep.2017.10.010.

Temple, S. (2001) 'The development of neural stem cells', *insight review articles*, 414(November).

TeSlaa, T., Setoguchi, K. and Teitell, M. A. (2016) 'Mitochondria in human pluripotent stem cell apoptosis', *Seminars in Cell & Developmental Biology*, 52, pp. 76–83. doi: https://doi.org/10.1016/j.semcdb.2016.01.027.

Thomson, M. *et al.* (2011) 'Pluripotency Factors in Embryonic Stem Cells Regulate Differentiation into Germ Layers', *Cell*. Elsevier Inc., 145(6), pp. 875–889. doi: 10.1016/j.cell.2011.05.017.

Thomson, M. *et al.* (2017) 'Pluripotency circuit members mediate germ layer fate choice of embryonic embryonic stem cells', *Cell*, 145(6), pp. 875–889. doi: 10.1016/j.cell.2011.05.017.Pluripotency.

Tickle, C., Towers, M. and Davey, M. (2017) 'Sonic Hedgehog Signaling in Limb Development', *Frontiers in Cell and Developmental Biology*, 5(February), pp. 1–19. doi: 10.3389/fcell.2017.00014.

Trounson, A. (2007) 'Embryonic Stem Cells', *Principles of Tissue Emgineering 3 Edition*.

Tsanov, K. M. *et al.* (2017) 'LIN28 phosphorylation by MAPK/ERK couples signaling to the post-transcriptional control of pluripotency', *Nature Cell Biology*, 19(1), pp. 60–67. doi: 10.1038/ncb3453.LIN28.

Tsialikas, J. and Romer-seibert, J. (2015) 'LIN28 : roles and regulation in development and beyond', *Development*, pp. 2397–2404. doi: 10.1242/dev.117580.

Tsz Kin Ng, Daniel Pelaez, V. R. F. and Cheung, J. G. and H. S. (2013) 'Pluripotent Adult Stem Cells: A Potential Revolution in Regenerative Medicine and Tissue Engineering', *inthecopen*, (chapter 2). Available at: http://dx.doi.org/10.5772/54366.

Uemura, Y. *et al.* (2017) 'Matrin3 binds directly to intronic pyrimidine-rich sequences and controls alternative splicing', *Genes to Cells*, 22(9), pp. 785–798. doi: 10.1111/gtc.12512.

Vallier, L. *et al.* (2009) 'Early Cell Fate Decisions of Human Embryonic Stem Cells and Mouse Epiblast Stem Cells Are Controlled by the Same Signalling Pathways', *PLoS ONE*, 4(6). doi: 10.1371/journal.pone.0006082.

Vencken, S. F. *et al.* (2014) 'An integrated analysis of the SOX2 microRNA response program in human pluripotent and nullipotent stem cell lines', *BioMedCentral*, pp. 1–16.

Viswanathan, S. R., Daley, G. Q. and Gregory, R. I. (2013) 'Selective blockade of microRNA processing by Lin-28', *Science*, 320(5872), pp. 97–100. doi: 10.1126/science.1154040.Selective.

Wakui, T. (2017) 'Method for evaluation of human induced pluripotent stem cell quality using image analysis based on the biological morphology of cells stem cell quality using image analysis based on', 4(4). doi: 10.1117/1.JMI.4.4.044003.

Wang, D. G. and J. (2014) 'RNA-binding proteins in pluripotency, differentiation, and reprogramming', *Front Biol*, 9(5), pp. 389–409. doi: 10.1007/s11515-014-1326-y.RNA-binding.

Wang, J. *et al.* (2006) 'A protein interaction network for pluripotency of embryonic stem cells', *Nature*, 444(November). doi: 10.1038/nature05284.

Wang, X. *et al.* (2015) 'N6-methyladenosine modulates messenger RNA translation efficiency', *Cell*. Cell Press, 161(6), pp. 1388–1399. doi: 10.1016/j.cell.2015.05.014.

Warkus, E. L. L. *et al.* (2016) 'Use of In Vitro Morphogenesis of Mouse Embryoid Bodies to Assess Developmental Toxicity of Therapeutic Drugs Contraindicated in Pregnancy', *SOT Society of Toxicology*, 149(1), pp. 15–30. doi: 10.1093/toxsci/kfv209.

Webster, D. M. *et al.* (2009) 'O-GlcNAc modifications regulate cell survival and epiboly during zebrafish development', *BMC Developmental Biology*, 24, pp. 1–24. doi: 10.1186/1471-213X-9-28.

Weed, M., Mundlos, S. and Olsen, B. R. (1997) 'The role of sonic hedgehog in vertebrate development', *Matrix Biology*, 16(2), pp. 53–58. doi: https://doi.org/10.1016/S0945-053X(97)90072-X.

Wei, F., Scho, H. R. and Atchison, M. L. (2007) 'Sumoylation of Oct4 Enhances Its Stability , DNA Binding ', *THE JOURNAL OF BIOLOGICAL CHEMISTRY*, 282(29), pp. 21551–21560. doi: 10.1074/jbc.M611041200.

Winanto *et al.* (2019) 'Spinal cord organoids add an extra dimension to traditional motor neuron cultures', *Neural Regeneration Research*, 14(9), pp. 1515–1516. doi: 10.4103/1673-5374.255966.

Wu, J. *et al.* (2016) 'An overview of mammalian pluripotency', pp. 1644–1648. doi: 10.1242/dev.132928.

Wu, R. *et al.* (2019) 'm 6 A methylation controls pluripotency of porcine induced pluripotent stem cells by targeting SOCS3 / JAK2 / STAT3 pathway in a YTHDF1 / YTHDF2-orchestrated manner', *Cell Death and Disease*. Springer US. doi: 10.1038/s41419-019-1417-4.

Xiao, Y. *et al.* (2018) 'ROS-related mitochondrial dysfunction in skeletal muscle of an ALS mouse model during the disease progression.', *Pharmacological research*, 138, pp. 25–36. doi: 10.1016/j.phrs.2018.09.008.

Xu, H. *et al.* (2009) 'WWP2 promotes degradation of transcription factor OCT4 in human embryonic stem cells', *Nature*, pp. 561–573. doi: 10.1038/cr.2009.31.

Xu, H. M. *et al.* (2004) 'Wwp2 , an E3 Ubiquitin Ligase That Targets Transcription Factor Oct-4 for Ubiquitination *', *THE JOURNAL OF BIOLOGICAL CHEMISTRY*, 279(22), pp. 23495–23503. doi: 10.1074/jbc.M400516200.

Xu, R. *et al.* (2009) 'NANOG is a Direct Target of TGFβ/Activin Mediated SMAD Signaling in Human ES Cells', *Cell Stem Cell*, 3(2), pp. 196–206. doi: 10.1016/j.stem.2008.07.001.NANOG.

Yamaguchi, A. and Takanashi, K. (2016a) 'FUS interacts with nuclear matrix- associated protein SAFB1 as well as Matrin3 to regulate splicing and ligand-mediated transcription', *Nature Publishing Group*. Nature Publishing Group, (September), pp. 1–14. doi: 10.1038/srep35195.

Yamaguchi, A. and Takanashi, K. (2016b) 'FUS interacts with nuclear matrix-associated protein SAFB1 as well as Matrin3 to regulate splicing and ligand-mediated transcription', *Scientific Reports*. Nature Publishing Group, 6(October), pp. 1–14. doi: 10.1038/srep35195.

Yang, D.-H. and Moss, E. G. (2003) 'Temporally regulated expression of Lin-28 in diverse tissues of the developing mouse', *Gene Expression Patterns*, 3(6), pp. 719–726. doi: https://doi.org/10.1016/S1567-133X(03)00140-6.

Young, R. A. (2012) 'Control of Embryonic Stem Cell State Richard', *Cell*, 144(6), pp. 940–954. doi: 10.1016/j.cell.2011.01.032.Control.

Yu, J. *et al.* (2012) 'Induced Pluripotent Stem Cell Lines Derived from Human Somatic Cells', *Science*, 1917(2007). doi: 10.1126/science.1151526.

Yun, S. *et al.* (2012) 'Neural stem cell specific fluorescent chemical probe binding to FABP7', *PNAS*, 109(26), pp. 10214–10217. doi: 10.1073/pnas.1200817109.

Zarei, S. *et al.* (2015) 'A comprehensive review of amyotrophic lateral sclerosis', *Surgical Neurology International*. doi: 10.4103/2152-7806.169561.

Zhang, J., Ratanasirintrawoot, S., Chandrasekaran, S., Wu, Z., *et al.* (2016) 'LIN28 Regulates Stem Cell Metabolism and Conversion to Primed Pluripotency', *Cell Stem Cell*, 19(1), pp. 66–80. doi: https://doi.org/10.1016/j.stem.2016.05.009.

Zhang, J., Ratanasirintrawoot, S., Chandrasekaran, S., Li, H., *et al.* (2016) 'LIN28 Regulates Stem Cell Metabolism and Conversion to Primed Pluripotency Article LIN28 Regulates Stem Cell Metabolism and Conversion to Primed Pluripotency', *Cell Stem Cell*, pp. 66–80. doi: 10.1016/j.stem.2016.05.009.

Zhang, K. *et al.* (2015) 'The C9orf72 repeat expansion disrupts nucleocytoplasmic transport', *Nature*, 525(7567), pp. 56–61. doi: 10.1038/nature14973.

Zhang, M., Schöler, H. R. and Greber, B. (2013) 'Rapid and Efficient Generation of Neurons from Human Pluripotent Stem Cells in a Multititre Plate Format', *Jove Journal of Visualized Experiments*, (March), pp. 1–7. doi: 10.3791/4335.

Zhang, P. *et al.* (2010) 'Kruppel-like Factor 4 (Klf4) Prevents Embryonic Stem (ES) Cell Differentiation by Regulating Nanog Gene Expression', *THE JOURNAL OF BIOLOGICAL CHEMISTRY*, 285(12), pp. 9180–9189. doi: 10.1074/jbc.M109.077958.

Zhang, S. and Cui, W. (2014) 'Sox2 , a key factor in the regulation of pluripotency and neural differentiation', *world journal of stem cells*, 6(3), pp. 305–311. doi: 10.4252/wjsc.v6.i3.305.

Zhang, Z. and Carmichael, G. G. (2001) 'The Fate of dsRNA in the Nucleus : A p54 nrb -Containing Complex Mediates the Nuclear Retention of Promiscuously A-to-I Edited RNAs', 106, pp. 465–475.

Zhao, M. *et al.* (2018) 'RNA-Binding Proteins in Amyotrophic Lateral Sclerosis', *Molecules and Cells*, 41(9), pp. 818–829.

Zhao, S. *et al.* (2004) 'SoxB transcription factors specify neuroectodermal lineage choice in ES cells', *Molecular and Cellular Neuroscience*, 27, pp. 332–342. doi: 10.1016/j.mcn.2004.08.002.

Zhu, H. *et al.* (2011) 'The Lin28 / let-7 Axis Regulates Glucose Metabolism', *Cell*, pp. 81–94. doi: 10.1016/j.cell.2011.08.033.

Zhuang, M. *et al.* (2019) 'The m 6 A reader YTHDF1 regulates axon guidance through translational control of Robo3 . 1 expression', *Nucleid Acids Research*. Oxford University Press, 47(9), pp. 4765–4777. doi: 10.1093/nar/gkz157.

Ziv, O. *et al.* (2015) 'Quantitative Live Imaging of Human Embryonic Stem Cell Derived Neural Rosettes Reveals Structure-Function Dynamics Coupled to Cortical Development', *PLoS ONE*, pp. 1–21. doi: 10.1371/journal.pcbi.1004453.

ACKNOWLEDGEMENTS

In conclusione, vorrei ringraziare chi mi ha dato la possibilità di lavorare a questo progetto fortemente voluto durante il mio dottorato. Colgo l'occasione quindi per ringraziare Prof. Alessandro Provenzani, che mi ha inserito nel suo gruppo di ricerca quattro anni fa, che mi ha dato poi la possibilità di realizzare il sogno di lavorare con cellule staminali e quello di aver potuto dire la "mia" nel mondo scientifico. Grazie! Colgo anche l'occasione per ringraziare Prof. Luciano Conti, che molto mi ha insegnato riguardo le cellule staminali.

Vorrei ringraziare di cuore Rosa Loffredo, colei che ha iniziato lo studio MATR3 nel nostro laboratorio e che quando ha dovuto muoversi all'estero mi ha lasciato in mano il progetto, mi ha insegnato, con molta pazienza, molto professionalmente ma soprattutto umanamente. Non smetterò mai di ringraziarla per quello che consapevolmente e inconsapevolmente mi ha dato da PostDoc e soprattutto da amica sia durante la sua permanenza al CIBIO che successivamente.

Ringrazio di cuore Marina Cardano, che mi ha insegnato a lavorare con cellule staminali e organoidi. Marina ha contribuito molto alla mia crescita professionale e umana, sempre disponibile ad aiutare le persone, non mi ha mai abbandonato ed ha sempre creduto in me.

Ringrazio il gruppo del lab. di Genomic Screening di cui faccio parte, dai tesisti che mi hanno affiancato durante il loro tirocinio come Weronika, i dottorandi, Mariachiara, Nausicaa, Caterina, Agata che hanno condiviso per questi 4 anni la loro quotidianità con la mia, in particolar modo vorrei ringraziare Mariachiara e Claudio, due veri amici, ed infine i PostDoc, Chiara e la nuova PostDoc Isabelle.

Ringrazio le facilties che hanno permesso diversi esperimenti, la facility di HTS che con la sua Operetta ha reso possibile l'impossibile, aiutandomi a vedere verde, Grazie Michael! Ovviamente ringrazio tutto lo staff di HTS, le bravissime Valentina Adami e Pamela Gatto, la facility di Imaging e la facility di proteomica.

Ringrazio il direttore del CIBIO Alessandro Quattrone e chi ha finanziato il progetto, fondi CARITRO e ARISLA.

Vorrei ringraziare i miei cari che mi hanno sempre supportato e con grande sacrifico nella vita mi hanno permesso di inseguire i miei sogni. Un grazie va anche alla mia sorellina, un vero orgoglio. Infine, il ringraziamento più importante di tutti va a chi mi ha supportato e sopportato 24 ore su 24, che ha sempre silenziosamente creduto in me supportandomi quando le cose non andavano e la prima a festeggiare ad ogni mio singolo traguardo raggiunto. La metà perfetta per condividere qualsiasi percorso della vita. Grazie veramente Simona per esserci.